ABSTRACT

Title of Document: TRUCK LOADING SIMULATION FOR THE FATIGUE ASSESSMENT OF STEEL HIGHWAY BRIDGES

Gengwen Zhao, Doctor of Philosophy, 2015

Directed By: Professor, Chung C. Fu, Department of Civil and Environmental Engineering

Fatigue is a common failure mode for steel bridges. About 80-90% of failures in steel structures are related to fatigue and fracture. Despite the deterioration caused by environmental factors, the increasing traffic volume and weight pose a premier threat of steel highway bridges. The total number of truck passages in the 75-year life of a highway bridge could exceed 100 million. With the aging of existing steel highway bridges and the accumulated damage under truck loading, the fatigue assessment for continuing service has become important for decisions making on the structure maintenance, component replacement, and other major retrofits. This research seeks to develop a framework for the fatigue assessment of steel highway bridges based on simulated truck loading. The I-270 Bridge over Middlebrook Road was numerically studied with the proposed methodology. With the help of the available long-term monitoring traffic data and information, truck loading was obtained through the probability-based full velocity difference model. Then, the three-dimensional finite

element (FE) global and local bridge models were studied subjected to the simulated truck loading. Meanwhile, the preliminary field test and the long-term monitoring test were also been conducted. The FE models were calibrated by the collected field measurements through monitoring systems, and the simulated numerical structural responses were validated. Lastly, Miner's rule and the rainflow counting algorithm were used in the analysis of simulated numerical structural responses to estimating the fatigue life. Thus, the proposed methodology could be used to realistically simulate the fatigue behavior of steel highway bridges under current or future truck loading, to direct the experimental designs and instrumentation plans before performing experiments on laboratory or on site, and to better understand the fatigue mechanism and prevent the fatigue damage of steel highway bridges.

TRUCK LOADING SIMULATION FOR THE FATIGUE ASSESSMENT OF STEEL HIGHWAY BRIDGES

By

Gengwen Zhao

Dissertation submitted to the Faculty of the Graduate School of the
University of Maryland, College Park, in partial fulfillment
of the requirements for the degree of
Doctor of Philosophy
2015

Advisory Committee:
Professor Chung C. Fu, Chair/Advisor
Professor M. Sherif Aggour
Professor Amde M. Amde
Professor Yunfeng Zhang
Professor Sung W. Lee

Acknowledgements

This work was sponsored by the US Department of Transportation's Office of the Assistant Secretary for Research and Technology (USDOT/OST-R), under The Commercial Remote Sensing and Spatial Information (CRS&SI) Technologies Program. This support is acknowledged and greatly appreciated.

First and foremost I wish to thank my advisor, Dr. Chung C. Fu, director of the Bridge Engine the Bridge Engineering Technology & Software (BEST) Center at University of Maryland. He has been very supportive since the first day I began working on this research. Besides, I would like to thank all the committee members: Dr. Amde M. Made, Dr. M. Sherif Aggour, Dr. Yunfeng Zhang and Dr. Sung W. Lee, for their guidance.

I also would like to thank all the members of BEST Center at University of Maryland, Dr. Yunfeng Zhang's group at University of Maryland, and Dr. Fuh-Gwo Yuan's group at North Carolina State University for their help throughout the course of the preliminary field test and the long-term monitoring test. Thank you to group member Tim Saad and Yunchao Ye for offering help on the topic of rainflow counting algorithm and vehicle-bridge interaction. In addition, Dr. Y. Edward Zhou from AECOM (formerly URS Corporation) kindly shared his knowledge on the finite element modeling.

Lastly, special thanks goes to my family. My father Xiaoping Zhao and my mother Baozhen Zhang have been a constant source of love, concern, support and strength all these years. I would like to express my heart-felt gratitude to my family. Particularly, my husband, Mr. Yang Lu has been continuously providing expertise on the

transportation related topics in this dissertation, and supporting throughout my Ph.D. study.

Table of Contents

List of Tables

List of Figures

Chapter 1 Introduction

1.1 Research Background

Fatigue is defined as a condition when a material weakens after repeated applied loadings. Figure 1.1 shows the most common constant amplitude cyclic fatigue loading. If the loads are above a certain threshold, microscopic cracks will begin to form at stress concentrators, and the induced structural damage will cumulate. Eventually a crack will propagate and reach a critical size, and then the structure will fracture.

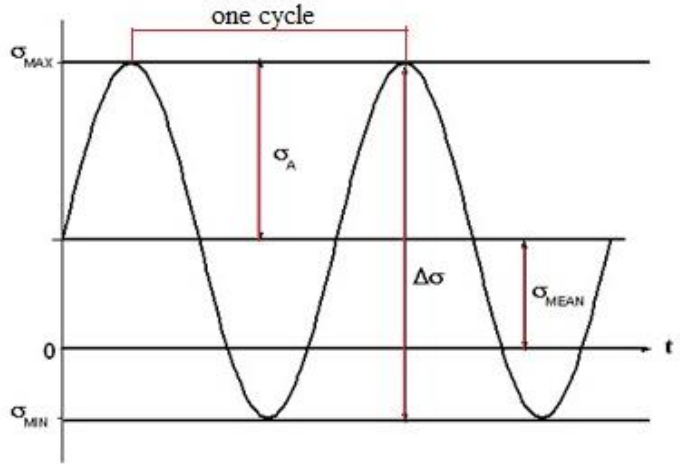

Figure 1.1 Constant Amplitude Cyclic Fatigue Loading

The fatigue failure is quite different with the failure mode caused by insufficient strength. The nominal maximum stress values that cause such damage may be much less than the strength of the material, typically quoted as the ultimate tensile stress limit, or the yield stress limit. Some characteristic of fatigue are listed below:

1. Macroscopic or microscopic discontinuities as well as component design features which cause stress concentrations are common locations for the

fatigue process begins;

2. Fatigue is usually associated with tensile stresses and stress reversals;
3. Fatigue is a process that has a degree of randomness;
4. Damage is cumulative, and materials do not recover when rested.

Therefore, steel structural components, of buildings or bridges, shall satisfy the requirements at all appropriate service: strength, extreme event limit states as well as fatigue state.

In the past 150 years, there have been a number of bridges damaged or collapsed attributed to fatigue in United States, which caused many casualties and large economic losses. On Dec. 29th 1876, Ashtabula River Railroad Bridge totally damaged as a result of possible fatigue failure of cast iron elements. Division Street Bridge, located in Spokane, Washington, collapsed in December 1915 because of metal fatigue. Similarly, in Greenwich, Connecticut, Mianus River Bridge also collapsed due to metal corrosion and fatigue in June 1983. There are also some cases reported that involve fatigue damage of highway bridges in service. For example:

1. Crack resulting from the typical web gap distortion near the bottom flange of welded plate girders were reported in the US 13 Bridge over Pocomoke River, Maryland. The distortion-induced stresses have initiated horizontal cracks in the web-to-flange welds and propagated into vertical cracks at the end of the web-to-connection plate welds.
2. On March 14th 2003, two large cracks were discovered in the webs of two steel girder on the I-895 Bridge over U.S. Route 1 and the Patapsco River in Elkridge, Maryland. The fracture originated at the top of the web-to-stiffener

weld. One crack propagated downward and diagonally, fractured the full height of the 90-inch web plate.

3. In 2009, fatigue cracking induced damages to the eye-bars of the existing San Francisco-Oakland Bay Bridge led to pieces of steel plummeting onto the roadway.

Figure 1.2 Typical Fatigue-induced Cracking

As can been seen, fatigue is a common failure model for steel bridges. About 80-90% of failures in steel structures are related to fatigue and fracture. (Banjara and Sasma, 2013) The passage of trucks across the steel highway bridge is the major cause of fatigue damage. The total number of truck passages in the 75-year life of a bridge could exceed 100 million. (AASHTO, Guide Specifications for Fatigue Evaluation of Existing Steel Bridges, 1990) Hence, fatigue design or evaluation, considering the most frequent load effect expected to occur, needs more attention in highway bridge design and evaluation.

1.2 Objectives

With the aging of existing steel highway bridges and the accumulated stress cycles under traffic loading, fatigue assessment for continuing service has become important for decisions making on the structure maintenance, component replacement, and other major retrofits. Given the uncertainties of the complicated traffic loading and

the complexity of the bridge structure, fatigue evaluation based on filed measurements under actual traffic flow is recommend by many researchers. However, there are still some difficulties in filed measurements. For example, some highway bridges is not accessible for field tests; the maintenance of monitoring system is difficulty, especially for long-term monitoring; and some highway bridges will not be considered for field tests under economic concerns. As the quality and quantity of the available long-term monitoring traffic data and information have improved, a set of methodologies has been developed to obtain a more realistic vehicular live load. The knowledge of actual traffic loading may reduce the uncertainty involved in the evaluation of the load-carrying capacity, estimation of the rate of deterioration, and prediction of remaining fatigue life.

The objectives of this research are to realistically simulate the fatigue behavior of steel highway bridges under current or future truck loading, taking advantage of the available long-term monitoring traffic data and information, and to better understand the fatigue mechanism and eventually prevent the fatigue damage of steel highway bridges. The proposed methodology could be used as a tool directing the experimental designs and instrumentation plans before performing experiments on laboratory or on site, accompanying a monitoring system program to obtain the fatigue reliability levels associated with the fatigue sensitive bridge details that were not monitored, and predicating the fatigue behavior of highway bridges under the continuous increased future traffic volume.

1.3 Organization

Based on the proposed research objectives, this study has been summarized into seven chapters.

Chapter 2 presents a detailed literature review on the current practice of fatigue design and evaluation criteria, especially on the fatigue load model. The current fatigue load model is insufficient for the actual loading, and the actual fatigue damage is often underestimated or overestimated by the code-specified fatigue truck. This chapter also provides a comprehensive review of the recent efforts on the subject of fatigue behavior simulations.

Compared with the methods of mainstream, the traffic load pattern is rarely considered in many studies, even the weigh-in-motion data is employed in the simulation. Usually, traffic load pattern was treated in multiple-presence statistics trucks as a function of traffic volume.

Chapter 3 proposes a probability-based full velocity difference model to realistically simulate the traffic loading of highway bridges, taking advantage of the available long-term monitoring traffic data and weigh station measurements on site. A simple span composite steel I-girder bridge is numerically studied with the proposed methodology. The traffic flow on the bridge with three traffic lanes is simulated by TSIS-CORSIM, a microscopic traffic simulation software as well, in order to evaluate the performance of the proposed microscopic simulation method – probability-based velocity difference model.

The three-dimensional global and local finite element model of the I-270 Bridge over Middlebrook Road are presented in Chapter 4 by two software. The efficient mesh size of elements is determined by the convergence test. The verification of the model is carried out with the help of the measured bridge model characteristics and standard vehicular live load analyses.

Chapter 5 focuses on conducting the time-history analysis of highway bridges under simulated truck loading. The single span composite steel I-girder bridge with inverted K-type bracing system is numerically studied. The simulated responses such as displacements and stresses of the bridge are examined. Later, the preliminary field test and the long-term monitoring test of the studied bridge are also introduced. Based on the field measurements, simulated numerical results are validated. Meanwhile, the vehicle-bridge interaction and the cause of fatigue cracks are discussed.

After obtaining the time-history result of stress at the welded connection from Chapter 5, the total fatigue life for this detail can be calculated as a function of stress range and number of cycles in Chapter 6. The widely used rainflow counting algorithm when determining the live load-induced stress range is introduced. The Miner's rule is then applied for an equivalent stress range representing the actual variable-amplitude cyclic loading. Case study is carried out in the last.

Chapter 7 summarizes findings and conclusions of this study. Furthermore, to complete this dissertation, this chapter states the on-going tasks for future work.

Chapter 2 Literature Review of Fatigue Design and Evaluation for Highway Bridges

2.1 Introduction

Generally speaking, fatigue of highway bridges can be categorized into two main types: load-induced fatigue and distortion-induced fatigue. Load-induced fatigue is due to the in-plane stresses in the steel plates. Distortion-induced fatigue is caused by secondary stresses in the steel plates (out-of-plane distortion). Usually, these in-plane stresses can be obtained easily by traditional calculation during bridge design and evaluation. On the contrary, the calculation of these out-of-plan stresses needs very refined methods of analyses. And, they cannot be calculated by the typical bridge design and evaluation procedures. In this study, only load-induced fatigue is discussed.

The results of several NCHRP reports, conducted by Dr. John Fisher in 1970s, confirm that for welded details, fatigue life is primarily a function of stress range, detail category, and the number of applied cycles. Therefore, each code, guide or handbook published after gives procedures for calculating the stress range at a detail, and the remaining cycles for this stress range.

This chapter provides background information regarding fatigue design and evaluation criteria, and reviews related studies over the past decades on the fatigue behavior simulation of highway bridges, especially the fatigue load modeling.

2.2 Code and Specifications

2.2.1 Fatigue Design

For load-induced fatigue considerations, each detail shall satisfy the design criteria:

$$\gamma(\Delta f) \leq (\Delta F)_n \qquad \text{Equation 2-1}$$

where, γ is the load factor for the fatigue load combination, Δf is the live load stress range due to the passage of the fatigue load, and $(\Delta F)_n$ is the nominal fatigue resistance.

The components of bridges are grouped into eight common detailed categories due to the construction detailing in *AASHTO LRFD Bridge Design Specifications (2013)*.The specific value of constant *A*, threshold$(\Delta F)_{th}$, and potential crack initiation point are provided for each type of detailed category. If the maximum stress range experienced by a detail is less than the constant-amplitude fatigue threshold, the fatigue life of this detail could be considered as theoretically infinite. If the maximum stress range exceeds the constant-amplitude fatigue threshold, the fatigue resistance and the finite life of the detail, in terms of cycles, could be determined by these equations:

$$(\Delta F)_n = (\frac{A}{N})^{\frac{1}{3}} \qquad \text{Equation 2-2}$$

$$N = (365)(75)n(ADTT)_{SL} \qquad \text{Equation 2-3}$$

where, *n* is the number of stress range cycles per truck passage, and $(ADTT)_{SL}$ is the single-lane *ADTT*. The fatigue design life has been considered to be 75 years in the Specifications. The following graphic in Figure 2.1 could represent the relationship

between the nominal fatigue resistance and the number of cycles according to the detailed category.

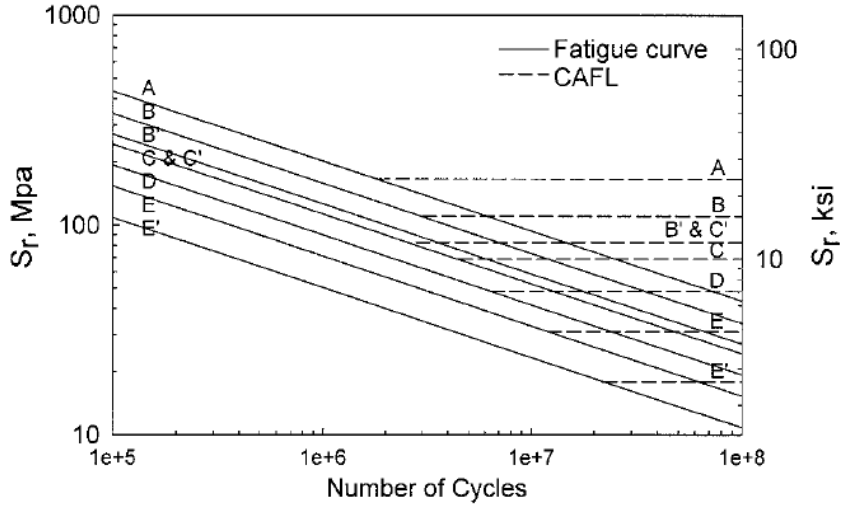

Figure 2.1Stress Range versus Number of Cycles (*AASHTO LRFD Bridge Design Specifications, 2013*)

2.2.2 Fatigue Evaluation

The procedure suggested by Section 7*"Fatigue Evaluation of Steel Bridges" in (AASHTO, Manual for Bridge Evaluation, 2010)* is to calculate the effective stress range through filed measurement while the bridge is under normal traffic, or to accurately determine the live load-induced stress range by analytical calculation.

$$(\Delta f)_{eff} = R_s \Delta f \qquad \text{Equation 2-4}$$

where, R_s is the stress-range estimate partial load factor, and Δf is the measured effective stress range, or 75 percent of the calculated stress range due to the passage of the fatigue truck.

Compared with analytical methods, field test is the most accurate method since no assumptions is needed for uncertainties in load distribution such as unintended composite action between structural components, contribution of nonstructural members, stiffness of

various connections, and behavior of concrete deck in tension. The actual strain histories experienced by bridge components are directly measured by strain gages at the areas of concern. The effects of varying vehicle weights and their random combinations in multiple lanes are also reflected in the measured strains.

After getting the nominal stress range, two levels of fatigue life evaluation would be checked. The first step is the infinite-life check. If satisfying the requirement below, the remaining fatigue life is taken as infinite.

$$(\Delta f)_{max} \leq (\Delta F)_{TH} \qquad \text{Equation 2-5}$$

where, $(\Delta f)_{max}$ is the maximum stress range due to the passage of the fatigue load, and $(\Delta F)_{TH}$ is the constant-amplitude fatigue threshold.

Only bridge details which fail the infinite-life check are subject to the further fatigue calculations, and calculate the remaining life for them using the following equation:

$$Y = \frac{R_R A}{365 n (ADTT)_{SL} ((\Delta f)_{eff})^3} \qquad \text{Equation 2-6}$$

where, Y is the total fatigue life in years, R_R is the resistance factor, A is the detail-category constant, n is the number of stress range cycles per truck passage, and $(ADTT)_{SL}$ is the single-lane *ADTT*.

Especially,

$$(ADTT)_{SL} = p \times ADTT \qquad \text{Equation 2-7}$$

ADTT is the number of trucks per day in one direction averaged over the design life, p is the fraction of trucks in the traffic, use 0.2 for rural interstate highways, 0.15 for other rural highways and urban interstate highway and 0.1 for other urban highways. Figure

2.2 could be used to estimate the average number of trucks per day in a single lane averaged over the fatigue life.

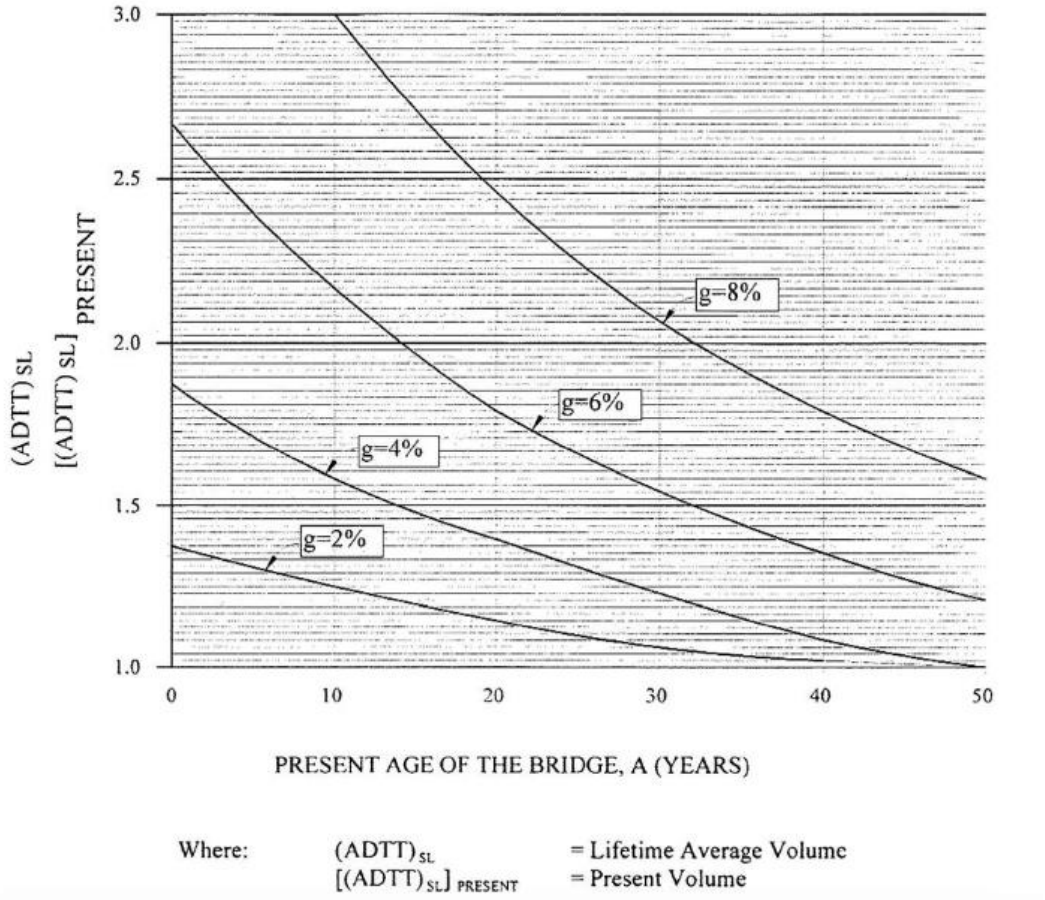

Figure 2.2 Lifetime Average Truck Volume for an Existing Bridge

2.2.3 Fatigue Load Model

The existing methodologies have been classified into three groups:

- the adjustment of static portion in early studies with the help of weigh station measurements or weigh-in-motion system;
- the proposed multi-freedom complicated truck models considering the dynamic effects of vehicle bridge interaction;
- traffic load pattern simulations using statistical projections approach and traffic flow simulation methods in order to generate traffic loading.

2.2.3.1 Magnitude and Configuration

The HL-93, designated as the vehicular live load in the *AASHTO LRFD Bridge Design Specifications (2013),* is defined as a combination of the design truck (HS20) or design tandem and the design land load. The weights and spacing of axles for the HS20 is specified in Figure 2.3, with a varied spacing between the two 32.0-kip axles for generating the most sever load effect. The design lane load of 0.64 klf uniformly distributed in the longitudinal direction with a width of 10.0 ft. And, the fatigue load defined in the *AASHTO LRFD Bridge Design Specification* (*2013)* is only one design truck HS20 but with a constant spacing of 30.0 ft between the two 32.0-kip axles.

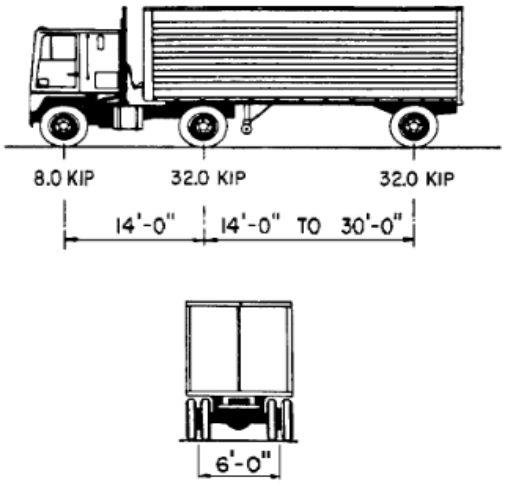

Figure 2.3 Design Truck (HS20) in the *AASHTO LRFD Bridge Design Specification (2013)*

"In the initial development of the notional live load model, no attempt was made to relate to escorted permit loads, illegal overloads, or short duration special permits. The moment and shear effects were subsequently compared to the results of truck weight studies (Csagoly and Knobel, 1981; Nowak, 1992), selected WIM data, and the 1991 OHBDC live load model. These subsequent comparisons showed that the notional load

could be scaled by appropriate load factors to be representative of these other load spectra." *AASHTO LRFD Bridge Design Specification (2013)* pointed out that the HL93 did not reflect all the load cases, and site-specific modification should be needed for some conditions. National Cooperative Highway Research Program published a report titled *Protocols for Collecting and Using Traffic Data in Bridge Design (2011)* also demonstrated that the designed vehicular live load was developed based on the truck magnitude and configuration from only one site in Ontario, Canada in the mid-1970s. Certainly, it cannot truly represent modern truck traffic conditions in the U.S., especially after almost 40-year's high-speed development in transportation.

To monitor and regulate the more and more larger and heavier trucks or commercial motor vehicles with goods traveling at highway speeds for long distances, technologies and facilities have been used to guarantee the safety of public transportation. And, this also provides realistic truck flow information and makes it possible for further studies on the more explicit vehicular live load modeling and more realistic behavior simulation of highway bridges under traffic loading. Traditionally, weigh stations are installed along a highway to inspect vehicular weights. A weigh station is a checkpoint equipped with truck scales. Trucks and commercial vehicle are subject to passing the scales at a very low speed, and they are allowed to return to the highway after necessary inspections. The measurements could be taken as static portion of live load. It was argued that weigh stations method cannot capture the true truckloads because the driver's manner has been disturbed, and some overweight trucks will chose other unmonitored route to avoid inspection intentionally. A more unbiased method has been developed in recent years. Weigh-in-motion (WIM) method is designed to capture and record axle

weights, gross weights, vehicle speeds and axle spacing as drives passing over a measurement site without knowledge. This makes the weighing process more efficient and realistic.

The weigh station measurements and weigh-in-motion data have been applied in many studies to assess current bridge design live loads, to model new design live loads, to develop new fatigue models, and assess existing models. *Guide Specifications for Fatigue Evaluation of Existing Steel Bridges* (1990) listed four ways to generate fatigue truck using the traffic data provided by the systems mentioned above:

1.

2. Evaluate the weight of the fatigue truck based on traffic survey data. (The procedure is given in NCHRP Report 299)

Comparing the results of fatigue evaluation using weigh station measurements /weigh-in-motion data and code-specified fatigue truck, several studies have found that the current load models are insufficient for the actual loading, and the actual fatigue damage is often underestimated or overestimated by the code-specified fatigue truck.

2.2.3.2 Frequency

Since the fatigue limit state is defined in terms of accumulated stress-range cycles, the frequency is another important component of fatigue loads. The frequency of the fatigue load is taken as the single-lane average daily truck traffic ($ADTT_{SL}$), despite the number difference carrying by different lanes.

$$ADTT_{SL} = p \times ADTT \qquad \text{Equation 2-8}$$

where, *ADTT* is the number of trucks per day in one direction averaged over the design life, same as the parameter discussed in section 2.2.2. Only the trucks on the shoulder lane were counted for fatigue evaluation.

In fact, ignoring trucks in other lanes can lead to an under-estimation of the real load, even though the shoulder lane carries most of the truck traffic under normal condition. Some studies shows that 70-90% of trucks use the shoulder lane when there are two lanes of traffic in each direction (Nowak, 1993). The truck percentage also varies by site. The frequency of fatigue load determined by the above method is only approximate estimation without the accurate traffic data.

2.3 Current Practice of Fatigue Behavior Simulation

2.3.1 Load Configuration

The live load of a bridge includes static and dynamic parts; the early research and studies focused on the static portion. Schilling (1984) and Raju et al (1990) suggested to improve the accuracy of the fatigue truck model by adjusting the fatigue truck axle weights in proportion to an equivalent total weight calculating from the specific site load distribution. The collected weigh station measurements, or data measured in stationary weight scales, were used by Nowak et al. (1993) to determine the truck-load spectra for highway bridges using on Highways I-75 and I-94. Later, Laman (1995) and Nowak (1996) developed a fatigue-load model from weigh station measurements and calculated the statistical parameters of stress for girder bridges. The results indicated that magnitude and frequency of truck load spectra are strongly site-specific and the live load stress spectra are strongly component-specific.

With the advent of weigh-in-motion (WIM) technology, the collection of large, representative samples of traffic load data has become more efficient and effective in late 1990s. Besides axle load information, a WIM system can also obtain information about speed, lane of operation, date and time of vehicle passage, and the number and spacing of axles. Furthermore, the average daily traffic (ADT) for a certain period of time, or the average annual daily traffic (AADT), can be calculated directly when a WIM system continuously counts and records all vehicles that pass through a WIM site.

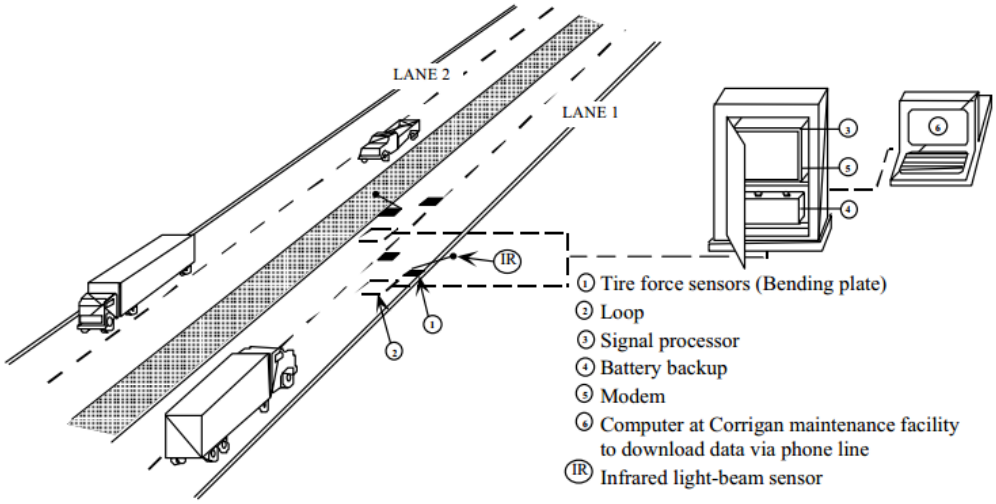

Figure 2.4 Layout of WIM System (Qu et al., 1997)

Miao and Chan (2002) developed a methodology by using 10 years of WIM data for deriving highway bridge live load models for short span bridges in Hong Kong. Based on the traffic data collected in Indiana, USA, Chotickai and Bowman (2006) proposed a three-axle fatigue truck to represent truck traffic on typical highways and a four-axle fatigue truck to represent truck traffic on heavy duty highways.

Protocols for Collecting and Using Traffic Data in Bridge Design (2011) developed a set of protocols and methodologies for using available national wide, state-

specific, or site-specific truck traffic data collected at different U.S. sites to obtain live-load models for LRFD superstructure design, fatigue design, deck design, and design for overload permits. The recommended protocols were summarized in 13 steps as follows:

Step 1. Define the type of traffic data and WIM sensor calibration for live load modeling;

Step 2. Select WIM sites for national, state-specific, route-specific, and site-specific data for bridge design;

Step 3. Decide the quantities of WIM data required for load modeling, for example one year's data, or one month's data;

Step 4. Ensure the data accuracy and reliability by WIM calibration and verification tests;

Step 5. Scrub the data and check the data quality;

Step 6. Generalize multiple-presence statistics for trucks as a function of traffic volume;

Step 7. Determine the one-lane load effects for superstructure design;

Step 8. Determine the two-lane load effects for superstructure design;

Step 9. Assemble axle load histograms for deck design as before, separate trucks into Strength I and Strength II;

Step 10. Filter WIM sensor errors/WIM scatter from WIM histograms;

Step 11. Accumulate fatigue damage and effective gross weight from WIM data;

Step 12. Determine Lifetime Maximum Load Effect L_{max} for superstructure design;

Step 13. Develop and calibrate vehicular load models for bridge design.

Both truck configuration and truck traffic flow pattern could be obtained with the help of WIM system. But, only truck configuration was considered in NCHRP Report 683 Method, and truck traffic flow pattern was treated in multiple-presence statistics trucks as a function of traffic volume. Besides, this method was highly dependent on the quality of WIM data.

An advanced traffic load model was developed based on weigh-in-motion data by Guo et al. (2012). This model took into account the uncertainties associated with the number of axles, axle weights, axle spacing and transversal position of vehicles. Combined with the traffic load model, a probabilistic finite element analysis approach was proposed to evaluate the time-dependent fatigue reliability levels of steel bridge details. The calculated results were in agreement with those obtained from monitored data.

Significant changes in vehicle loads have occurred in China due to the development of the automobile industry and transportation within the past two decades, particularly the rapid increase in traffic flow and the large-scale emergence of heavy trucks. However, the codes used in China are relatively old and there are no explicit formulations for calculating the fatigue of components with specific loading patterns, loading values, and fatigue stress amplitudes. Ten representative vehicle types were obtained from traffic flow data collected on an urban expressway in a logistics zone by Chen et al. (2014), using weigh-in-motion system, and the fatigue load spectrum was studied. Based on the axle weight and axle space of ten representative vehicle types, six equivalent vehicle models were established using the equivalent fatigue damage theory

and a simplified fatigue vehicle load spectrum was developed for urban expressway bridges.

2.3.2 Vehicle Bridge Interaction

Highway bridges are subjected to the dynamic forces imposed by moving vehicles. The corresponding dynamic effects result in deterioration of the bridges, consequently increasing the maintenance cost and decreasing the service life. It has important economical and safety implications and helps to make management decisions such as establishing permissible weight limits or issuing overload permits. To further study the dynamic impacts of multi-girder bridges, Wang et al. (1992) and Huang et al. (1993) developed a three-dimensional nonlinear truck model and applied on grillage bridge models.

Based on data collected by weigh-in-motion (WIM) measurements, Wang and Liu (2005) synthesized truck traffic by type and loading condition. Three-dimensional nonlinear models for the trucks with significant counts were developed from the measured data. Six simply supported multi-girder steel bridges with spans ranging from 35 ft to 140 ft were analyzed using the proposed method. Road surface roughness was generated as transversely correlated random processes using the autoregressive and moving average model. The dynamic impact factor was taken as the average of 20 simulations of good road roughness. Live-load spectra were obtained by combining static responses with the calculated impact factors. A case study of the normal traffic from a specific site on the interstate highway I-75 was illustrated. Static loading of the heaviest in each truck type was compared with that of the American Association of State Highway

and Transportation Officials standard design truck HS20-44. Several important trucks causing fatigue damage was found.

MacDougall et al. (2006) focused on the fatigue damage caused in steel bridge girders by the dynamic tire forces that occur during the crossing of heavy transport vehicles. This work quantified the difference in fatigue life of a short-span and a medium-span bridge due to successive passages of either a steel-sprung or an air-sprung vehicle. The bridges were modeled as beams to obtain their modal properties, and air-sprung and nonlinear steel-sprung vehicle models were used. Bridge responses were predicted using a convolution method by combining bridge modal properties with vehicle wheel forces. A linear elastic fracture mechanics model was employed to predict crack growth. For the short-span bridge, the steel-sprung vehicle caused fatigue failure up to 6.5 times faster than the air-sprung vehicle. For the medium-span bridge, the steel-sprung vehicle caused fatigue failure up to 277 times faster than the air-sprung vehicle. A two dimensional nonlinear vehicle simulation program NLVSP was developed and validated by extensive field tests Cole and Cebon (1992) to predict the tire forces of articulated vehicles with well-damped suspension modes, operating under typical conditions of speed and road roughness. Figure 2.5 illustrates the leaf-sprung vehicle model used in the NLVSP. It has a total of 11 degrees of freedom, and nonlinear suspension elements simulate leaf springs.

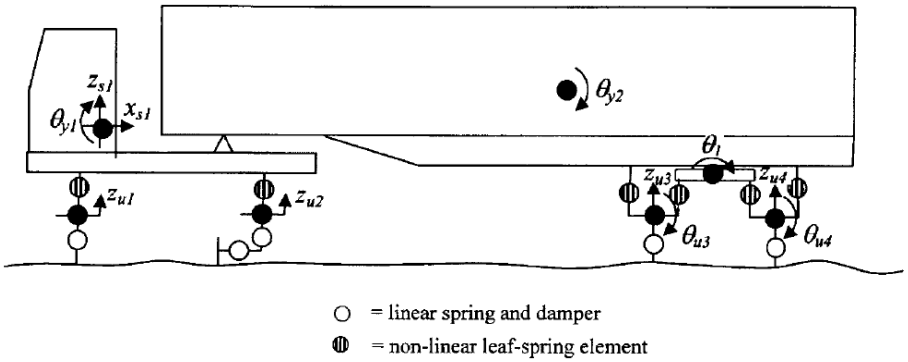

(a) Tractor and Trailer Vehicle Model with Leaf-Sprung Suspension

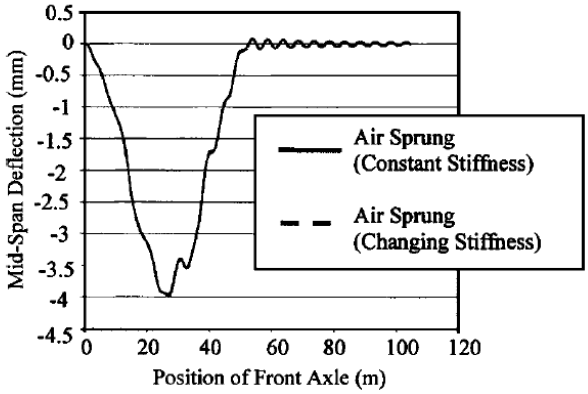

(b) Midspan deflection of Holowka's bridge due to air-spring vehicle

Figure 2.5 Dynamic Vehicle Load Modeling (MacDougall et al., 2006)

Chen and Cai (2007) claimed in the current AASHTO LRFD specifications, the fatigue design considers only one design truck per bridge with 15% dynamic allowance. While this empirical approach may be practical for regular short and medium span bridges, it may not be rational for long-span bridges e.g., span length 500 ft that may carry many heavy trucks simultaneously. Some existent studies suggested that fatigue may not control the design for many small and medium bridges. However, little research on the fatigue performance of long-span bridges subjected to both wind and traffic has been reported and if fatigue could become a dominant issue for such a long-span bridge design was still not clear. Regardless if the current fatigue design specifications were

sufficient or not, a real understanding of the traffic effects on bridge performance including fatigue was desirable since the one truck per bridge for fatigue design does not represent the actual traffic condition. As the first step toward the study of fatigue performance of long-span cable-stayed bridges under both busy traffic and wind, the equivalent dynamic wheel load approach was proposed in the this study to simplify the analysis procedure. Based on full interaction analyses of a single-vehicle–bridge–wind system, the dynamic wheel load of the vehicle acting on the bridge can be obtained for a given vehicle type, wind, and driving condition. As a result, the dimension of the coupled equations was independent of the number of vehicles, through which the analyses can be significantly simplified. Such simplification is the key step toward the future fatigue analysis of long-span bridges under a combined action of wind and actual traffic conditions.

2.3.3 Traffic Loading Simulation

In the early studies, it was commonly assumed that a certain percentage of the total weight was loaded on the front axle or rear axle for the magnitude and configuration. Further, there was no real traffic simulation considering the truck flow pattern. For bridge behavior simulations under truck loading, it was usually performed using the Monte Carlo method. Obviously, Monte Carlo method is only a statistical projections approach because of its generic nature, and does not considering any vehicle and driver behavior models to simulate truck traffic flow. In recent years, traffic flow simulation method has been applied to provide instantaneous information of individual vehicle by many researchers. Chen and Wu (2011) developed a general framework of modeling the live load from traffic for a long-span bridge by using the cellular

automation (CA) traffic flow simulation technique. A typical four-lane long-span bridge was studied using the proposed method. Each lane is divided into cells with an equal length of 7.5 m. Three conditions, the free flow, the moderate flow and busy flow, were considered in the simulation. A simple comparison between the simulated static traffic load and the AASHTO LRFD HL-93 design load was made. The results showed the HL-93 may be insufficient for busy flow condition.

2.4 Summary

In summary, this chapter presented a detailed literature review on the current practice of fatigue design and evaluation criteria, especially on the fatigue load model. The current fatigue load models are insufficient for the actual loading, and the actual fatigue damage is often underestimated or overestimated by the code-specified fatigue truck. This chapter also provided a comprehensive review of the recent efforts on the subject of fatigue behavior simulations and prediction of remaining fatigue life. The existing methodologies has been classified into three groups: the adjustment of static portion in early studies with the help of weigh station measurements and weigh-in-motion system, the proposed multi-freedom complicated truck models considering the dynamic effects of vehicle-bridge interaction, and the truck flow simulation using statistical projections approach and traffic flow simulation methods in order to generate traffic loading. Compared with the methods of mainstream, realistic traffic flow pattern was rarely considered in many studies, even the weigh-in-motion data were employed in the simulation. Usually, truck traffic flow pattern was treated in multiple-presence statistics trucks as a function of traffic volume.

Each individual passage causes one complex stress cycle that may include several peaks and valleys. The main stress variation is caused by the changing position of the truck, but small vibration stresses are superimposed on this main variation. The vibration stresses that are superimposed on the main stress variation have two effects: (1) they increase the maximum stress and the stress range of the complex cycle; and (2) they add wiggles which increase the equivalent number of cycles for a truck passage. A study of available experimental data shows that the second effect is small and normally can be neglected. The passage of two or more closely spaced trucks across a bridge produces one complex stress cycle. Depending on the truck spacing and bridge span, this single cycle may cause more or less fatigue damage than the two or more cycles that would have resulted if the same trucks had crossed individually.

As a result, the desired modeling process is probability-based microscopic traffic loading simulation, with the combination of both advantages.

Chapter 3 Microscopic Traffic Loading Simulation

3.1 Introduction

Since the fatigue behavior of steel highway bridges is controlled by passages of trucks across the bridge, the effectiveness of fatigue analyses is determined by the accuracy of the traffic load model and the structure model. The purpose of this chapter is to obtain an accurate traffic load model from weigh station measurements and the traffic flow simulation, which is capable of capturing realistic traffic flow on highway bridges, and can be employed as the simulated truck loading for finite element models during fatigue analyses.

In fact, there are two major components of the traffic loading. One is the loading magnitude and configuration, including axle weights and axle spacing. The other is the traffic load pattern, which refers to the way of truck passages, containing the vehicle speed, lane distribution, vehicle position, and headways. For example, trucks pass through a highway bridge one by one, side by side, or staggered. Section 3.2 and 3.3 introduce two main approach when simulating the traffic load pattern. The first one is Monte Carlo simulation, which consider the traffic load pattern as the frequency of the traffic loading according to assumed statistical probability distribution. The second approach is traffic flow simulations, which describe the vehicle movement on roadways.

The proposed probability-based full velocity difference model is the full velocity difference model together with the probabilistic models of loading configuration established, explained in Section 3.4. And the I-270 Bridge over Middlebrook Road is

taken as a case study in Section 3.5. The traffic loading of the I-270 Bridge over Middlebrook Road has been simulated by the proposed method as well as the traffic simulation commercial software.

3.2. Monte Carlo Simulation

Monte Carlo method has been widely used in regard to uncertainties arising from traffic load models. The original source of Monte Carlo method was from playing and recording results in a real gambling casino. It is a broad class of computational algorithms that rely on repeated random sampling to obtain numerical results. Typically, one runs simulations many times over in order to obtain the distribution of an unknown probabilistic entity, especially useful when it is difficult or impossible to obtain a closed-form expression, or unfeasible to apply a deterministic algorithm.

For fatigue analyses of highway bridges, Monte Carlo simulation is carried out in order to account for randomness of the traffic loading. The simulation procedure could be summarized in the following steps: (Boulent M. Lmam, Timothy D. Righiniotis, and Marios K. Chryssanthopoulos, 2008)

1. Obtain the static stress ranges from the deterministic analysis of the bridge under the passage of an individual vehicle;
2. Obtain a factor α sampled from the assumed probability distribution in order to account for randomness.
3. Multiply the static stress ranges from Step 1 with the factor α from Step 2. For each individual vehicle crossing, a different value of α will be applied. This process of calculating the deterministic stress ranges will be carried out *n* times, where *n* is the annual frequency of a certain vehicle type in any given

time period.

Since the frequency *n* of a certain vehicle type is taken to be random, the above process is repeated many times, in order to capture the uncertainty in the traffic loading.

3.3 Traffic Flow Simulation

As the quality and quantity of the available long-term monitoring traffic data and information has improved, a set of methodologies has been developed to obtain a more realistic vehicular live load. Originally, the traffic flow simulation is to offer a comprehensive model capable of capturing the complexity of the real traffic in the design and control of transportation systems. Since the simulation technique has gained rapid development during the past decades, it provides some useful tools to model the traffic loading for bridge engineers.

Generally speaking, there are two major types of traffic flow models: microscopic and macroscopic. The former one describes the traffic behavior based on discrete time and space. The results, emerging from discrete entities interacting with each other, can provide detailed time variant information of individual trucks and passenger cars. On the contrary, macroscopic models are concerned with describing the aggregate behavior of the whole traffic low in a large scale. The microscopic traffic flow simulation is more suitable for simulating the traffic loading, since the detailed information of each vehicle can be obtained by this method.

For the microscopic traffic flow simulation, many models and methodologies have been proposed to describe the behavior of realistic traffic flow, liked the cellular automation-based simulation mention, full velocity difference model, and comprehensive traffic simulation software.

3.3.1 Cellular Automation

Cellular automaton (CA), a microscopic scale traffic flow simulation model, can generate probabilistic traffic information by simulating individual vehicle's behavior. The CA model is able to provide detailed instantaneous information of each vehicle through replicating major traffic phenomena on highways. Thus it becomes an ideal technology to be integrated into the advanced bridge analysis considering live load in a more accurate manner (Suren Chen and Jun Wu, 2011). The cellular automation adopted the following assumptions:

1. Both time and space are discrete, and each lane is divided into cells with an equal length, as described in Figure 3.1.
2. Each cell can be empty or occupied by at most one vehicle at a time.
3. The velocity of a vehicle is decided by the number of cells a vehicle can move in one time step.

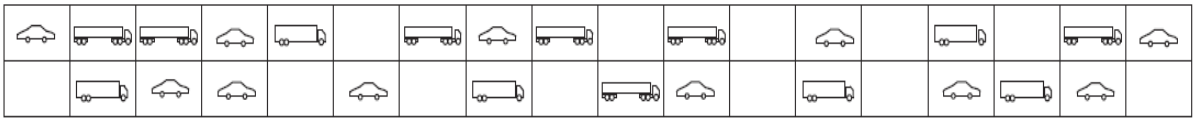

Figure 3.1 CA Traffic Model (Suren Chen and Jun Wu, 2010)

3.3.2 Full Velocity Difference Model

The full velocity difference model was developed based on the classical car-following model, which introduced the relationships among position, velocity and acceleration for a linear system from Kinematics. The classical model of car-following is described as

$$\frac{dv_{n+1}}{dt}(t+\Delta t) = \lambda \Delta v \quad \text{Equation 3-1}$$

$$\Delta v = v_n(t) - v_{n+1}(t) \quad \text{Equation 3-2}$$

$$\lambda = \begin{cases} a: s \le s_c \\ b: s > s_c \end{cases} \quad \text{Equation 3-3}$$

$$s = x_n(t) - x_{n+1}(t) \quad \text{Equation 3-4}$$

where, the *(n+1)*th car is following the *n*th car in a single traffic lane; $v_n(t)$ and $v_{n+1}(t)$ are the velocities of these two cars; Δt is the time lag of response; λ is the sensitivity; *s* is the headway; $x_n(t)$ and $x_{n+1}(t)$ are the positions of these cars; *a*, *b*, and s_c are constants.

However, the car-following behavior not only depends on the velocity difference but also relates to the driver's behavior. In 1995, Bando et al, presented the optimal velocity model from the psychology perspective. In this model, the author assumed that the driver had an optimal velocity objective, and would try to maintain this speed during the car-following process.

$$\frac{dv_{n+1}}{dt}(t) = \kappa[V(s) - v_{n+1}(t)] \quad \text{Equation 3-5}$$

where, κ and $V(s)$ are the sensitivity constant and the optimal velocity that the driver prefer. Then, Helbing and Tilch carried out a calibration of the optimal velocity model, and adopted the optimal velocity as

$$V(s) = V_1 + V_2 \tanh[C_1(s - l_c) - C_2] \quad \text{Equation 3-6}$$

where, the length of the vehicle was considers as parameter lc. V_1, V_2, C_1, and C_2, are constants.

Taking advantage of both the classical car-following and the optimal velocity model, Rui Jiang et al proposed a full velocity difference model. In this model, both the

optimal velocity and the velocity difference contribute to the acceleration of the following vehicle.

$$\frac{dv_{n+1}}{dt}(t) = \kappa[V(s) - v_{n+1}(t)] + \lambda\Delta v \qquad \text{Equation 3-7}$$

Comparing with the cellular automation simulation model, the full velocity difference model is more suitable for short or medium-span highway bridges. Since the span length of these highway bridges is relatively short, the car-following behavior is the primary behavior of traffic flow in contrast with lane-changing behavior. Another reason is the difference between the total length of one truck with the total length of one passage car cannot be ignored. The space of one vehicle occupied will determine the capacity of single traffic lane of the highway bridge.

3.3.3 Traffic Simulation Software TSIS-CORSIM

Besides the two traffic flow simulation models mentioned above, there are several well-developed commercial traffic simulation software. TSIS-CORSIM is a comprehensive microscopic traffic simulation, applicable to surface streets, freeways, and integrated networks with a complete selection of control devices (i.e., stop/yield sign, traffic signals, and ramp metering). It simulates traffic and traffic control systems using commonly accepted vehicle and driver behavior models. CORSIM combines two of the most widely used traffic simulation models, NETSIM for surface streets, and FRESIM for freeways. Considering the computational efficiency and accuracy, CORSIM has advantage over cellular automation simulation model. In this study, traffic simulation by CORSIM was employed for model validation of the proposed method.

3.4 Probability-based Full Velocity Difference Model

Combining the existing traffic monitoring data and weigh station measurements for truck regulation, the traffic loading on highway bridges could be determined by the probability based full velocity difference model. The weigh station measurements are used to generate the load configuration and magnitude based on the probability analysis, and the existing traffic monitoring data is used to simulate the traffic load pattern by the full velocity difference model. The probability-based full velocity difference model was developed in the MATLAB environment. The analysis flow is shown in Figure 3.2, and was performed in the following procedure:

1. According to the collected weigh station measurements, trucks crossing the bridge could be classified into several types according to the number of axles. Axle weights and axle spacing of each truck type were represented in terms of random variables, which follow an empirical probability distributions, and each variable was represented by a variable designation consisting of letters and numbers. (Truck classification)

An empirical distribution is a distribution generated from the observed data themselves. It could happen that the measured or monitoring data cannot be fitted by a theoretical distribution. In the circumstances, the empirical distribution is used to describe the probability distribution of random variables.

2. The relationship of axle weights and axle spacing of each truck type has been studied in order to determine the generated random number for each variable. Some variables had a strong correlation. Others were not. In this study, 0.8 is defined as the dividing line. Greater than it, it is assumed that the relationship between these two

variables is so strong that one variable may be determined by the other. Otherwise, they could be treated as independent variables, and the correlations between these axle weights and axle spacing could be neglected to simplify the analysis. (Variable correlation)

3. The real time monitoring traffic flow data of one year was been gathered, studied and summarized in one typical weekday data. One typical weekday could be divided to several time periods according to the different traffic flow per hour. The total vehicle number, truck percentage, lane distribution of truck traffic were provided. (Traffic flow data)

4. Before starting the simulation, a uniformly distributed variable *T* is defined regarding the vehicle type, and *m* numbers are generated in the value domain of [0, 1], which are used in *m* times to simulate *m* vehicles crossing the bridge in a certain time period. In each time, the vehicle type is determined by the value of *T*. For instance, if *T*< *the percentage of vehicle type 1*, the generated vehicle will be determined as *type 1*; if *the percentage of vehicle type 1*< *T*< *the percentage of vehicle type 2*, the generated vehicle will be determined as *type 2*, etc.

5. A uniformly distributed variable *L* is defined to determine the lane in which the vehicle travels. Similar to *T*, m numbers are generated in the value domain of [0, 1], and the value of *L* determines the transversal position of the vehicle loads. For instance, if the generated vehicle will be determined as type 1 and *L* < *the percentage of lane 1*, the vehicle should be applied in the first lane; if *the percentage of lane 1*< *L* < *the percentage of lane 2*, the vehicle should be applied in the second lane; etc.

6. After setting the vehicle type and lane occupancy, the last step before simulation is to define the magnitude and configuration. *x* random numbers are generated for each variable of axle weights and axle spacing, according to their PDFs. And the correlations between axle weights and axle spacing are considered during the analysis. For example, if the axle weight 1 and axle weight 2 has a correlation greater than 0.8, the axle weight 2 will be defined when the axle weight 1 has been generated. If axle weight 1 and axle weight 2 has a correlation less than 0.8, the correlations between these axle weights are neglected, and the random numbers are generated for each axle weights respectively.

5. The full velocity difference model was applied in MATLAB environment to simulate the car-following behavior of all vehicles passing through the studied bridge. The vehicle type, the transversal position of vehicle loads, axle loads and the axle spacing of the vehicle determined in the above three steps become the input of the simulation network.

6. The results of the simulation will provide the magnitude and configuration of vehicles, the speed of vehicles passing through the site, and the position of vehicle loads at every simulation time step.

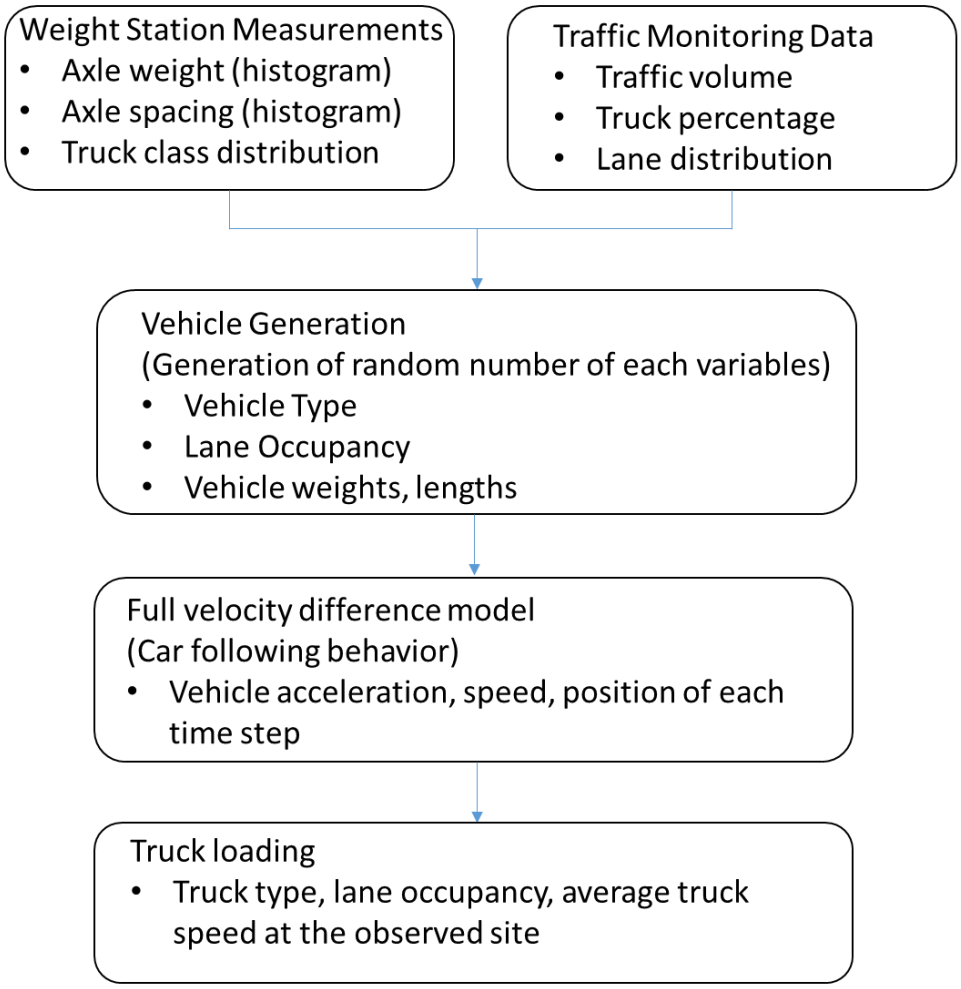

Figure 3.2 Analysis Flowchart

3.5 Case Study of I-270 Bridge over Middlebrook Road

3.5.1 Bridge Location

MD Bridge No.15042 is a simple-span composite steel I-girder bridge with a span length of 140 ft, located at I-270 over Middlebrook Road near Germantown, Maryland. The bridge is comprised of two structures for the northbound (NB) and southbound (SB) roadways respectively, separated at the centerline. It carries three traffic lanes in the south and four traffic lanes in the north with equal lane width of 12 ft.

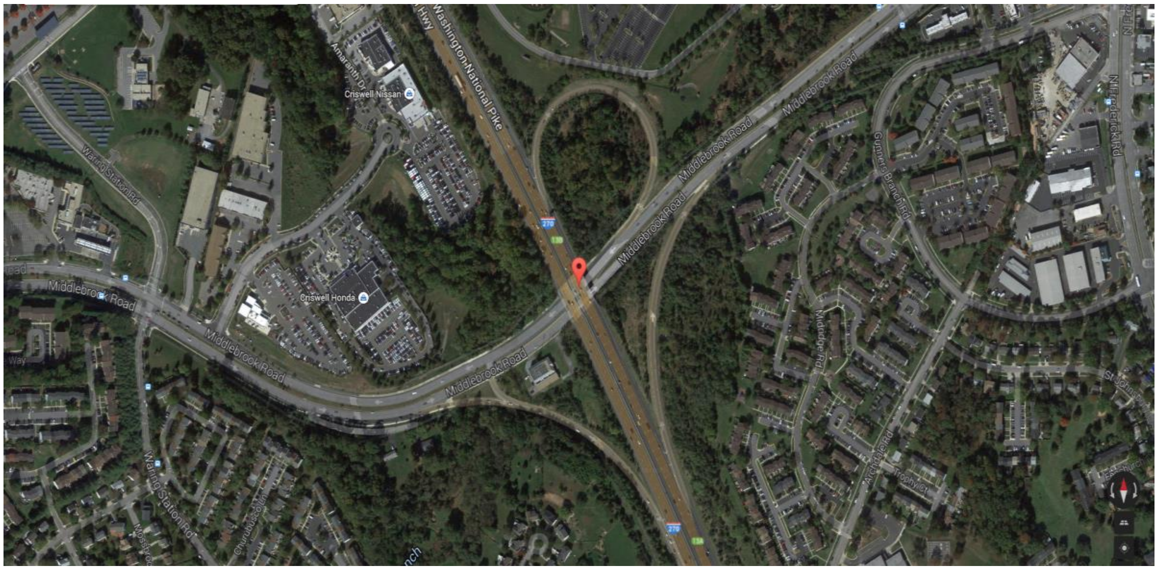

Figure 3.3 Location of I-270 Bridge over Middlebrook Road

(a)Plan View (b) Elevation View

Figure 3.4 Photo view (a), (b) of I-270 Bridge over Middlebrook Road

3.5.2 Traffic Data Collection

From the presentation of *Maryland State Highway Administration (MD SHA) Bridge Management System (Roby, 2010)*, there are 2500+ bridges owned by MD SHA, and 2500+ non MD SHA owned bridges. Therefore, the total number of bridge in Maryland is over 5000 by 2010. However, from the report *Protocols for Collecting and Using Traffic Data in Bridge Design (2011)*, there is only one WIM site in Maryland

covering one traffic lane. Obviously, the data from this site cannot capture all the truck information for every bridge in Maryland.

From Traffic Monitoring System Program (2010), published by Highway Information Services Division, Maryland State Highway Administration, the Traffic Monitoring System program has been responsible for the collection, processing, analysis, and management of Maryland highway traffic data since 1997. Maryland's Traffic Monitoring Program includes 79 permanent continuous Automatic Traffic Recorders (ATRs) counting traffic continuously throughout the year, and over 3,800 short term (48 hour) program count locations throughout the state, taken during the week on either Tuesday and Wednesday or Wednesday and Thursday to reflect typical weekday travel patterns.

Comparing these two different data sources in Maryland, Traffic Monitoring System Program has an advantage over WIM motion. Traffic Monitoring System Program covers almost the entire area of Maryland and monitors most of the arterials, freeways, and interstate. Apparently, using traffic data from the Traffic Monitoring System Program to generate truck loading in Maryland is more accessible and reliable.

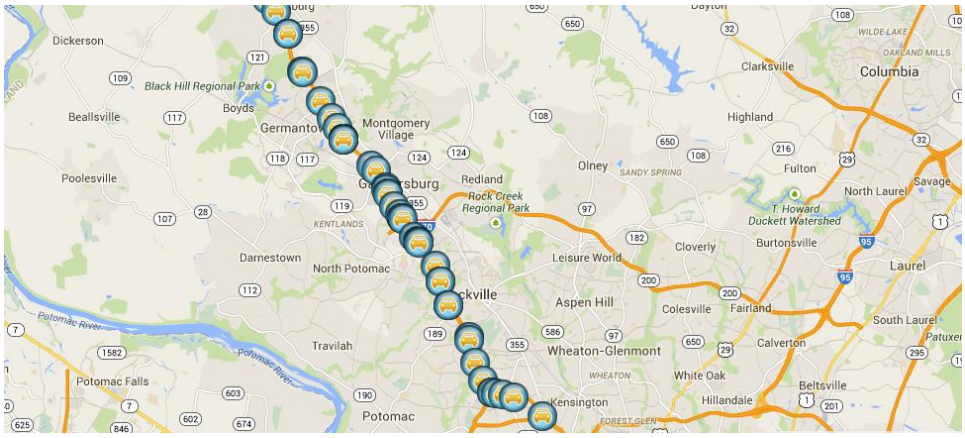

Figure 3.5 Observation points on I-270 in Montgomery County

Besides, Maryland currently has thirteen fixed commercial motor vehicles weigh and inspection stations with permanent static scales. Six of these stations are located on Interstate highways, and the remaining seven are located on Maryland and U.S. highway routes. Some of these fixed weigh and inspection stations are operational in both directions. These stations provide adequate data source for magnitude and configuration of truck loading.

3.5.2.1 Weigh Station Measurements

The Hyattstown Weigh and Inspection Station is located approximately 10 miles north of I-270 Bridge over Middlebrook Road, along Interstate 270 (I-270). It was built and is owned by the Maryland State Department of Transportation State Highway Administration (MDOT/SHA).

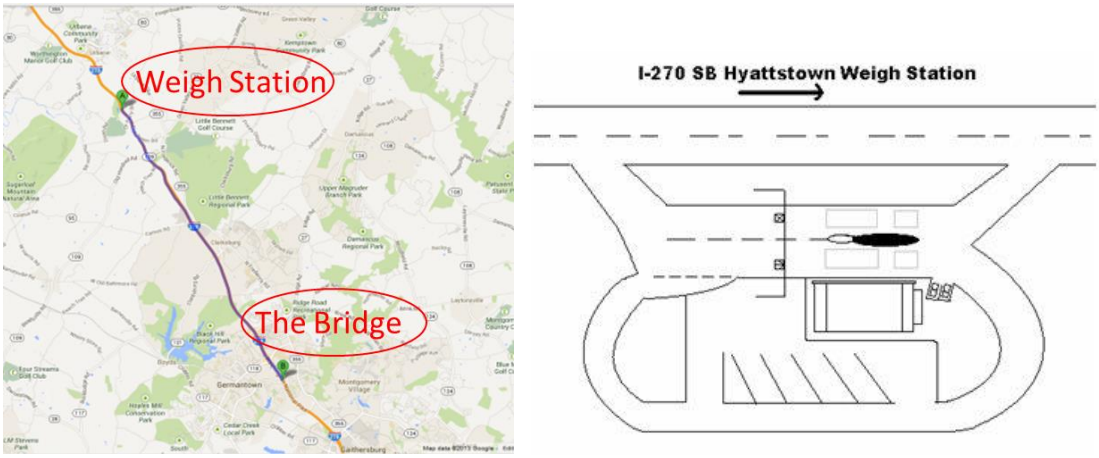

Figure 3.6 The Hyattstown Weigh Station Location and configuration

The Maryland State Police Commercial Vehicle Enforcement Division (MSP/CVED) is responsible for operating the site. The primary features of the Hyattstown Weigh Station include the scale house, static scales, and inspection pit. The static scales are located near the end of the ramp directly in front of the scale house. This inspection pit is located in the large parking lot behind the static scales and scale house.

A schematic layout of the facility is shown in Figure 3.6.The southbound facilities were operated using computers and other equipment housed in the static scales during all of the baseline data collection activities.

2200 samples during one year were chosen as the database to generate the truck information. The measured data were filtered before the statistical analysis were made, five (5) samples were deleted. All the trucks were cataloged into seven (7) classes based the number of axles (Figure 3.7). Obviously, 2-axle trucks and 5-axle trucks were in the majority, and took percentage of 24.87 and 67.99, respectively. The 3-axle trucks, 4-axle trucks and the heaviest 6-axle trucks and over accounted for 1.61%, 2.98% and 2.55%, respectively. And they only took percentage of 7.14 in total.

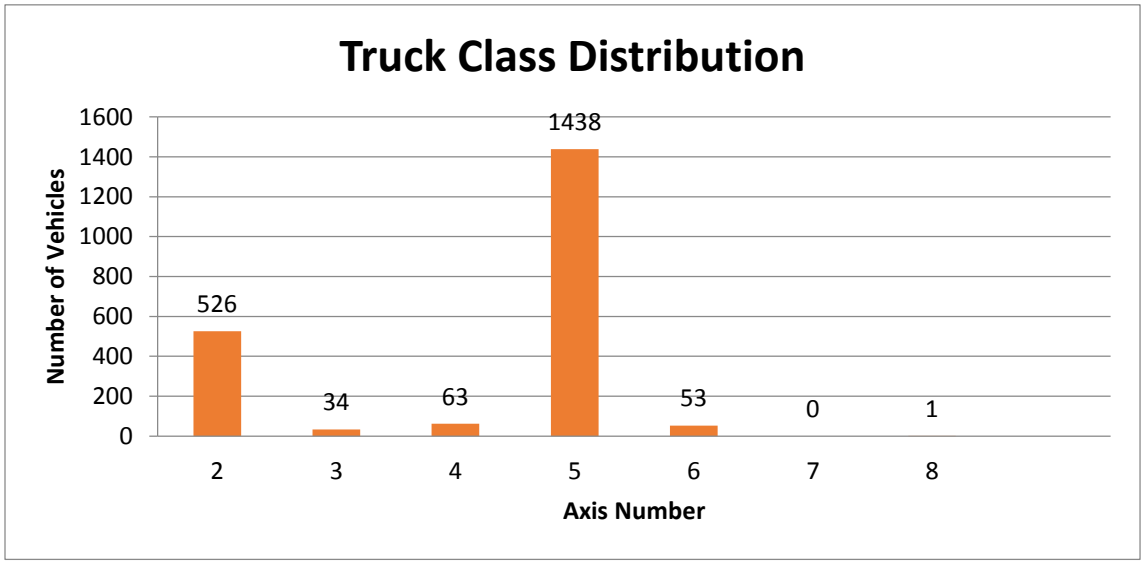

Figure 3.7 Truck Class Distribution

3.5.2.2 Traffic Flow Data

The Internet Traffic Monitoring System (I-TMS), operated by Maryland State Highway Administration, provides access to detailed traffic count data. Similar to annual average daily truck (AADT) Locator, I-TMS also has Address Search and Route Search options wherein the user can filter for the required locations. The tool then displays the

locations in the results tab. The user can select an individual location to view reports (class, volume, lane distribution, etc.) Based on the hourly traffic volume, one typical day was divided into four different time periods: midnight, early morning and night, morning peak hour, and noon to evening, shown in the Table 3-1 below. And the durations for these four time period are five (5) hours, five (5) hours, five (5) hours, nine (9) hours, correspondingly. The average hourly volume varied from 505 to 4215, and the truck percentage also varied from 10.39 to 20.10. Lane distribution of I-270 Bridge over Middlebrook Road is shown in Table 3-2. The main purpose of this time division is to realistically simulate the major characteristics of the traffic flow for each time period.

Table 3-1 Time Period

Time Period	Time	Average Total Volume (per hour)	Passenger Car	Truck					Truck Percentage
				2-Axle	3-Axle	4-Axle	5-Axle	6-Axle	
1. Midnight	23:00-24:00 0:00-3:00 (5 hours)	505	403	25	2	3	69	3	20.10%
2. Early Morning & Night	4:00-5:00 19:00-23:00 (5 hours)	1934	1712	55	4	7	150	6	11.40%
3.Moring Peak	5:00-10:00 (5 hours)	4215	3759	113	7	14	310	12	10.82%
4. Noon to Evening	10:00-19:00 (9 hours)	3021	2707	78	5	9	213	8	10.39%

Table 3-2 Lane Distribution of One Typical Day

Vehicle Type	Left Lane	Middle Lane	Right Lane
Total (Passage Car and Truck)	31.87%	30.62%	37.51%
Truck	1.45%	44.84%	53.71%

3.5.3 Probability-based Full Velocity Difference Model

3.5.3.1 Correlation of axle weights and axle spacing

Table 3-3 Schematic Diagram

Vehicle Type	Truck Configurations	Variable
2-axle	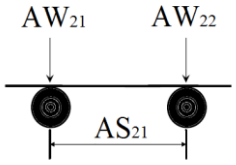	AW_{21} AW_{22} AS_{21}
3-axle	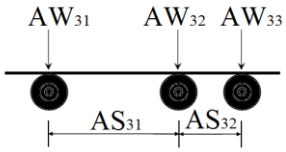	AW_{31} AW_{32} AW_{33} AS_{31} AS_{32}
4-axle	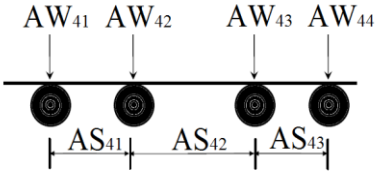	AW_{41} AW_{42} AW_{43} AW_{44} AS_{41} AS_{42} AS_{43}
5-axle	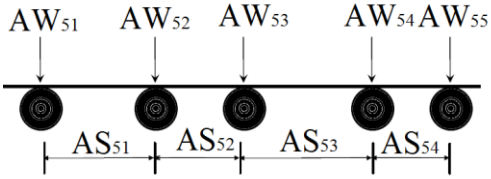	AW_{51} AW_{52} AW_{53} AW_{54} AW_{55} AS_{51} AS_{52} AS_{53} AS_{54}

6-axle	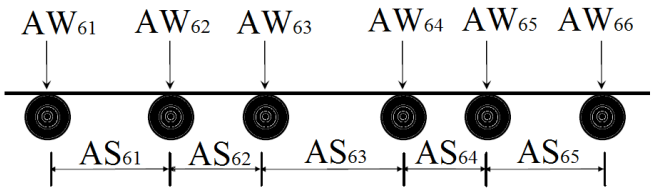	AW61 AW62 AW63 AW64 AW65 AW66 AS61 AS62 AS63 AS64 AS65

Axle weights and axle spacing of each vehicle type were represented in terms of random variables, which follow certain probability distributions, and each variable in Table 3.3 is represented by a variable designation consisting of four letters and numbers. The first two letters “AW” and “AP” represent “axle weight” and “axle spacing”, respectively. The first digit following the two letters represents the type of vehicles (the number of axle), and the second digit denotes the serial number of the axle weight or the axle spacing.

Table 3-4 Correlation between Axle Weight and Axle Spacing of 2-Axle Truck

	AW_{21}	AW_{22}	AS_{21}
AW_{21}	1	0.946099	0.937138
AW_{22}	0.946099	1	0.916605
AS_{21}	0.937138	0.916605	1

Table 3-5 Correlation between Axle Weight and Axle Spacing of 3-Axle Truck

	AW31	AW32	AW33	AS31	AS32
AW31	1	0.31584	0.522189	0.373476	-0.40691
AW32	0.31584	1	0.842602	0.123877	0.270663
AW33	0.522189	0.842602	1	0.165804	-0.00936
AS31	0.373476	0.123877	0.165804	1	-0.59633
AS32	-0.40691	0.270663	-0.00936	-0.59633	1

Table 3-6 Correlation between Axle Weight and Axle Spacing Of 4-Axle Truck

	AW_{41}	AW_{42}	AW_{43}	AW_{44}	AS_{41}	AS_{42}	AS_{43}
AW_{41}	1	0.43316	0.831297	0.810507	0.32113	-0.43735	-0.05542
AW_{42}	0.43316	1	0.254649	0.256759	0.329698	0.131624	-0.07658
AW_{43}	0.831297	0.254649	1	0.981835	0.107333	-0.65552	-0.09954
AW_{44}	0.810507	0.256759	0.981835	1	0.131666	-0.67778	-0.01997
AS_{41}	0.32113	0.329698	0.107333	0.131666	1	-0.1916	0.284203
AS_{42}	-0.43735	0.131624	-0.65552	-0.67778	-0.1916	1	-0.13314
AS_{43}	-0.05542	-0.07658	-0.09954	-0.01997	0.284203	-0.13314	1

Table 3-7 Correlation between Axle Weight and Axle Spacing of 5-Axle Truck

	AW51	AW52	AW53	AW54	AW55	AS51	AS52	AS53	AS54
AW51	1	0.333782	0.357301	0.292537	0.294484	0.376357	-0.13998	0.179732	-0.14324
AW52	0.333782	1	0.973951	0.844237	0.844549	0.038626	0.083291	0.04935	0.089767
AW53	0.357301	0.973951	1	0.858239	0.854743	0.077744	-0.04454	0.133813	0.001559
AW54	0.292537	0.844237	0.858239	1	0.973042	0.08592	-0.04221	0.074877	0.076426
AS51	0.294484	0.844549	0.854743	0.973042	1	0.079632	-0.07043	0.110853	0.040574
AS52	0.376357	0.038626	0.077744	0.08592	0.079632	1	-0.15665	0.159391	-0.03326
AS53	-0.13998	0.083291	-0.04454	-0.04221	-0.07043	-0.15665	1	-0.74235	0.677787
AS54	0.179732	0.04935	0.133813	0.074877	0.110853	0.159391	-0.74235	1	-0.73204
AS55	-0.14324	0.089767	0.001559	0.076426	0.040574	-0.03326	0.677787	-0.73204	1

Table 3-8 Correlation between Axle Weight and Axle Spacing of 6-Axle Truck

	AW61	AW62	AW63	AW64	AW65	AW66	AS61	AS62	AS63	AS64	AS65
AW61	1	0.033866	0.081027	-0.23213	0.494108	0.54817	0.266537	-0.55651	-0.29876	-0.34338	-0.50136
AW62	0.033866	1	0.917806	0.346707	0.17858	0.230484	0.396535	0.459944	0.773229	-0.36938	-0.39438
AW63	0.081027	0.917806	1	0.459465	0.354502	0.402092	0.397757	0.230639	0.597779	-0.06677	-0.46974
AW64	-0.23213	0.346707	0.459465	1	0.520469	0.467473	-0.06734	0.211694	0.043736	0.449869	0.343592
AW65	0.494108	0.17858	0.354502	0.520469	1	0.941108	0.153847	-0.48241	-0.39915	0.168179	-0.13609
AW66	0.54817	0.230484	0.402092	0.467473	0.941108	1	0.153536	-0.47102	-0.33296	0.098325	-0.24542
AS61	0.266537	0.396535	0.397757	-0.06734	0.153847	0.153536	1	0.148067	0.377068	-0.20922	-0.28047
AS62	-0.55651	0.459944	0.230639	0.211694	-0.48241	-0.47102	0.148067	1	0.775222	-0.21238	0.347188
AS63	-0.29876	0.773229	0.597779	0.043736	-0.39915	-0.33296	0.377068	0.775222	1	-0.43455	-0.23045
AS64	-0.34338	-0.36938	-0.06677	0.449869	0.168179	0.098325	-0.20922	-0.21238	-0.43455	1	0.403921
AS65	-0.50136	-0.39438	-0.46974	0.343592	-0.13609	-0.24542	-0.28047	0.347188	-0.23045	0.403921	1

The relationship of axle weights and axle spacing of each truck type has been studied in order to determine the generated random number for each variable. In this study, 0.8 is defined as the dividing line. Greater than 0.8, it is assumed that the relationship between these two variables is so strong that one variable may be determined by the other. Otherwise, they could be treated as independent variables, and the correlations between these axle weights and axle spacing could be neglected to simplify the analysis. As can be seen in Table 4.5 to 4.9, for 2-axle trucks, the correlations between AW_{21}, AW_{22} and AS_{21} are very strong and cannot be neglected. For 3-axle trucks, only AW_{32} and AW_{33} have a strong correlation. Other variables could be treated as independent variables. For 4-axle trucks, it is observed that axle weight 3 and axle weight 4 correlated with axle weight 1. And, there is a tight connection between those two variables. For 5-axle trucks, AW_{53}, AW_{54} and AW_{55} are linked closely with AW_{51}, and AW_{53}, AW_{54} and AW_{55} interrelate with each other. For 6-axle trucks, only the relationship between AW_{62} and AW_{63} and the relationship between AW_{65} and AW_{66} need to be considered.

3.5.3.2 Histograms of Axle Weights and Axle Spacing

Figures 3.8 to 3.12 show the probability densities of axle weights and axle spacing for each type of trucks. Unlike it was observed by other studies (Tong Guo, Dan M. Frangopol, Yuwen Chen, 2012), the variables cannot be described by normal or lognormal probability density functions (PDFs). The variables of this location cannot fit in these two probability density functions. This verified the site-specific nature of traffic loading. Hence, random numbers are generated for each variable of axle weights and axle spacing according to their own PDFs, during the simulation.

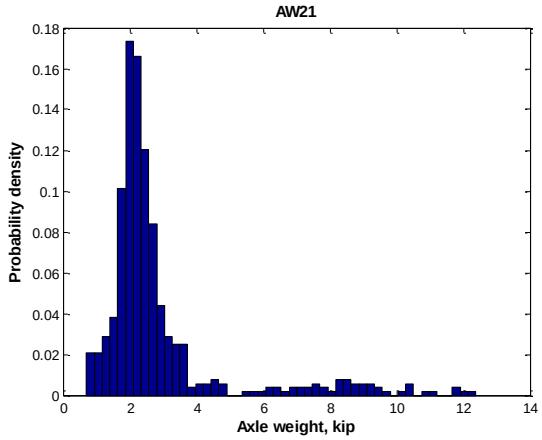

(a) Axle Weight 1 of 2-Axle Truck

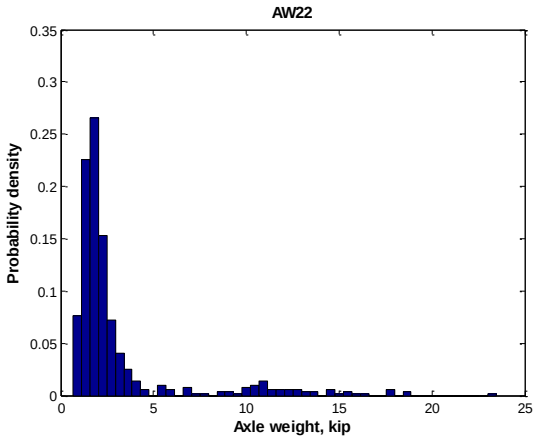

(b) Axle Weight 2 of 2-Axle Truck

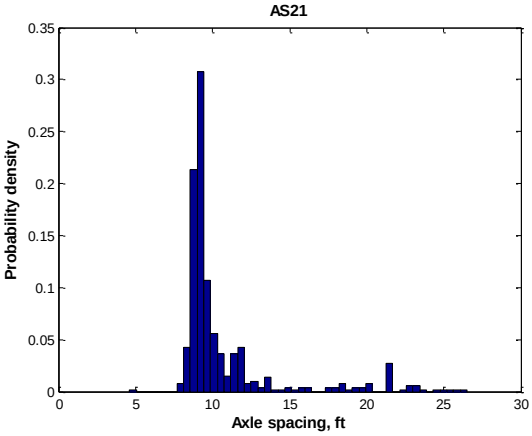

(c) Axle Spacing of 2-Axle Truck

Figure 3.8 Probability Densities of Axle Weights and Axle Spacing for 2-Axle Truck

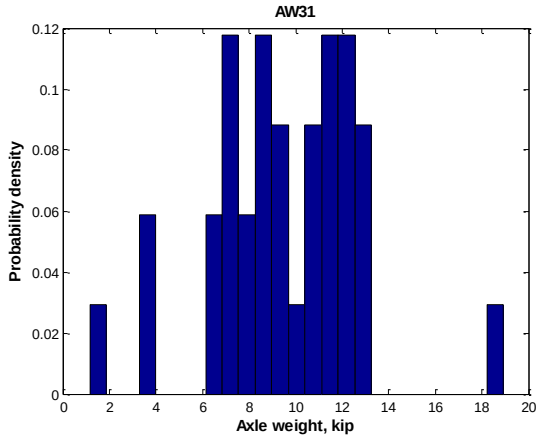

(a) Axle Weight 1 of 3-Axle Truck

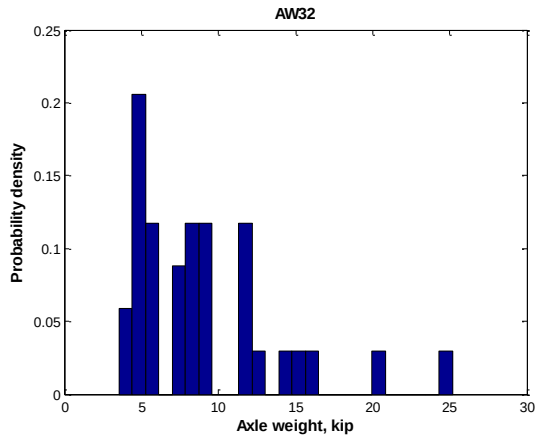

(b) Axle Weight 2 of 3-Axle Truck

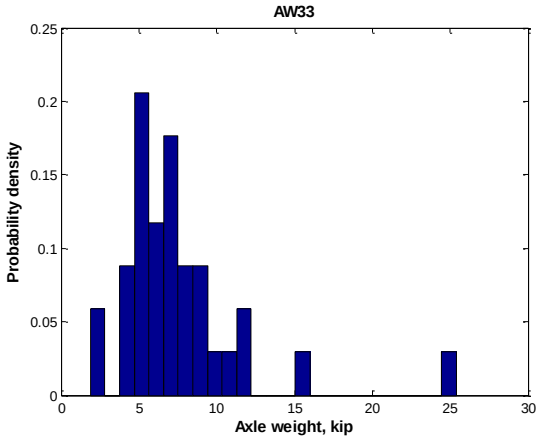

(c) Axle Weight 3 of 3-Axle Truck

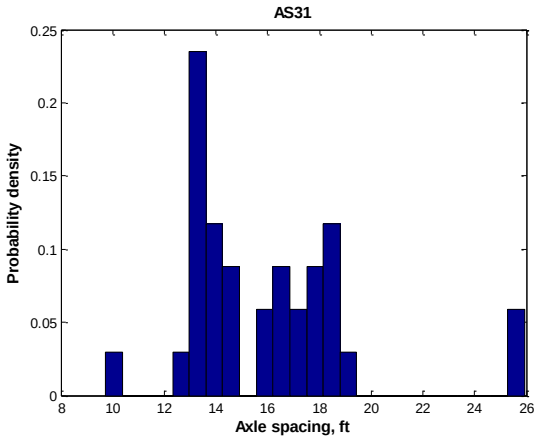

(d) Axle Spacing 1 of 3-Axle Truck

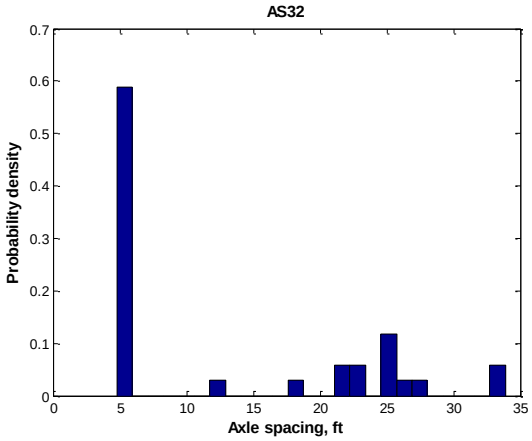

(e) Axle Spacing 2 of 3-Axle Truck

Figure 3.9 Probability Densities of Axle Weights and Axle Spacing for 3-Axle Truck

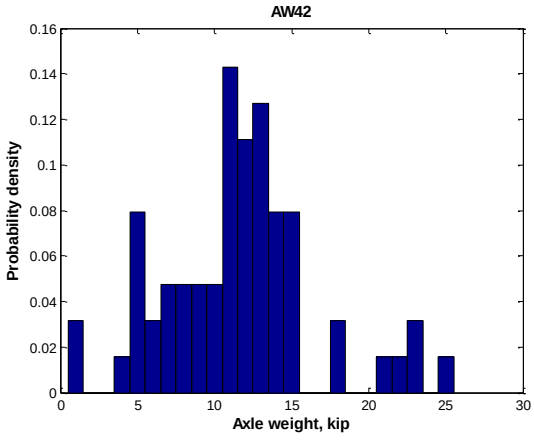

(a) Axle Weight 1 of 4-Axle Truck

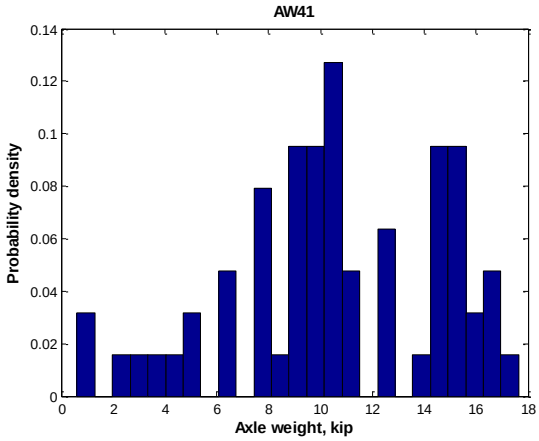

(b) Axle Weight 2 of 4-Axle Truck

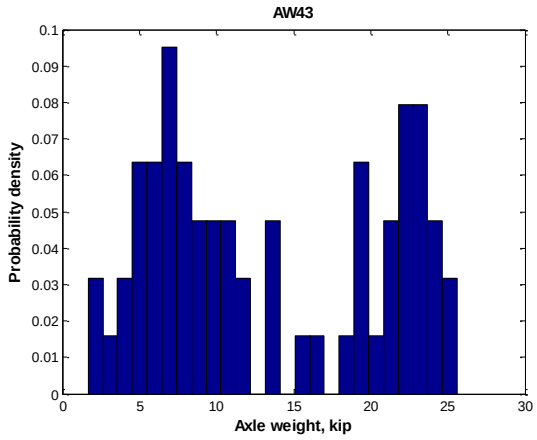

(c) Axle Weight 3 of 4-Axle Truck

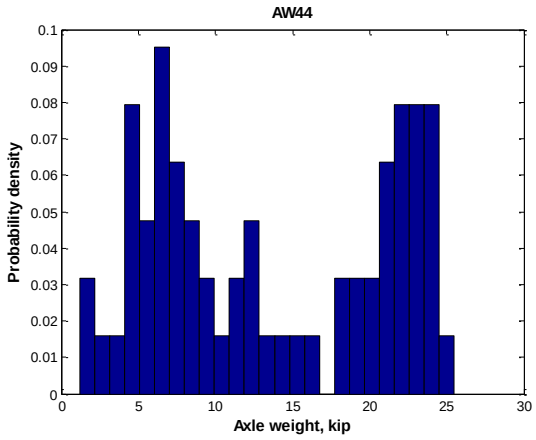

(d) Axle Weight 4 of 4-Axle Truck

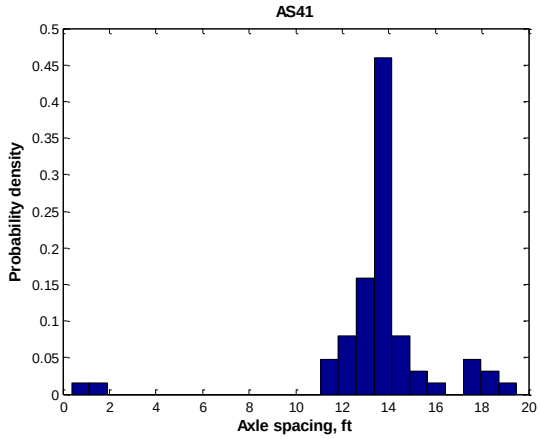

(e) Axle Spacing 1 of 4-Axle Truck

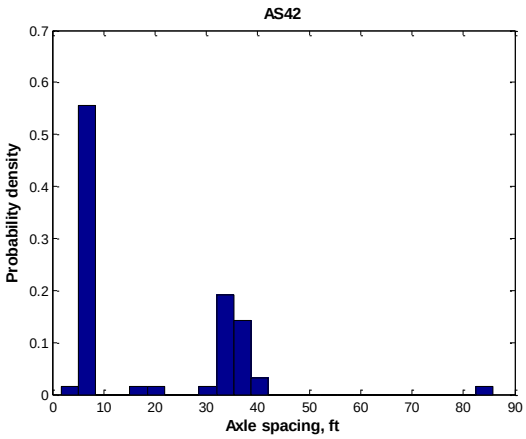

(f) Axle Spacing 2 of 4-Axle Truck

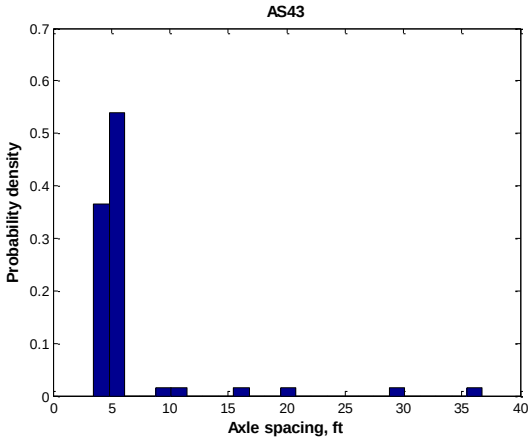

(g) Axle Spacing 3 of 4-Axle Truck

Figure 3.10 Probability Densities of Axle Weights and Axle Spacing for 4-Axle Truck

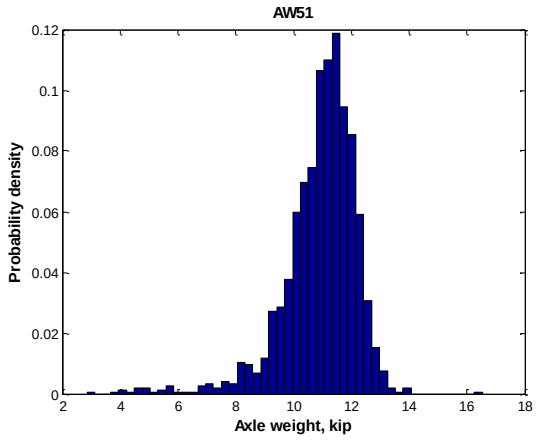

(a) Axle Weight 1 of 5-Axle Truck

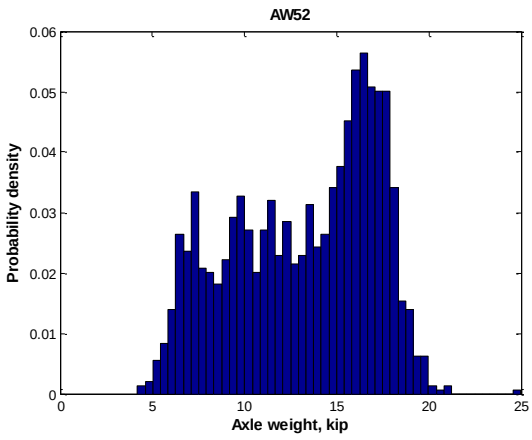

(b) Axle Weight 2 of 5-Axle Truck

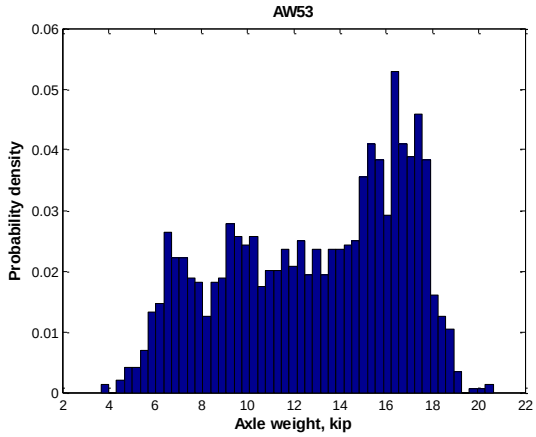

(c) Axle Weight 3 of 5-Axle Truck

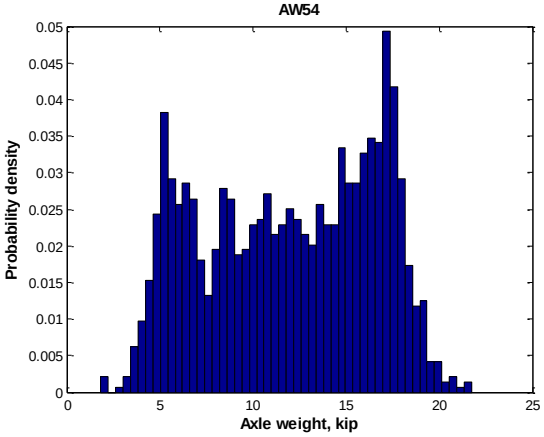

(d) Axle Weight 4 of 5-Axle Truck

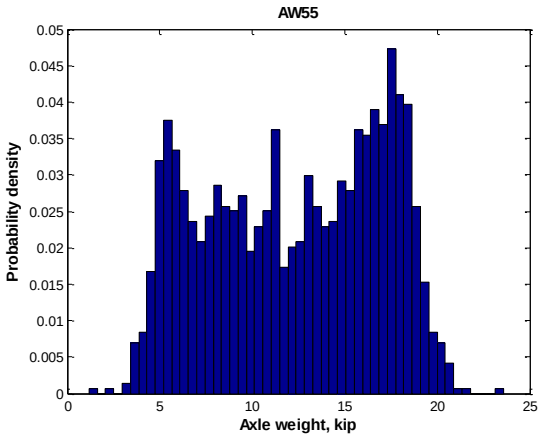

(e) Axle Weight 5 of 5-Axle Truck

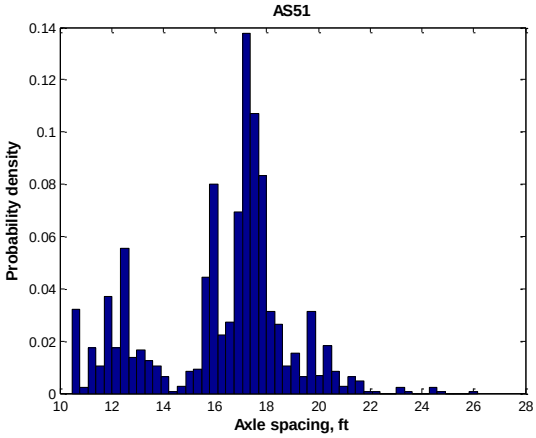

(f) Axle Spacing 1 of 5-Axle Truck

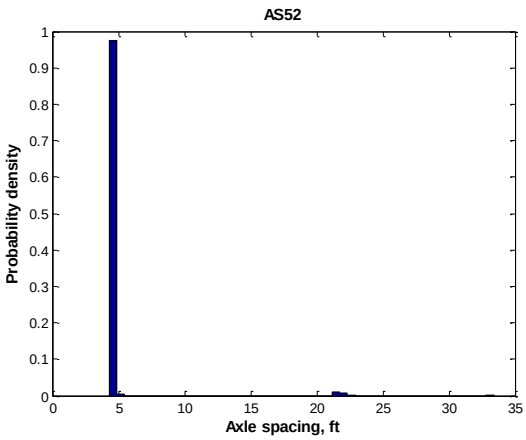

(g) Axle Spacing 2 of 5-Axle Truck

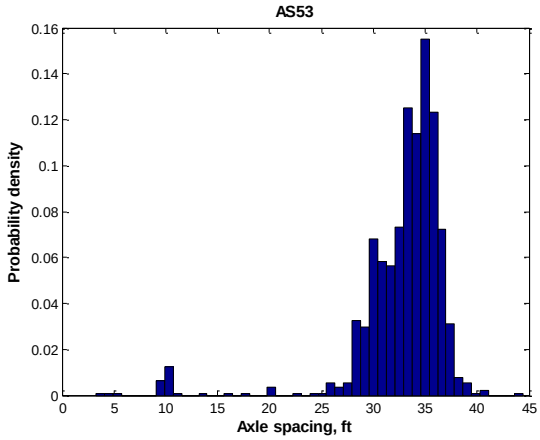

(h) Axle Spacing 3 of 5-Axle Truck

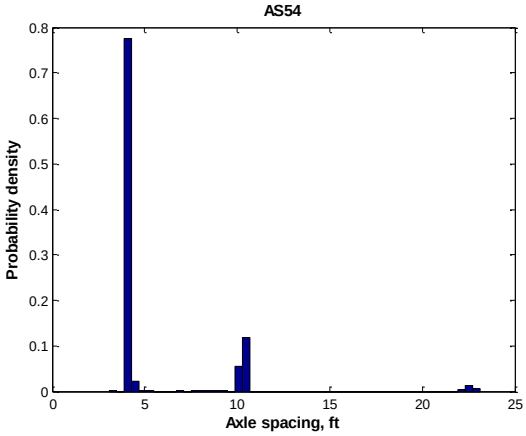

(i) Axle Spacing 4 of 5-Axle Truck

Figure 3.11 Probability Densities of Axle Weights and Axle Spacing for 5-Axle Truck

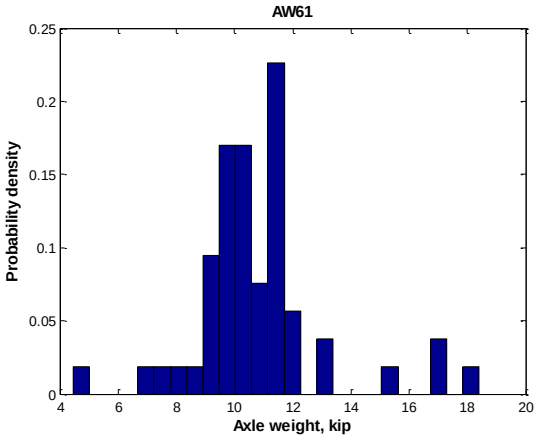

(a) Axle Weight 1 of 6-Axle Truck

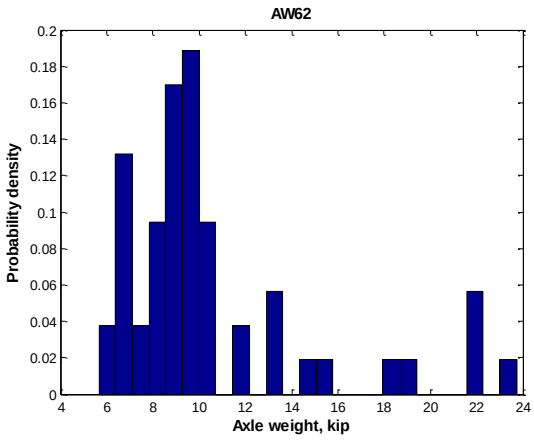

(b) Axle Weight 2 of 6-Axle Truck

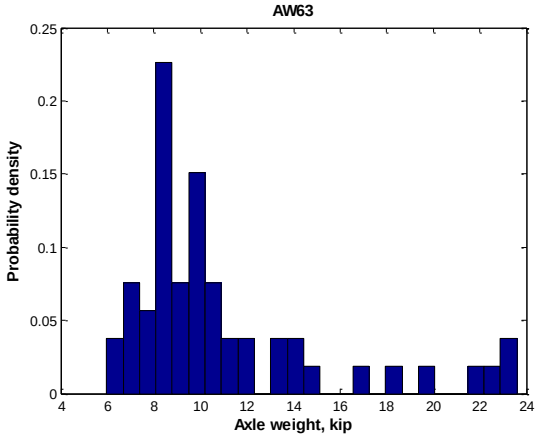

(c) Axle Weight 3 of 6-Axle Truck

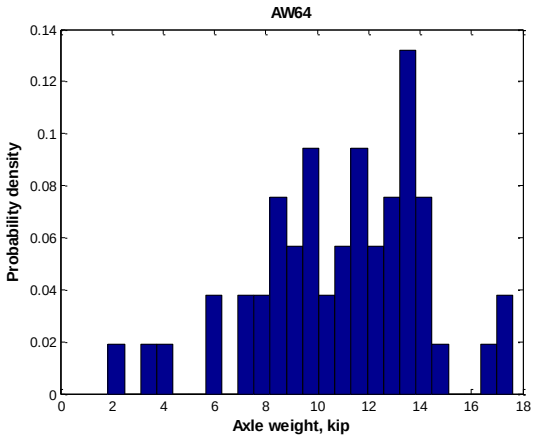

(d) Axle Weight 4 of 6-Axle Truck

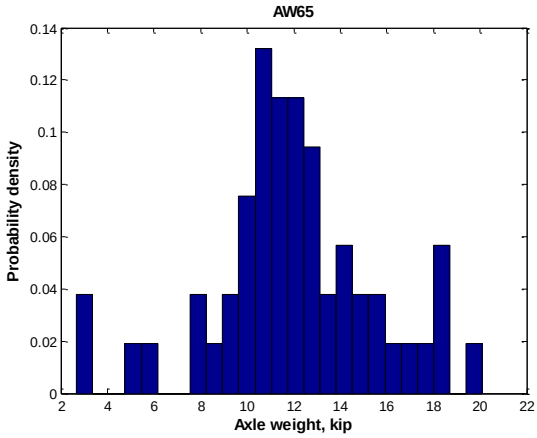

(e) Axle Weight 5 of 6-Axle Truck

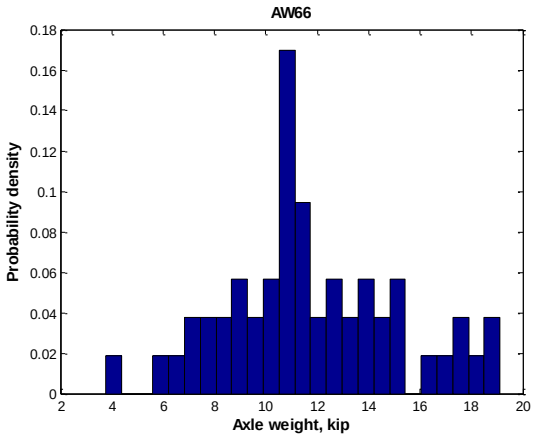

(f) Axle Weight 6 of 6-Axle Truck

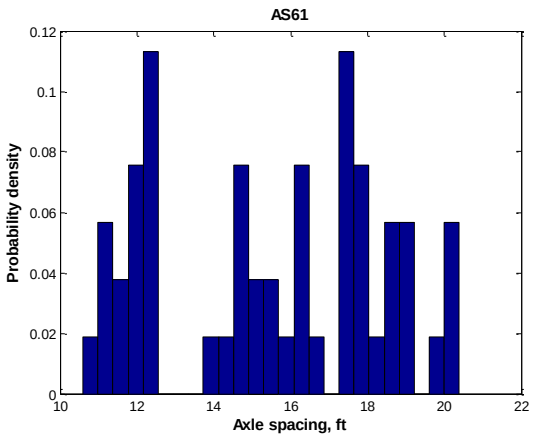

(g) Axle Spacing 1 of 6-Axle Truck

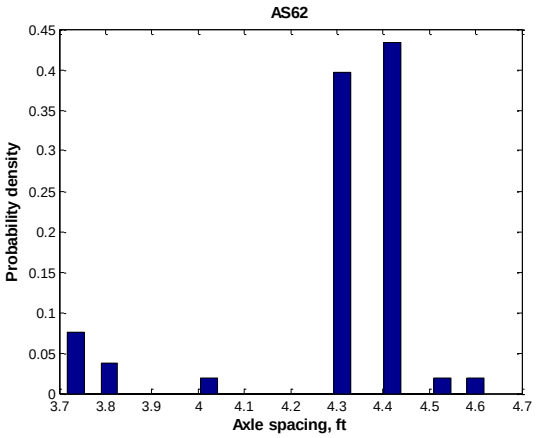

(h) Axle Spacing 2 of 6-Axle Truck

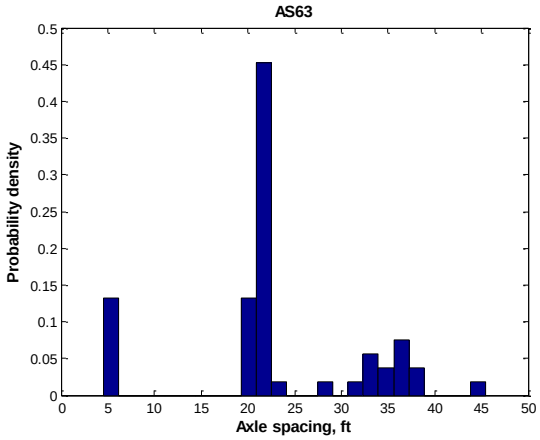

(i) Axle Spacing 3 of 6-Axle Truck

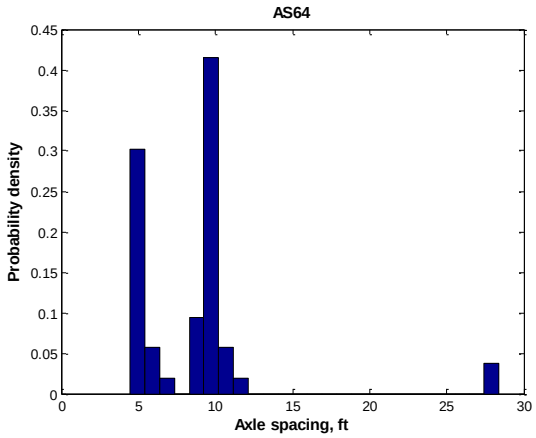

(j) Axle Spacing 4 of 6-Axle Truck

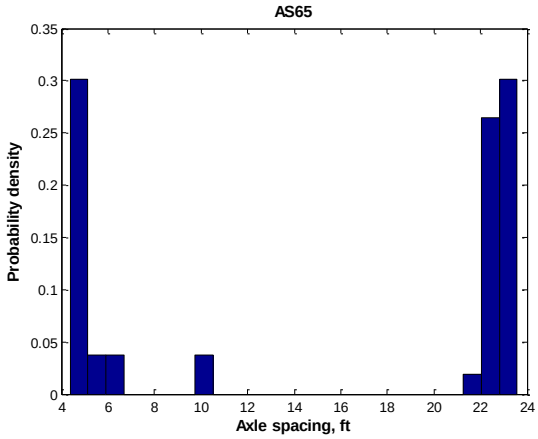

(k) Axle Spacing 5 of 6-Axle Truck

Figure 3.12 Probability Densities of Axle Weights and Axle Spacing for 6-Axle Truck

3.5.3.3 Traffic Simulation by Probability based Full Velocity Difference Model

Following the procedure describe in Section 3.4, the MATLAB code of traffic simulation can be found in Appendix B.

3.5.4 Traffic Simulation using CROSIM

3.5.4.1 Three Main Types of Fatigue Trucks

Following the specifications of *Guild Specifications for fatigue evaluation of existing steel bridges* (1989), through weigh station measurements at Hyattstown Weigh Station to obtain a gross-weights histogram for the truck traffic and calculate the gross

weight of the fatigue truck. Because of the limitation of the traffic simulation software CORSIM, only three different types of trucks can be defined during traffic simulation: the small truck, the medium truck, and the large truck. Since 2-axle trucks and 5-axle trucks were in the majority, the small truck consisted of 2-axle trucks and 3-axle trucks, and the medium truck consisted of 4-axle trucks and 5-axle trucks. For safety consideration, the heaviest 6-axle trucks and over were also been considered as the third main type, although it only takes a very small percentage.

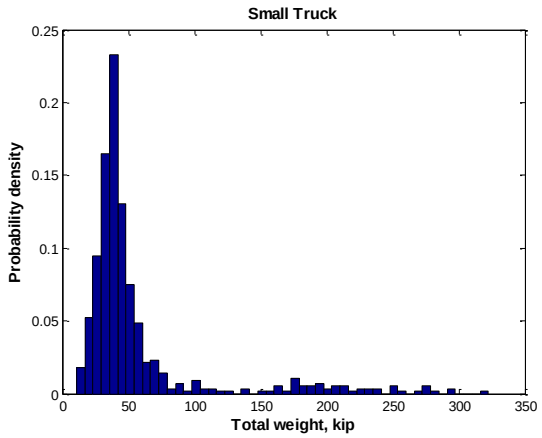

(a) Small Truck

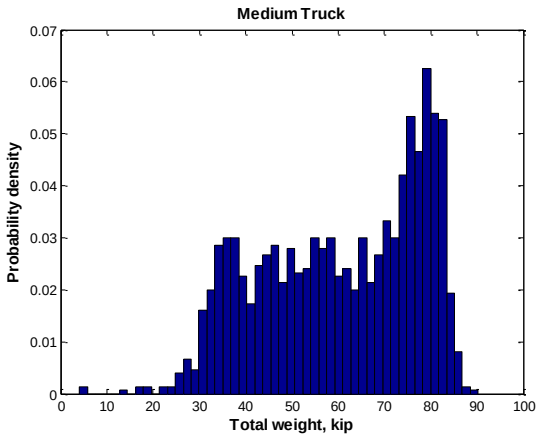

(b) Medium Truck

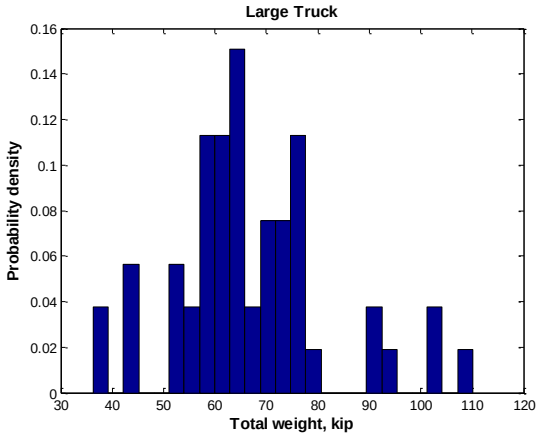

(c) Large Truck

Figure 3.13 Gross-weight Histogram (a) Small Truck; (b) Medium Truck; (c) Large Truck

Calculate the gross weight of the fatigue truck from

$$W = (\sum f_i W_i^3)^{1/3}$$ Equation 3-8

Here, f_i is the fraction of gross weights within an interval. And, W_i is the midwidth of the interval.Distribute the gross weight to axles in accordance with site data. The final fatigue truck configurations are shown in Figure 3.14.

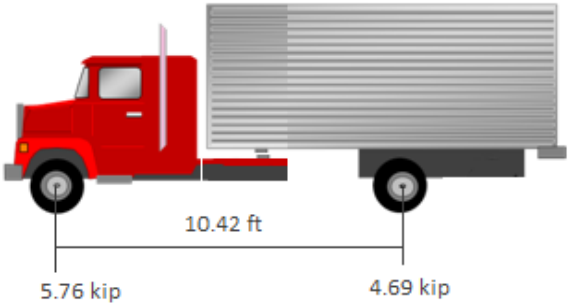

(a) Small truck

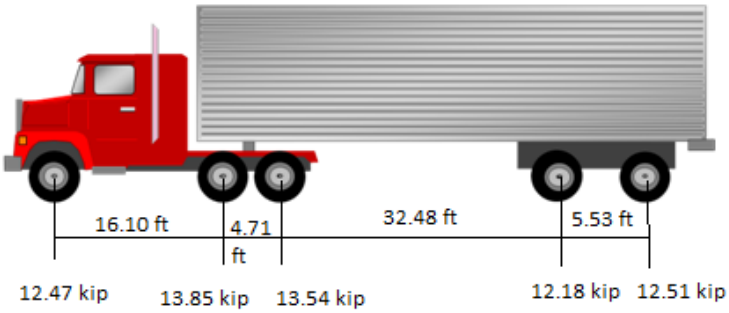

(b) Medium truck

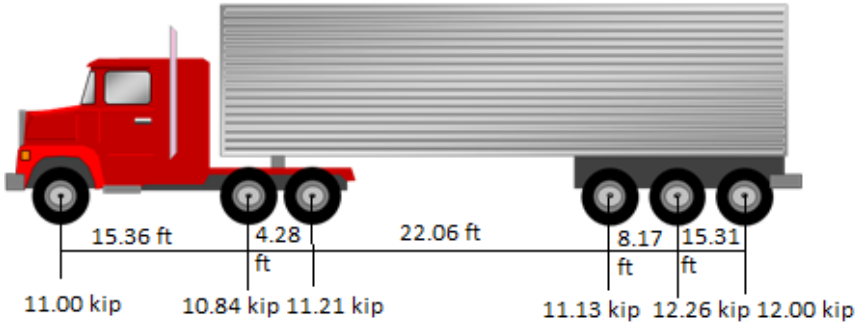

(c) Large truck

Figure 3.14 Fatigue Truck Configurations (a) Small truck; (b) Medium truck; (c) Large truck

4.4.4.2 Traffic Simulation by CORSIM

As interrelated components of a whole transportation network, the actual traffic flow through a bridge is affected by the traffic on the connecting roadways. Therefore, in order to realistically capture the major characteristics of the traffic flow, a road network system consisting of the bridge, highway, and two near ramps is to be studied in the present work. The detailed procedure could be summarized in four steps:

(1) Build the simulation network (Figure 3.15) in TSIS5.1 around the MD Bridge No. 1504200 I-270 over Middlebrook Road based on the background map obtained from Google Map. The background map is adjusted to the correct scale and the simulation network is drawn along the real roadway segment. The network contained the mainline of I270 and adjacent on-ramps of the bridge in the studies. Since we only focus on the southbound of the bridge, the network only contains one-way southbound link. The simulation time is set to be one hour.

(2) Use the time varying vehicle count data collected from nearby detectors and combine with the weigh station measurements collected from the Hyattstown southbound station as the input data for the simulation model. Vehicle count report can be found from the Internet Traffic Monitoring System operated by the Maryland Department of Transportation State Highway Administration. The truck count data is converted to truck percentage (truck count/ total vehicle count) as the input for CORSIM simulation.

(3) Set three different types of trucks corresponding to fatigue trucks generated in last section. Install three loop detectors at the bridge in the created simulation network, one for each lane in order to record the speed, type and passage time of the detected vehicles.

(4) Simulation result after the simulation network was completely created, the traffic demand was input and calibrated, and the detectors were installed, the CORSIM simulation could be started. The simulation could provide the following meaning results for the analysis. First, it records the animation of the simulation, which is used to observe the passage time of the trucks. Second, it provides text output including the volume and speed statistics by each interval (set to be 1s here). Combining the above two output, the passage time and the lane occurred and speed of the truck could be successfully matched.

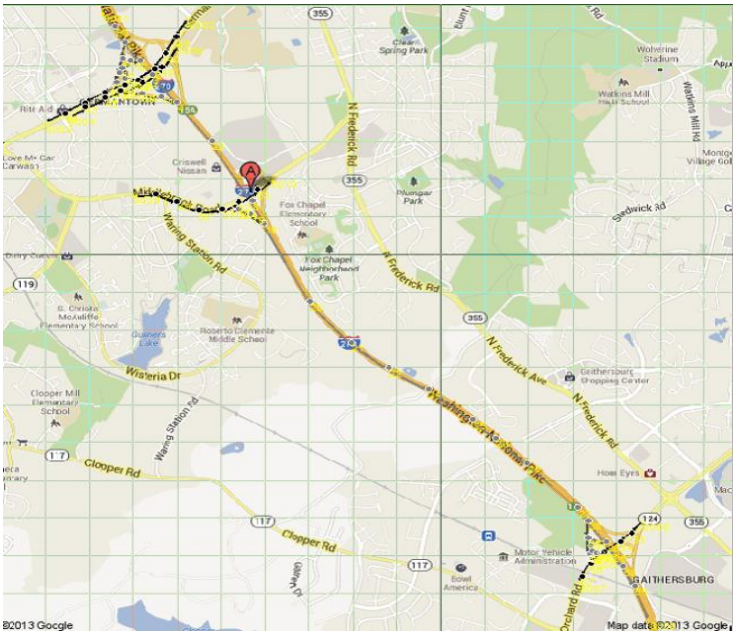

Figure 3.15 Network of the Traffic Simulation Model

3.5.5 Results

From the perspective of a bridge engineer, the actual traffic loading applying on the bridge is of the utmost importance. Based on the microscopic traffic flow simulated for difference time periods, the average static loads from all the vehicles on the bridge for the (1) Midnight, (2) Early Morning and Night, (3) Morning Peak, and (4) Noon to

Evening can be calculated for any instant. The time-history results for the four traffic conditions were shown in Figure 3.17-20, respectively. The horizontal axis showed the time period, 120 steps corresponding to 20 minutes.

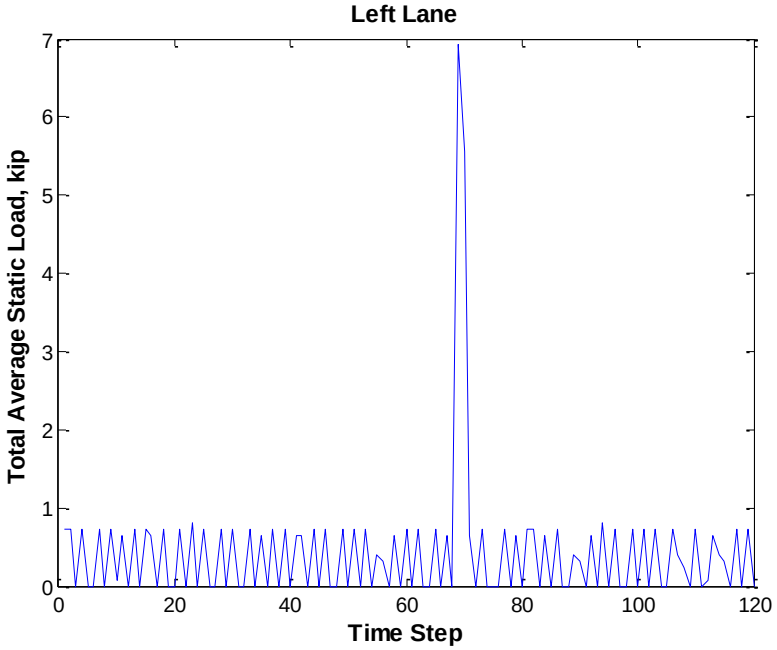

(a) Total Average Static Load of Left Lane

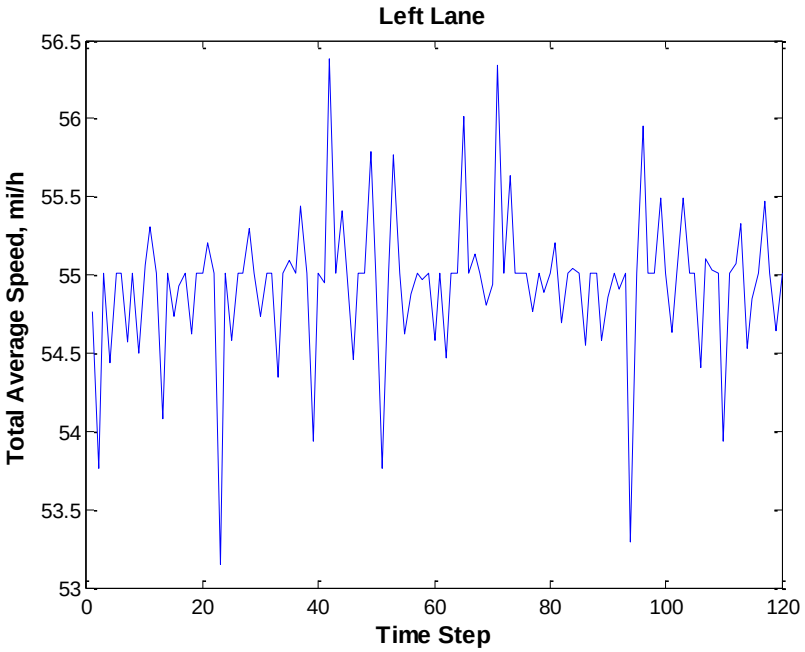

(b) Total Average Speed of Left Lane

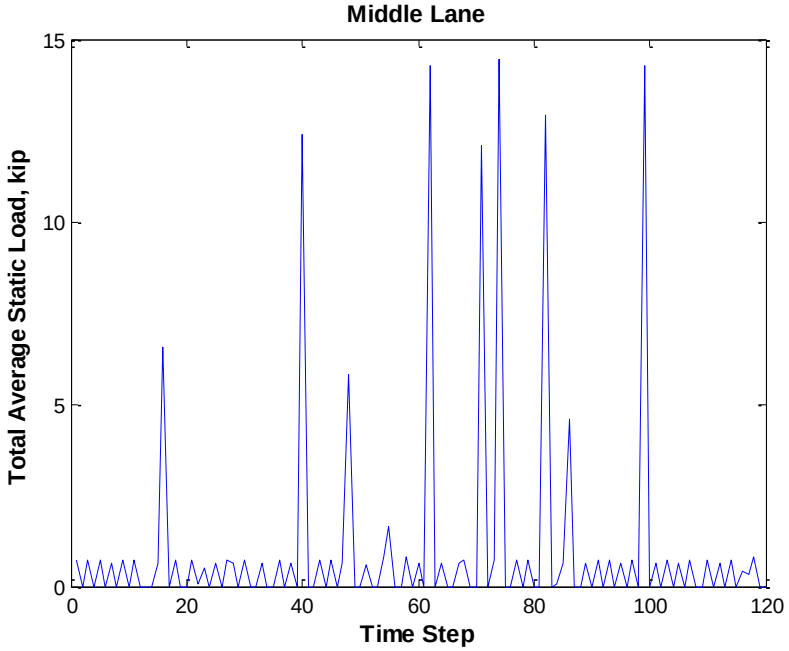

(c) Total Average Static Load of Middle Lane

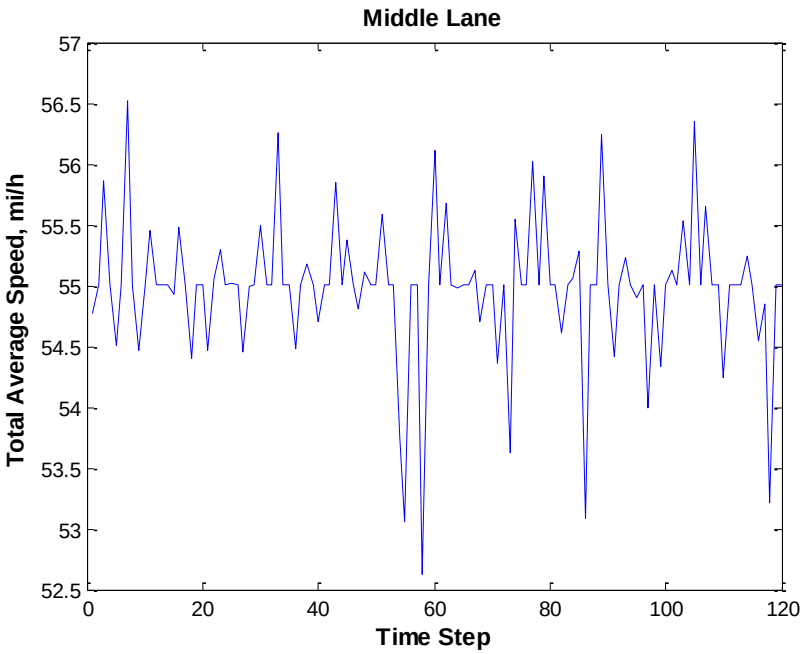

(d) Total Average Speed of Middle Lane

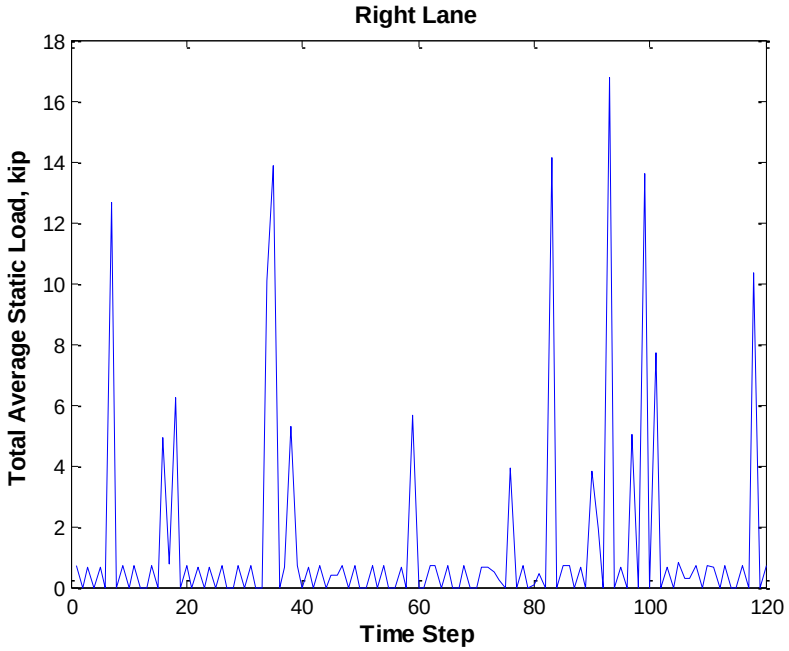

(e) Total Average Static Load of Right Lane

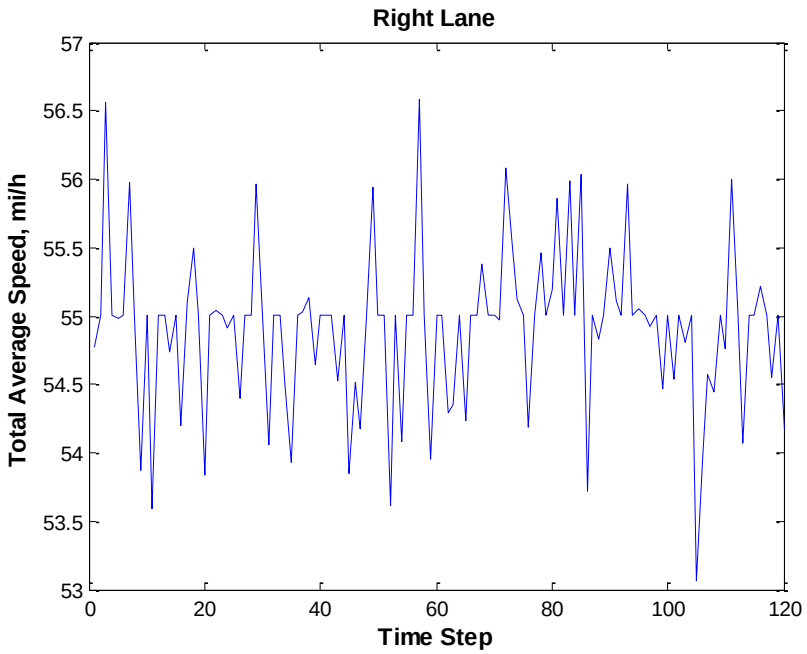

(f) Total Average Speed of Middle Lane

Figure 3.16 20-min Simulation Results for Time Period of Midnight

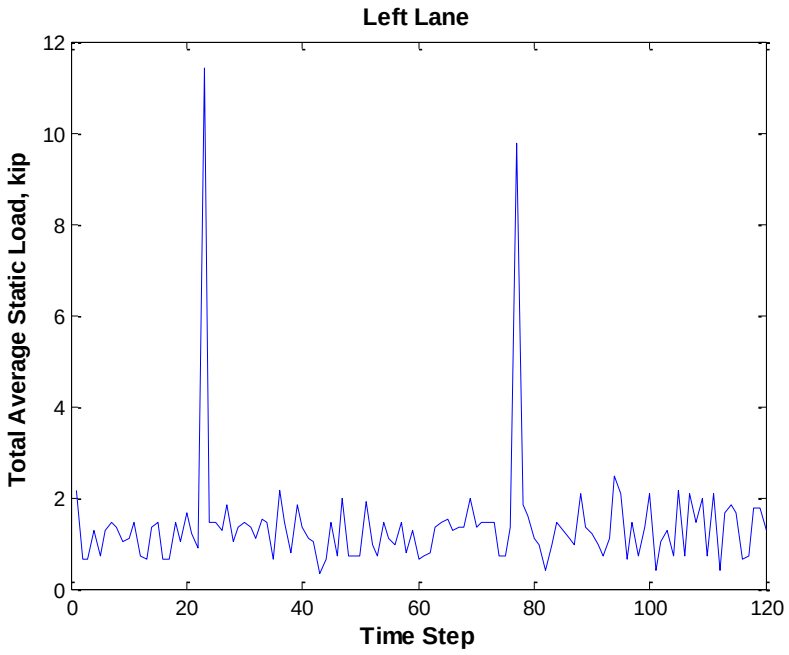

(a) Total Average Static Load of Left Lane

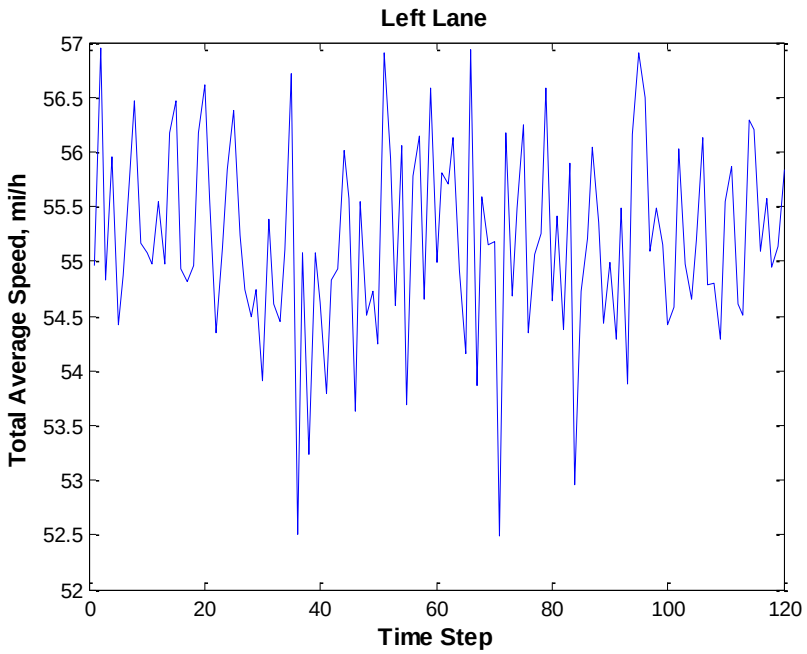

(b) Total Average Speed of Left Lane

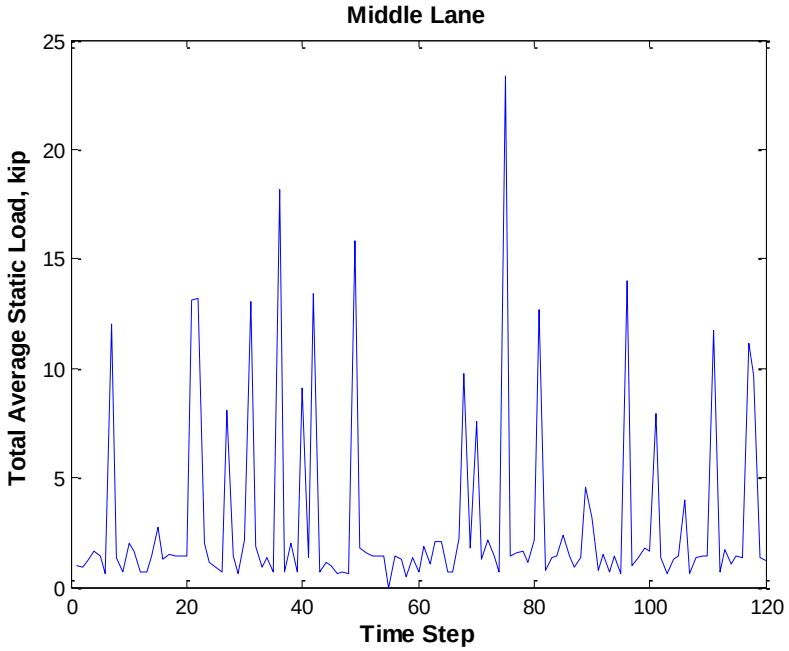

(c) Total Average Static Load of Middle Lane

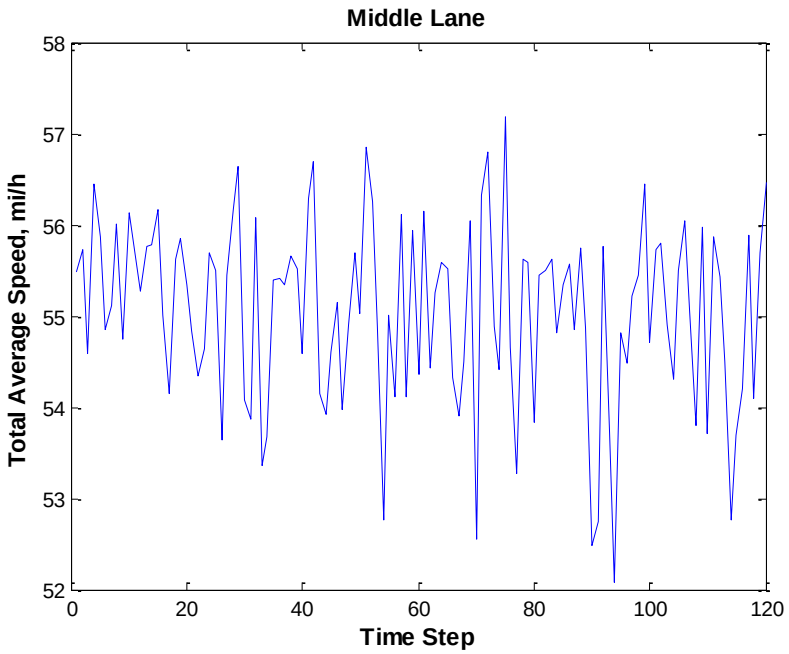

(d) Total Average Speed of Middle Lane

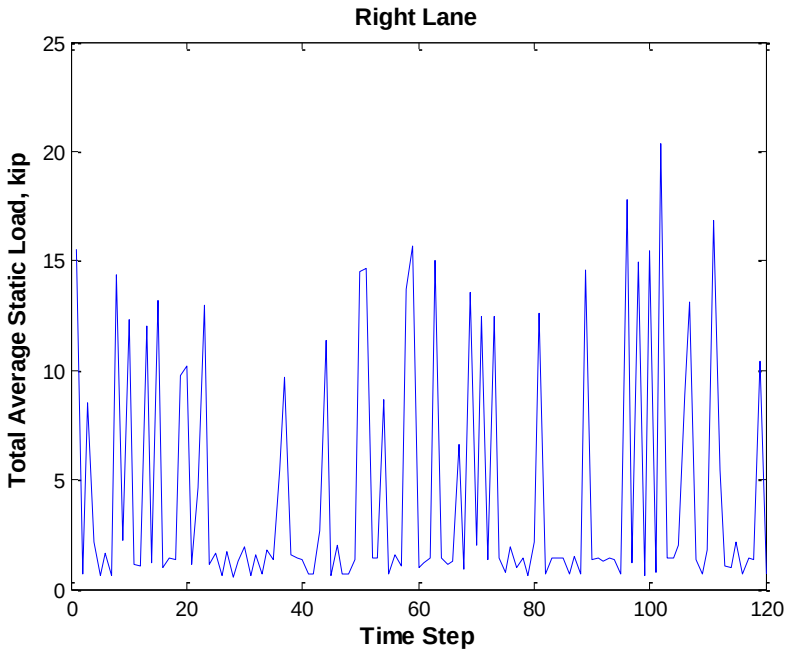

(e) Total Average Static Load of Right Lane

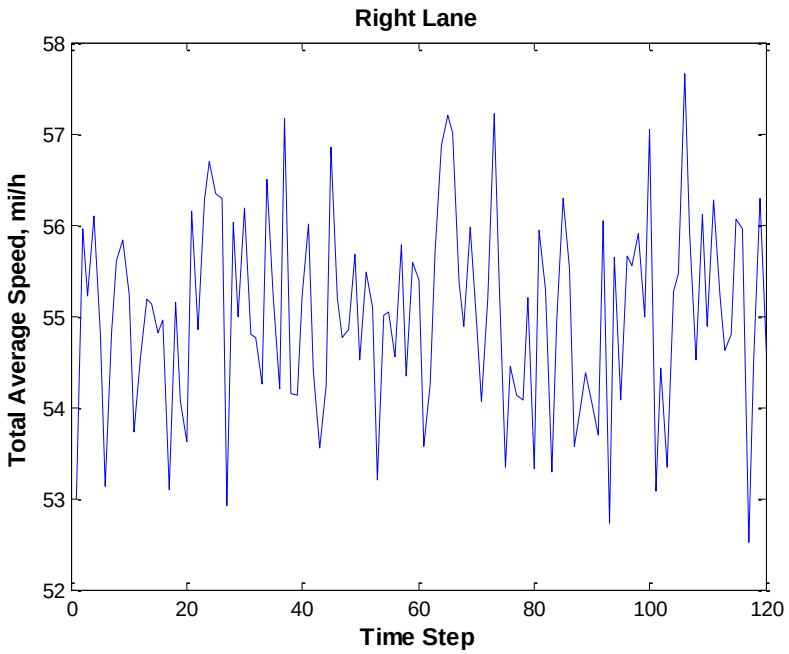

(f) Total Average Speed of Middle Lane

Figure 3.17 20-min Simulation Results for Time Period of Early Morning and Night

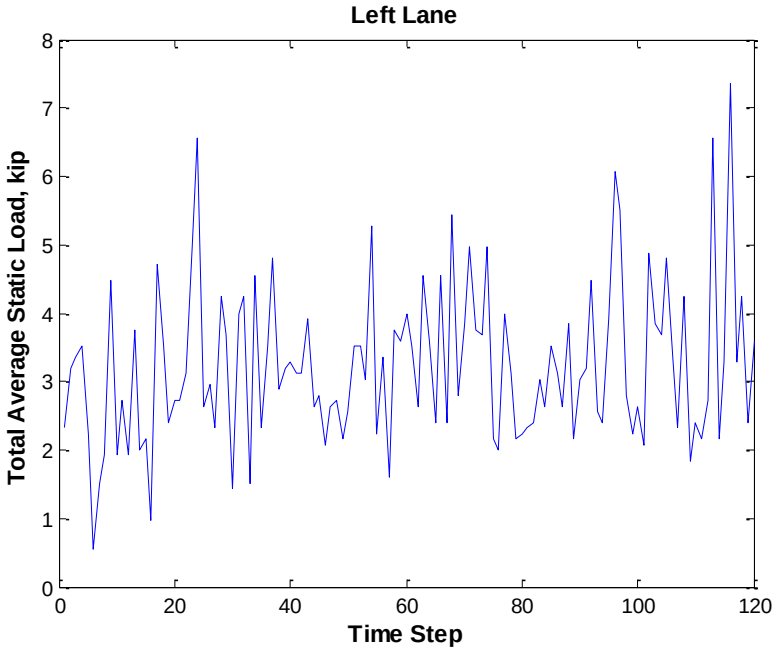

(a) Total Average Static Load of Left Lane

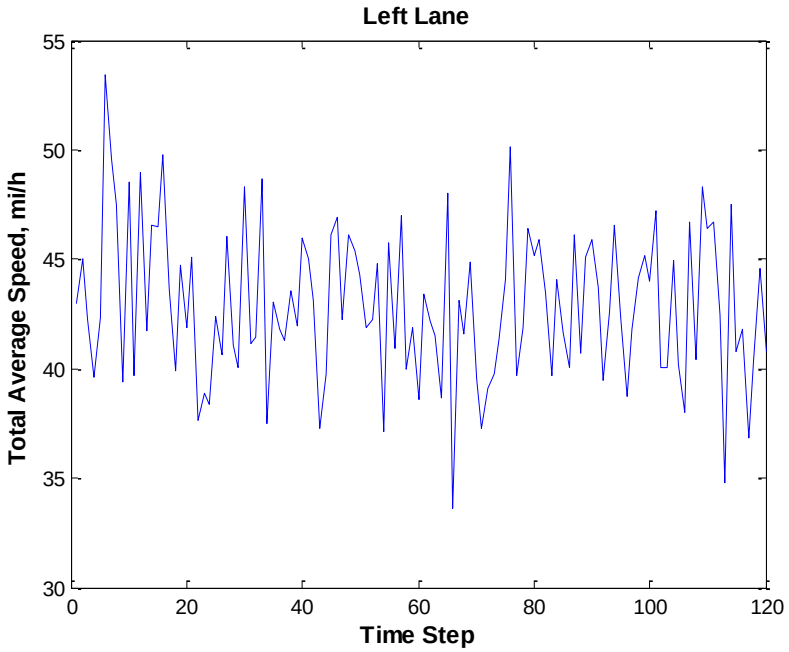

(b) Total Average Speed of Left Lane

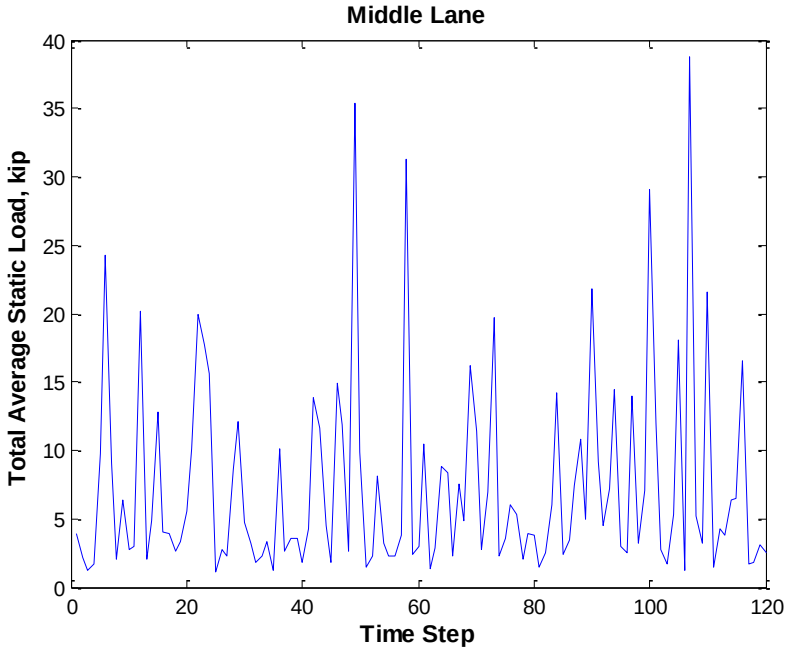

(c) Total Average Static Load of Middle Lane

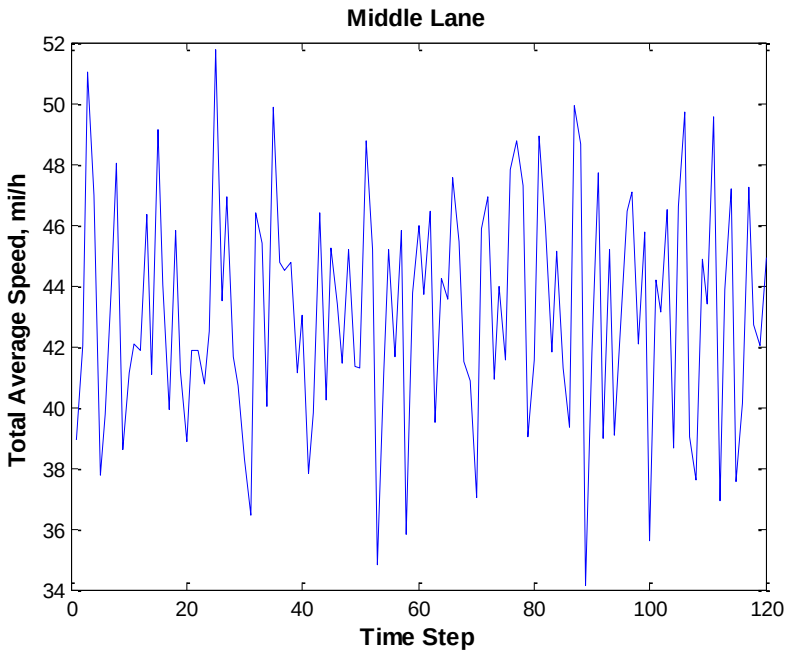

(d) Total Average Speed of Middle Lane

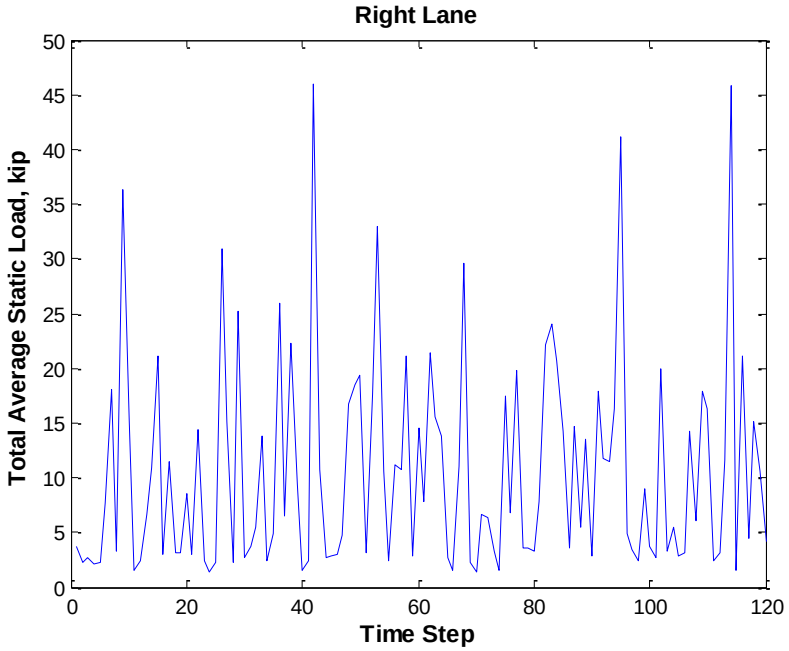

(e) Total Average Static Load of Right Lane

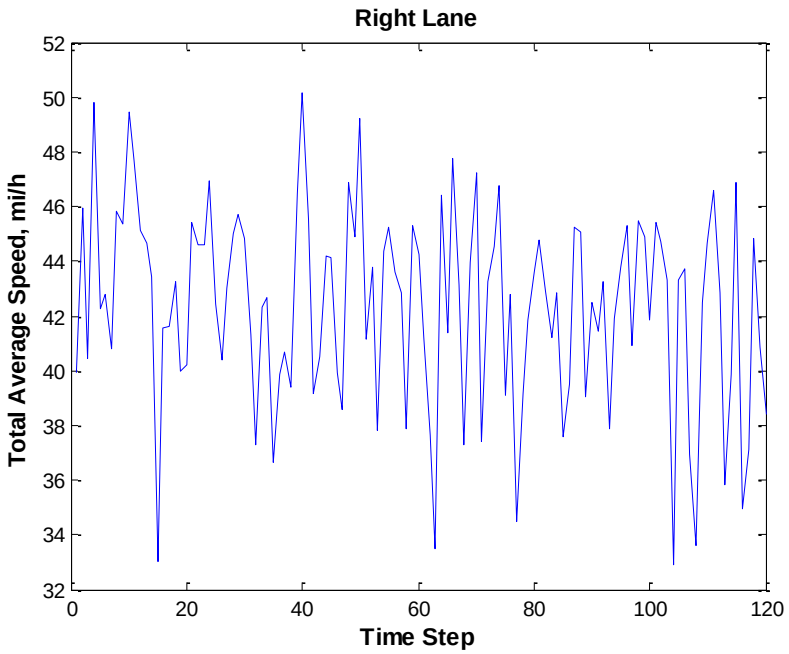

(f) Total Average Speed of Middle Lane

Figure 3.18 20-min Simulation Results for Time Period of Morning Peak

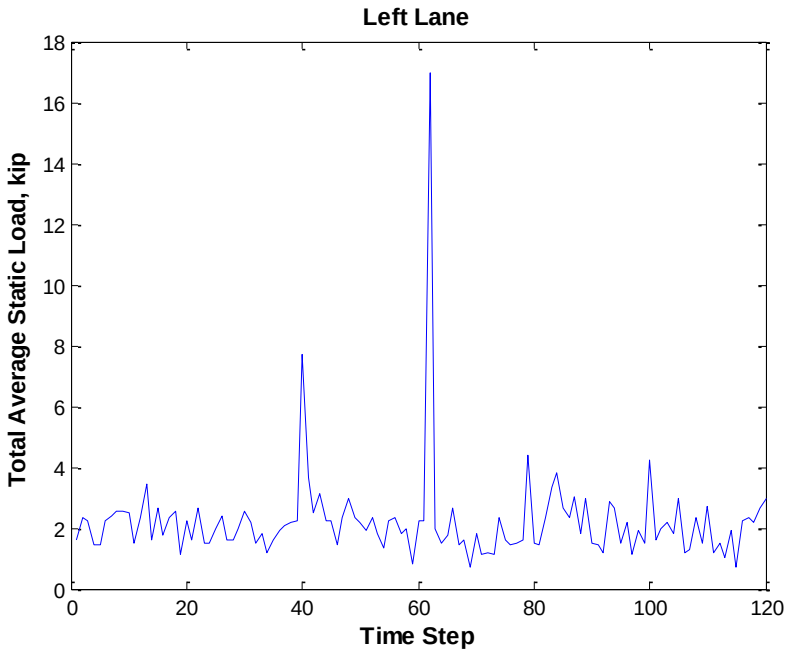

(a) Total Average Static Load of Left Lane

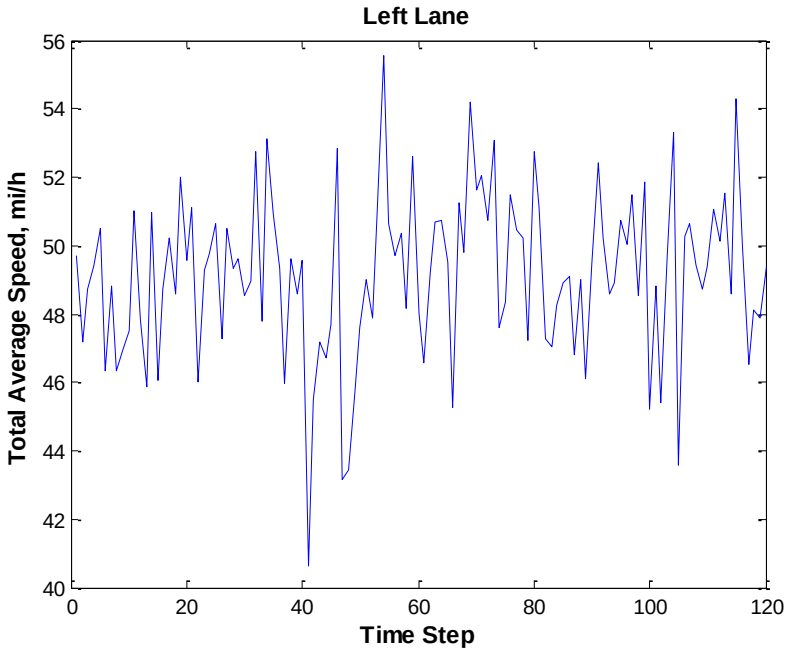

(b) Total Average Speed of Left Lane

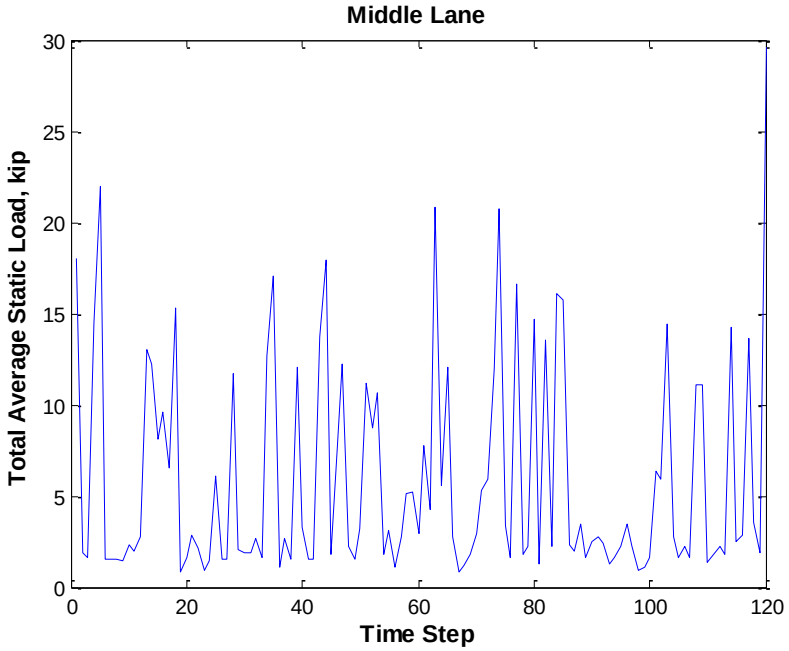

(c) Total Average Static Load of Middle Lane

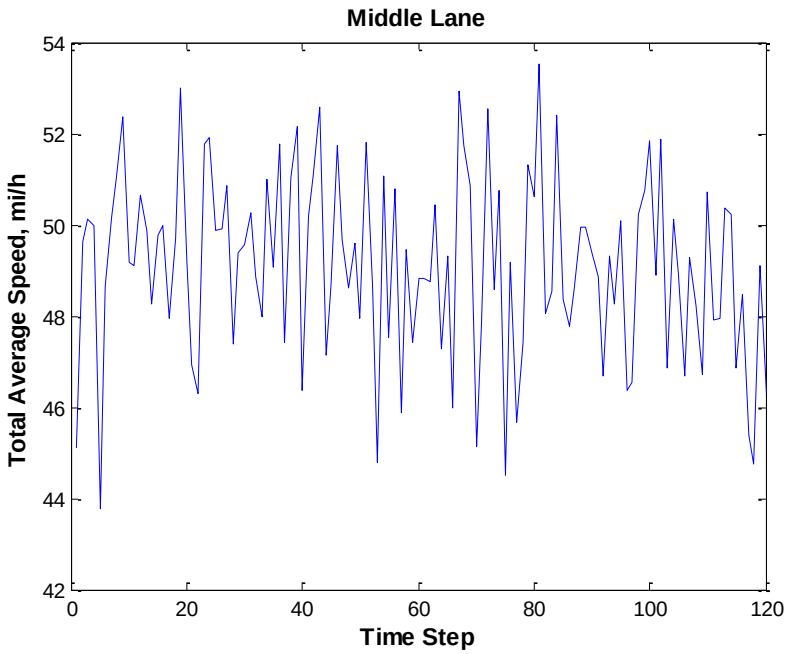

(d) Total Average Speed of Middle Lane

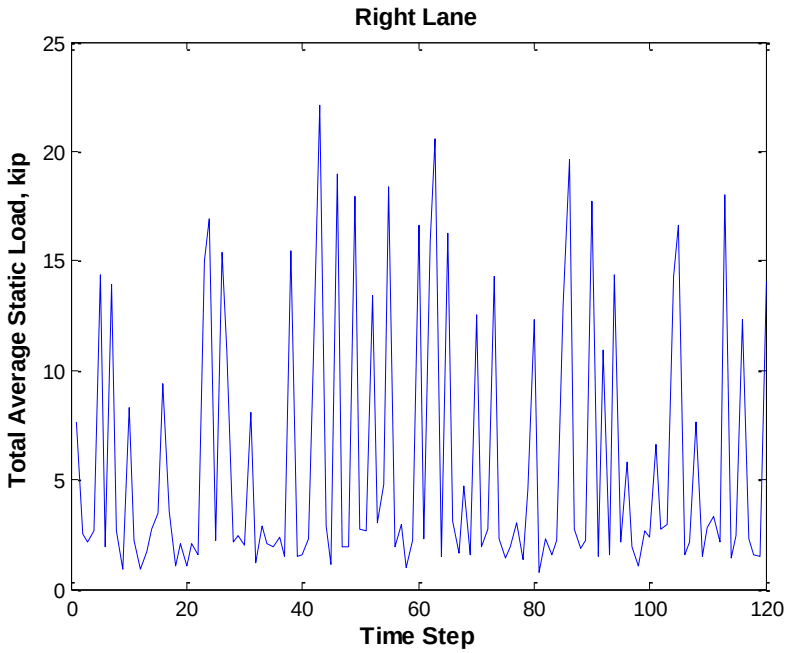

(e) Total Average Static Load of Right Lane

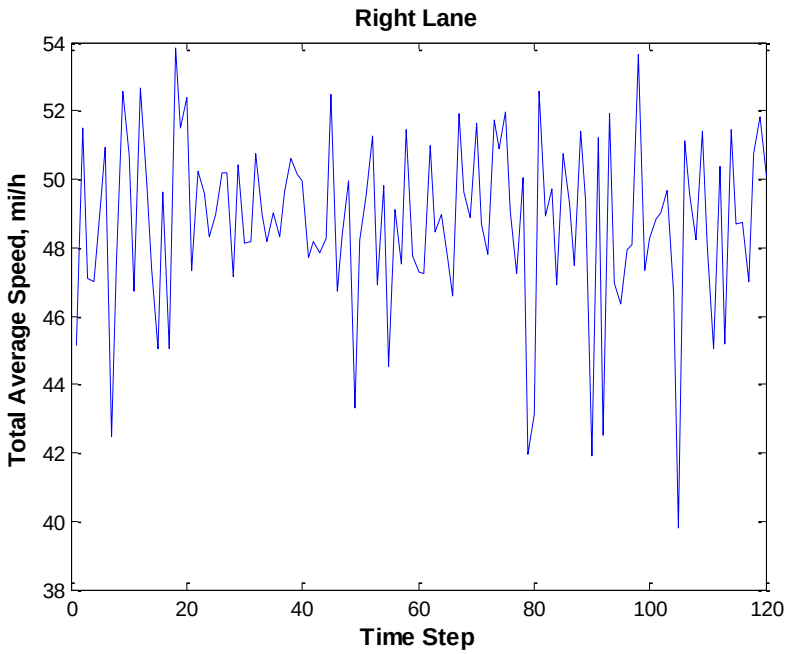

(f) Total Average Speed of Middle Lane

Figure 3.19 20-min Simulation Results for Time Period of Noon to Evening

It can be found that the total average static traffic load, including the weight of trucks and passage cars on the bridge, generally has some variations over time due to the stochastic nature of the traffic flow. Among the four different traffic conditions and the different traffic lanes, the time period of Midnight was found to cause the minimum mean static traffic loads on the bridge, while the time period of Morning Peak caused the maximum mean static traffic loads. The left lane carried the minimum mean static traffic loads on the bridge, while the right lane carried the maximum mean static traffic loads for all the four different time periods. Comparatively, the total average static traffic load has larger variations when the traffic volume gets higher. For the time period of Morning Peak, the total average static traffic load had the most fluctuations over time, which was likely because of the number of trucks passing through the bridge increased due to the increased traffic volume.

Due to the increased traffic volume, the total average speed went down reasonably. The time period of Midnight was found to have the maximum mean average speed on the bridge, while the time period of Morning Peak had the minimum average speed.

Table 3-9 Statistical Results Comparison of Truck Loading

Time Periods	The probability based full velocity difference model			CORSIM		
	Average Speed (mph)	Number	Average Headway (s)	Average Speed (mph)	Number	Average Headway (s)
Midnight	55.00	34	35.29	53.69	32	37.5
Early Morning and	54.68	74	16.22	52.94	78	15.38
Morning Peak	38.33	168	7.14	35.45	165	7.27
Noon to Evening	47.32	104	11.54	42.07	98	12.24

The statistical results on the time histories of the static traffic load can provide useful information to evaluate the actual traffic loads. Before the analytical fatigue assessments of highway bridges under traffic loading were conducted, the statistical results from the probability based full velocity difference model and the commercial software CORSIM were studied. Table 3-9 showed the comparison for the four different time periods. The average truck speed of the probability based full velocity difference model was a little bit higher than that of the software CORSIM, which was likely because of the different assumptions for the mechanical properties of truck models in these two methods. The results of the total truck number and the average headway were pretty close. It was found from the results that the 20-min simulation period currently used can lead to stable pattern and matched results. The results also suggested that the

probability based full velocity difference model were capable of capturing the traffic flow pattern and simulating the truck loading for the four different simulation time periods.

3.6 Summary

This chapter proposed a probability-based full velocity difference model to simulate real traffic loading of steel highway bridges combing the traffic monitoring data and weigh station measurements. A case study of I-270 Bridge over Middlebrook Road was studied with the proposed methodology.

According to the traffic volume of the historical traffic monitoring data, one typical day has been divided into four time periods: (1) Midnight, (2) Early Morning and Night, (3) Morning Peak, and (4) Noon to Evening. The simulation duration has been set to one hour for each time period. The traffic flow on the bridge with three traffic lanes was simulated by full velocity difference model, as well as the microscopic traffic simulation software TSIS-CORSIM for validation. The simulated vehicles were generated based on the historical truck information from the weigh station measurements. Each simulated vehicle were inputted to the simulated network representing the studied bridge, and would follow the full velocity difference model of car-following behavior.

The results could provide the axle weight, axle spacing, vehicle position and speed at each time step of the simulation. Comparisons were carried out between the results of the proposed methodology and CORSIM, in terms of truck speed, truck number, and average headways. It was found from the results that the 20-min simulation period currently used can lead to stable pattern and matched results. The results also suggested that the probability based full velocity difference model were capable of

capturing the traffic flow pattern and simulating the truck loading for the four different simulation time periods.

Chapter 4 Global and Local Modeling of Highway Bridges using Finite Element Method

4.1 Introduction

Finite element method (FEM) is a numerical technique for finding approximate solutions to boundary value problems for partial differential equations. It uses subdivision of a whole problem domain into different parts and adopts variational methods to solve the problem by minimizing an associated error function. Analogous to the idea that connecting many tiny straight lines can approximate a larger circle, the finite element method encompasses methods for connecting many simple element equations over many small subdomains to approximate a more complex equation over a larger domain.

To study fatigue behavior of highway bridges under traffic loading, the analysis for an existing bridge is predominantly based on stress analysis, which means to get the distribution of stress in structures. The finite element method is a highly valuable tool as a basis for the evaluation of fatigue behavior. It can be used to determine the critical locations due to fatigue damage before field tests. It also can provide guidance for experimental designs and instrumentation plans. Furthermore, the finite element method is considered a rigorous method for structural fatigue stress analysis, especially for those bridges without any field measurement.

In recent years, the engineer's ability of modeling has increased drastically with the development of advanced powerful analysis software packages, such as LUSAS,

CSiBridge, and ANSYS. With the help of these facilities, a wide range of engineering problems have been more efficiently modeled and accurately analyzed.

The purpose of this chapter is to obtain a validated model from the finite element modeling process, which is capable of simulating and predicting the actual behavior of highway bridges subjected to traffic loading. Section 4.2 introduces the material models using in finite element modeling. Then, the global modeling and local modeling of I-270 Middlebrook Bridge are discussed in Section 4.3 and 4.6.

4.2 Material Properties

Bridge systems consist of super- and sub structures. The most commonly used material for super- and sub structures are concrete and steel.

4.2.1 Concrete

Concrete is a quasi-brittle material and has different behavior in compression and tension. The tension strength of concrete is typically 8-15% of the compressive strength. In compression, the stress-strain curve of concrete is linearly elastic up to about 30 percent of the maximum compressive strength. Above this point, the stress increase gradually up to the curve descends into a softening region, and eventually crushing failure occurs at an ultimate strain. In tension the stress-strain curve for concrete is approximately linearly elastic up to the maximum tensile strength. After this point the concrete cracks and the strength decreases gradually to zero.

Concrete is defined as isotropic material and is not affected by temperature change. The mass density is specified as 2.248E-07 kip/in^3, using for calculating the mass

of the element. The total mass of the element equals the product of the mass density and the volume of the element. The weight density is specified as 8.681E-05 kip/in^3, using for calculating the self-weight of the element. The total weight of the element is the product of the weight density and the volume of the element. Typically the mass density is equal to the weight density of the material divided by the acceleration due to gravity. Actually, only elastic linear behavior is considered under the vehicular load. The modulus of elasticity is equal to 3605 ksi, Poisson's ratio is 0.2, coefficient of thermal expansion is defined as 5.5E-06, shear modulus is taken as 1502 ksi, and the concrete compressive strength is specified as 4.5 ksi.

4.2.2 Steel

The characteristics of mild structure steel under tensile test can be summarized in four steps:

1. Proportional limit: the relationship between stress and strain is linear up to the proportional limit; the material is said to follow Hooke's Law.

2. Elastic limit: up to this stress, the specimen can be unloaded without permanent deformation.

3. Yield limit: a peak value, the upper yield point, is quickly reached after elastic limit, followed by a leveling off at the lower yield point. The stress remains constant, even though the strain continues to increase. Usually, the lower yield point is defined as the yield tensile strength.

4. Ultimate tensile limit: at a strain of approximately 12 times the strain at yield, strain hardening begins, and additional load is required to cause additional elongation. A maximum value of stress decreases with increasing strain, and fracture occurs.

Steel is defined as isotropic materials, independent of the direction of loading or the orientation of the materials for fatigue analysis. In addition, shearing behavior is uncoupled from extensional behavior. All the elastic material properties used in this study is temperature independent, which means that the properties used by an element are assumed to be constant regardless of any temperature changes experienced by the structure. The modulus of elasticity is equal to 29000 ksi, Poisson's ratio is 0.3, coefficient of thermal expansion is defined as 6.5E-06, and shear modulus is taken as 11153.846 ksi. The minimum yield stress F_y is 50 ksi, the minimum tensile stress F_u is equal to 65 ksi, effective yield stress F_{ye} is defined 55 ksi, effective tensile stress F_{ue} is taken as 71.5 ksi. Material damping, and time-dependent properties, including creep, shrink age, and age-dependent elasticity, are not be considered.

4.3 Global Model

To study the behavior of the bridge, the entire superstructure was first analyzed by a large, coarse finite element model. The global model contains only the main components of the bridge and is mainly for modal analysis, displacement output of the whole bridge, critical fatigue location determination, and so on.

4.3.1 Bridge Introduction

MD Bridge No.15042 is a simple-span composite steel I-girder bridge with a span length of 140 ft. The bridge is comprised of two structures for the northbound (NB) and southbound (SB) roadways respectively, separated at the centerline. It carrie with three traffic lanes in the south and four traffic lanes in the north with equal lane width of 12".

The southbound superstructure provides a curb-to-curb roadway width of 61’-2” and consists of eight identical welded steel plates girders with a composite reinforce concrete deck constructed with shear connector. The eight girders are equally spaced at 7’-11” and each girder has a constant web depth of 60” throughout the entire bridge. For the northbound superstructure, it provides a curb-to-curb roadway width of 73’-1” and consists of nine identical welded steel plates girders with a composite reinforce concrete deck constructed with shear connector. The nine girders are equally spaced at 8’-5” and each girder has a constant web depth of 60” throughout the entire bridge. This bridge has a 76^{o} parallel skew of its bearing lines. The bridge diaphragms are inverted K-type braces with bottom chords only. All of them are parallel to the bearing lines. Girders of the southbound are numbered as G1 through G8 from the exterior to the centerline of the bridge. The general plan view and the cross section are depicted in Figure 4.1.

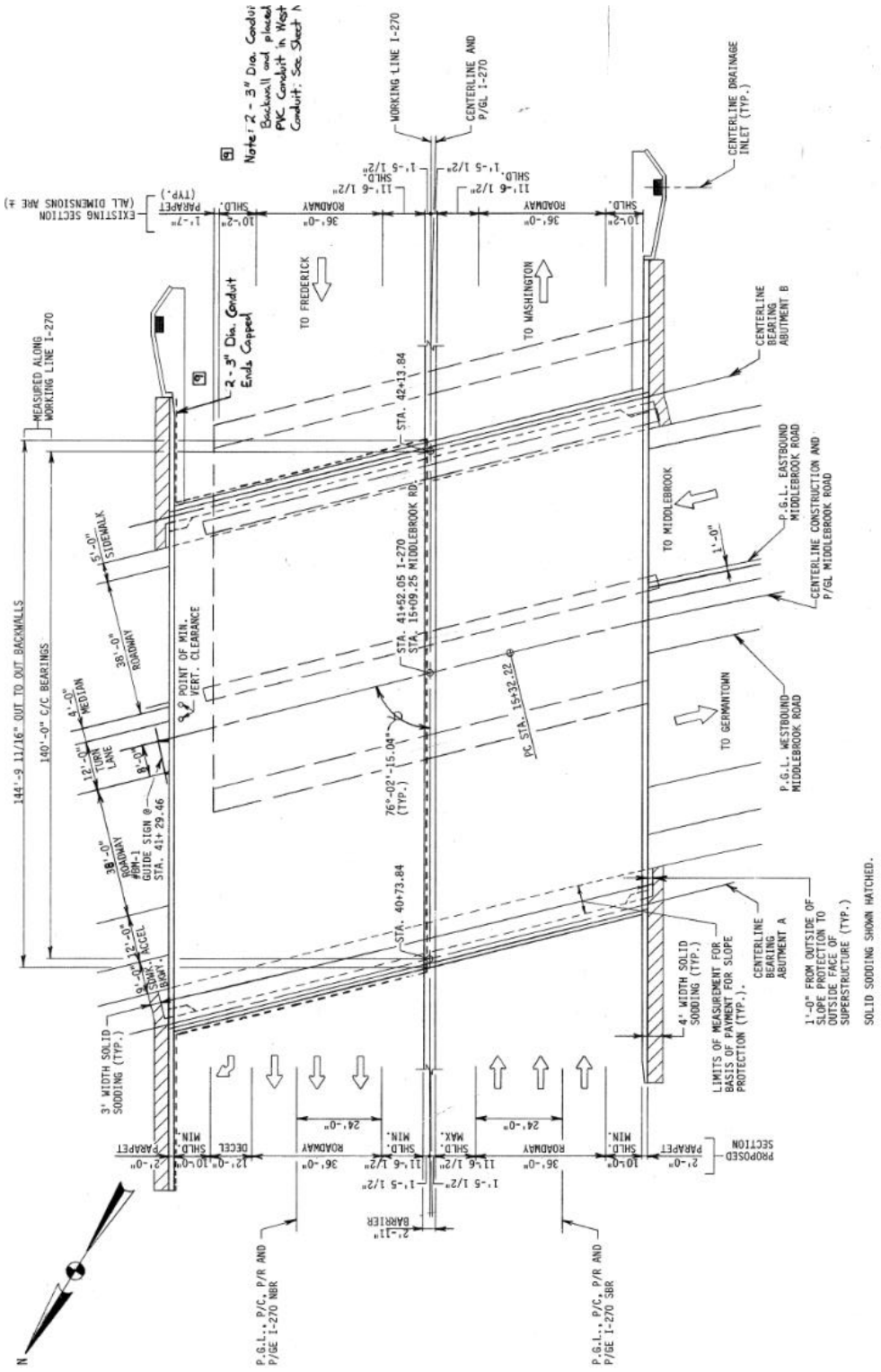

(a) General Plan

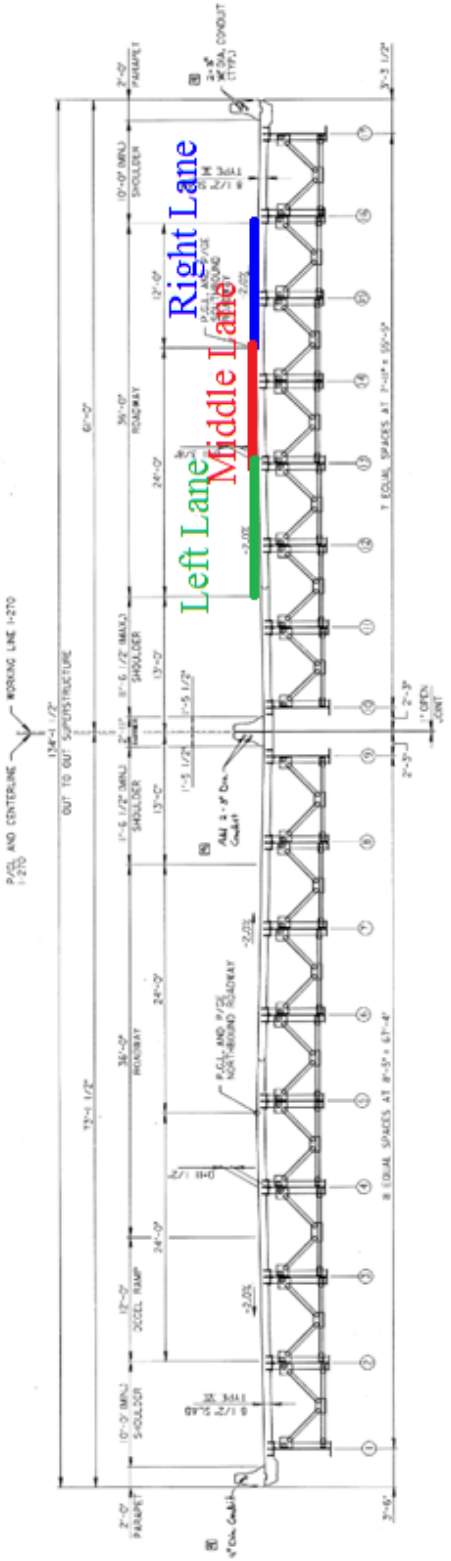

(b) Cross Section with Lane Position

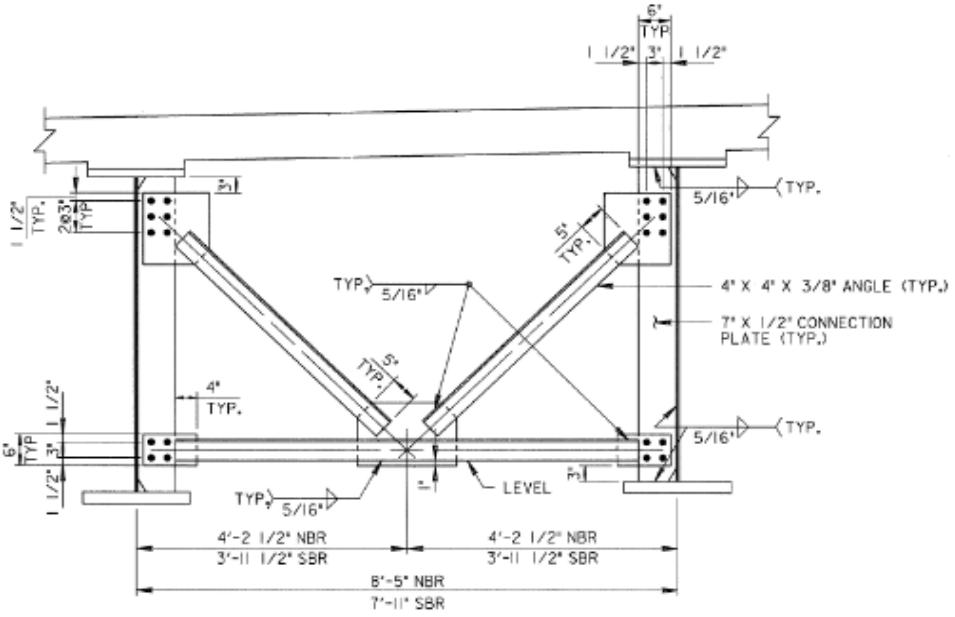

(c) Cross Frame Detail

Figure 4.1 Bridge Geometry (a) Plan View; (b) Cross Section (Looking South) (c) Cross Frame Detail

(a) Girder 3 Bay 2 Diaphragm 3

(b) Girder 4 Bay 3 Diaphragm 3

Figure 4.2 Typical fatigue cracks in cross frame connection plate-to-girder bottom flange weld at (a) G3B2D3 and (b) G4B3D3

Designed in 1988, the I-270 Bridge over Middlebrook Road has been built for over 20 years. Despite the deteriorating caused by environmental factors, the increasing traffic volume and weight pose a premier threat of the bridge structure. Four fatigue cracks were reported in the June 2011 Bridge Inspection Report, and all in the welded connection between the lower end of the cross frame connection plate and the girder

bottom flange of the Southbound. Figure 4.2 shows two of the four crack locations at G3B2D3 (Girder 3 Bay 2 Diaphragm 3) and G4B3D3 (Girder 4 Bay 3 Diaphragm 3). The detailed information was summarized in Table 4-1.

Table 4-1 Description of I-270 Bridge Southbound over Middlebrook Road

Structure Identification		Southbound of MD No.15042
Structure Type		Steel I-girder bridge with concrete deck
Geometry	Span Length	140 ft
	Curb-to-Curb Roadway Width	61’-2”
	Girder Number	8
	Girder Equal Spacing	7’-11”
	Web Plate	60”×9/16”
	Top Flange	16”×1 ½”
	Bottom Flange	18”×1 5/8” and 20”×2”
	Bearing Skew Angle	76°
Martials	Concrete	Mix No.6 (4500 psi)
	Structural Steel	ASTM A-572, Fy=50 ksi
Cross Frame	Type	Inverted K-Type with bottom chord only
	Equal Spacing	23’-4”
	Section	4”×4”×3/8” Angle
Connection Plate	Section	7”×1/2”
Crack Locations		Connection plate to girder bottom flange weld G3B2D3 G3B2D4 G4B3D3 G4B3D4

4.3.2 Global Model in CSiBridge

To investigate the fatigue performance of the bridge, a three-dimensional finite element model was developed by using the CSiBridge for linear-elastic structural analyses, as depicted in Figure 4.3. The model of the southbound consisted of eight I-girders. The concrete deck, the eight I-girders, and connection plates which connecting cross frames and girder webs were modeled by shell elements, while all the cross frames were modeled by spatial frame along their enter-of-gravity. Special link members were defined to connect the girder elements and concrete deck elements at the actual spatial points where these members intersect. The translations of x-, y-, z-directions were fixed at the abutments to represent actual characteristics of support and continuity.

It is very complicated to establish a finite element model of a large practical structure for fatigue damage analysis, as the finite element model should embody the sectional properties of structural members. Moreover, in considering that fatigue damage is a local failure mode and often occurs around welded regions, a global model with refined meshing around the welded connection between the connection plats and the bottom flanges was built for analysis.

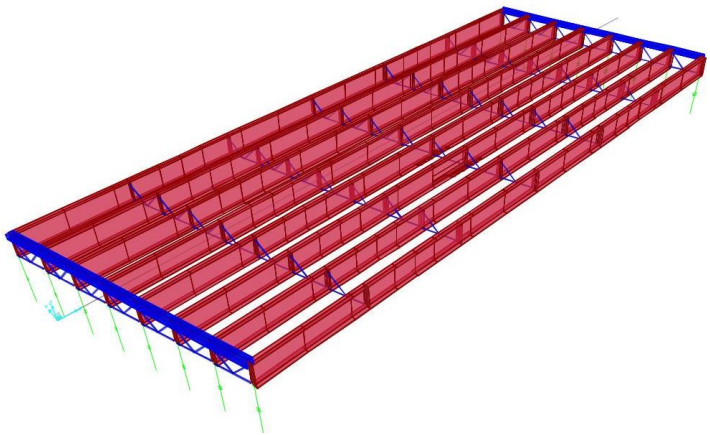

(a) Eight I-girders without concrete deck

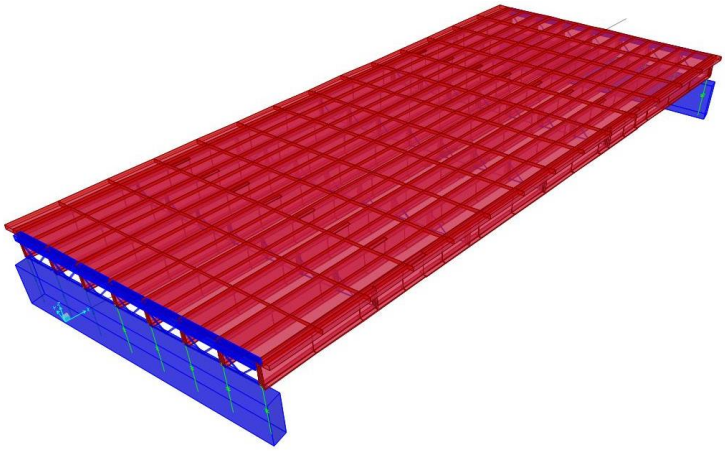

(b) Isometric View of FEM for I-270 Bridge

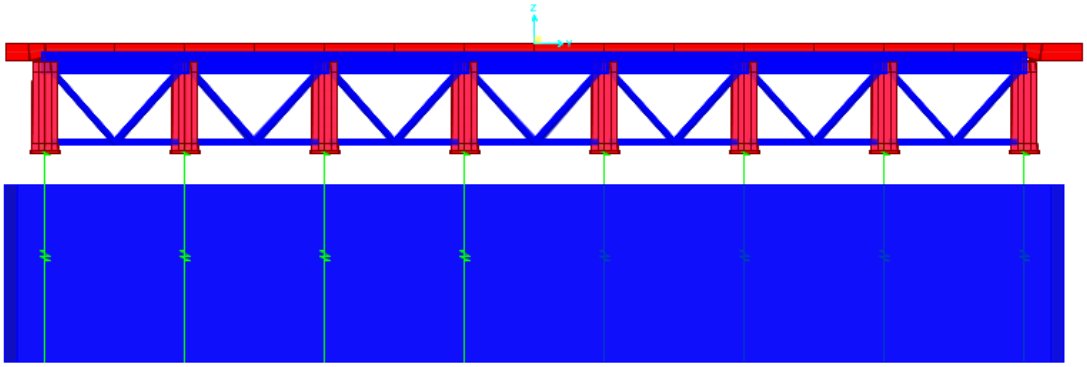

(c) Cross Section of FEM for I-270 Bridge

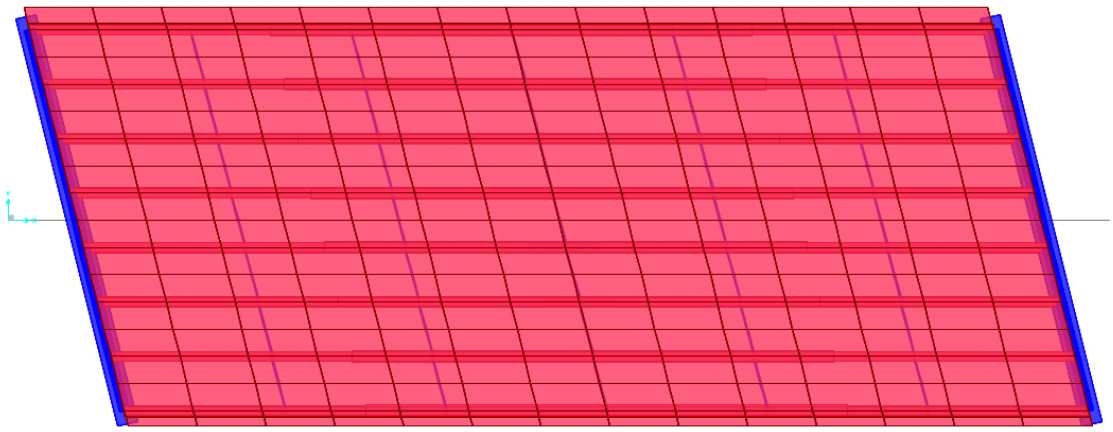

(d) Plan View of FEM for I-270 Bridge

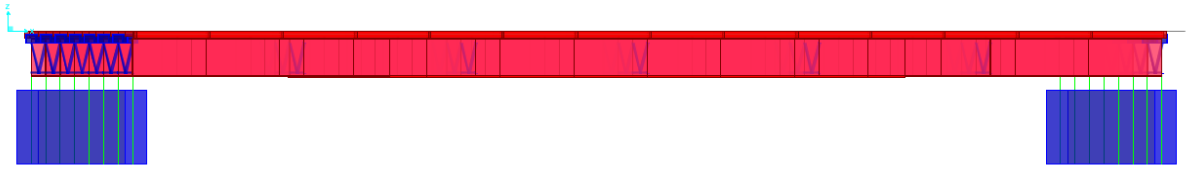

(e) Side Elevation of FEM for I-270 Bridge

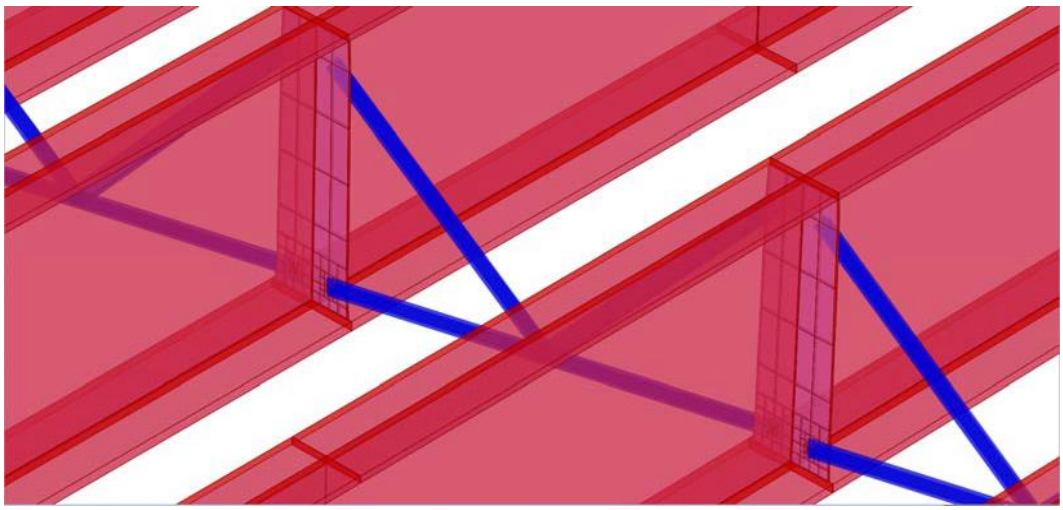

(f) Zoom-in View (Refined Meshing around the Weld)
Figure 4.3 Finite Element Model of I-270 Bridge in CSiBriddge

4.3.3 Global Model in ANSYS

Meanwhile, a three-dimensional finite element model was developed by using the ANSYS APDL for linear-elastic structural analyses, as depicted in Figure 4.4. APDL stands for ANSYS Parametric Design Language, a scripting language that can be used to automate common tasks or even build the model in terms of parameters (variables). While all ANSYS commands can be used as part of the scripting language, the APDL commands discussed here are the true scripting commands and encompass a wide range of other features such as repeating a command, macros, if-then-else branching, do-loops, and scalar, vector and matrix operations. APDL is the foundation for many sophisticated features. In this study, all the ANSYS models were established through APDL

The model of the southbound consisted of eight I-girders. The concrete deck was generated by SOLID185 element, the eight I-girders and connection plates which connecting cross-frames and girder webs were modeled by SHELL 181 element, and all

the cross-frames were modeled by BEAM 188 along their enter-of-gravity. Special coupled nodes were defined to connect the girder elements and concrete deck elements at the actual spatial points where these members intersect. The translations of x-, y-, z-directions were fixed at the abutments to represent actual characteristics of support and continuity. In order to locate the crack detailing, a global model with refined meshing around the weld between the connection plats and the bottom flanges was built for analysis. Based on the convergence test results, the mesh size of solid element and shell element was set around 20 in.

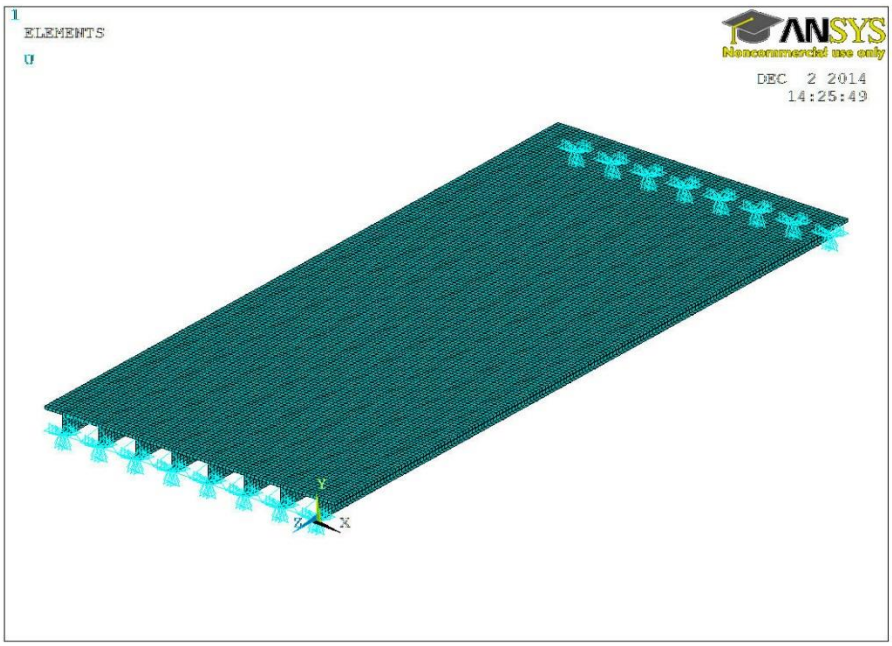

(a) Isometric View of FEM for I-270 Bridge

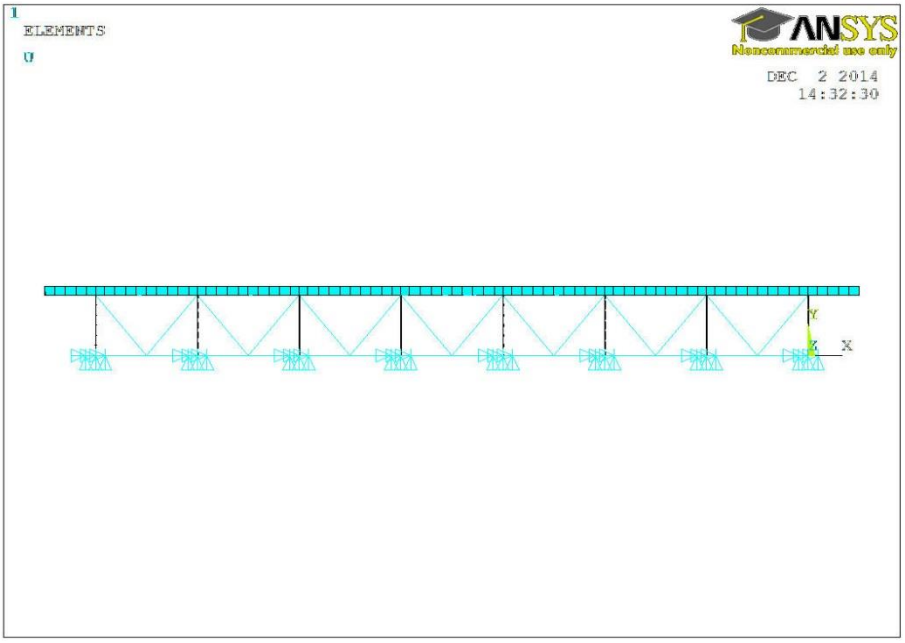

(b) Cross Section of FEM for I-270 Bridge

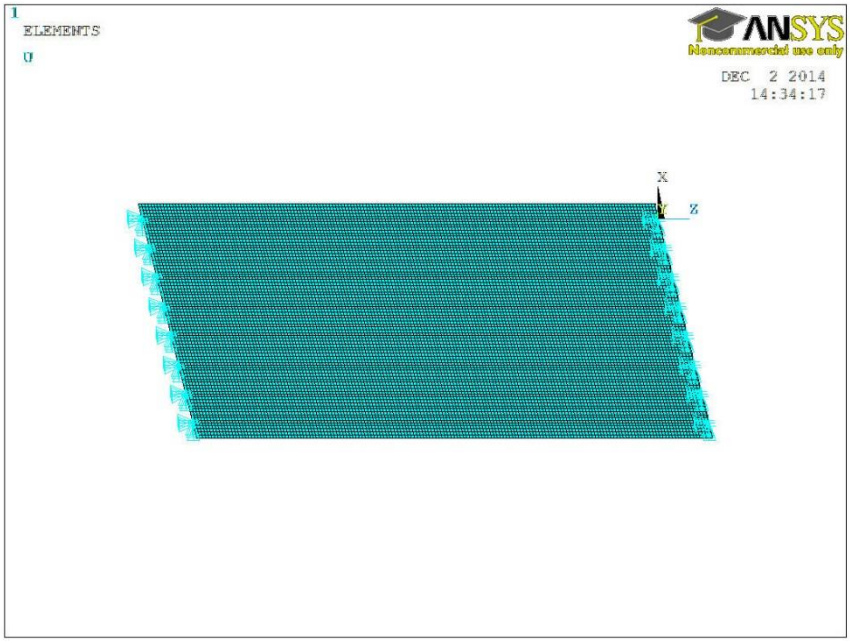

(c) Plan View of FEM for I-270 Bridge

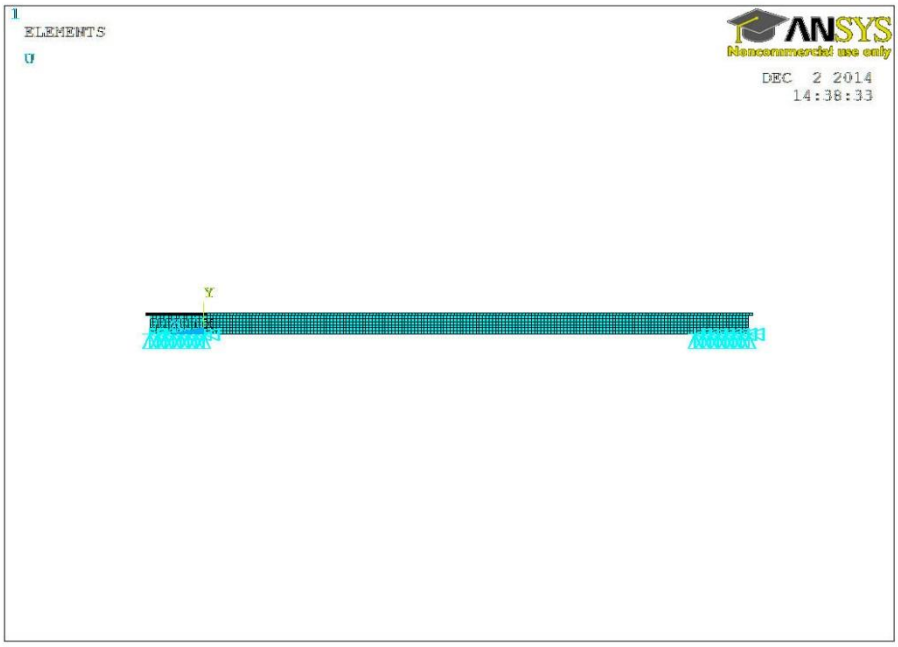

(d) Side Elevation of FEM for I-270 Bridge
Figure 4.4 Finite Element Model of I-270 Bridge in ANSYS

4.4 Convergence Test

The accuracy of a finite element analysis depends on the mesh size of the elements. Basically, the smaller size of the elements, the higher accuracy of the analysis. However, the calculation accuracy and computational time should compromise on each other. This convergence test in finite element analysis is a procedure used to determine appropriate mesh size for a model. The measurement of a finite element model's mesh should depend on the purpose of the model. Since the bridge model was to investigate the vertical stress or shear stress in the cracked connection weld, then it needed to have a very fine mesh in the connection area but needed to transition gradually to coarser meshes because otherwise the model would become unnecessarily too large. Then it may be able to use a uniform mesh along the bridge length for all the girders. However, there are multiple parameters for the measurement of a two-dimensional or three-dimensional

finite element models, including the dimensions and aspect ratios of the elements for the girder top flange, bottom flange, and web, as well as the bridge deck. To simplify the convergence test for these finite element models of I-270 Bridge over Middlebrook Road, a consistent refined mesh around the weld region was employed in all the models, and the maximum element size was used in control the uniform mesh along the bridge longitudinal length for all the girders and the deck, depicted in Figure 4.5.

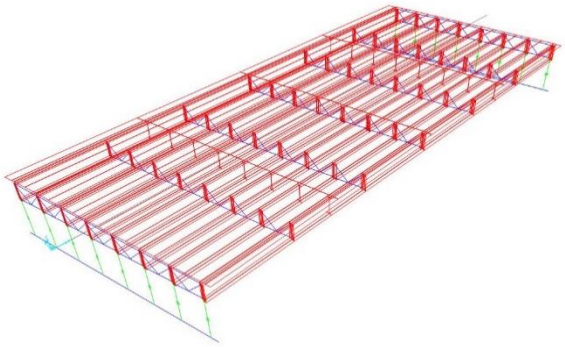

(a) Element Maximum size 500”

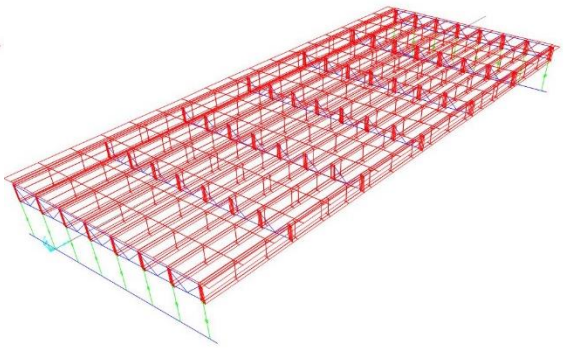

(b) Element Maximum size 100”

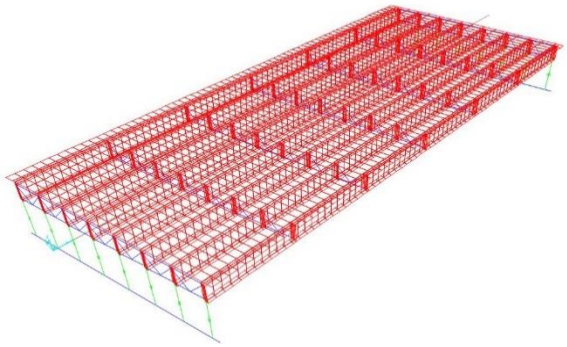

(c) Element Maximum size 25”

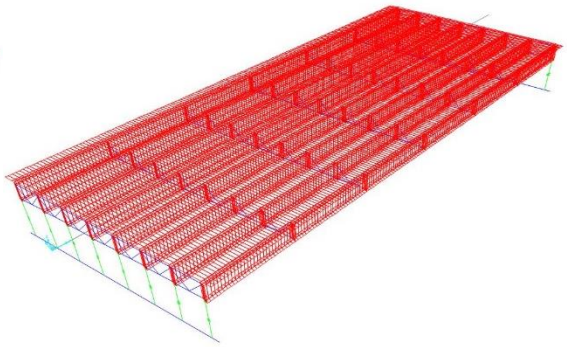

(d) Element Maximum size 10”

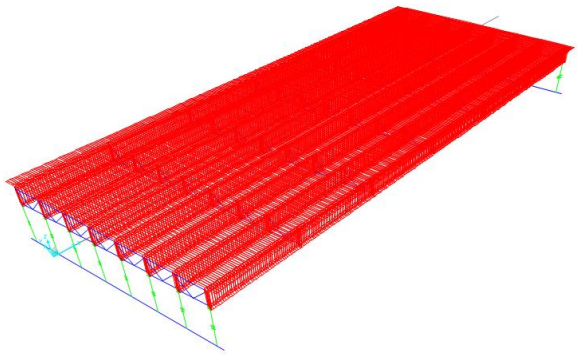

(e) Element Maximum size 0.5”
Figure 4.5 Mesh of I-270 Bridge over Middlebrook Road

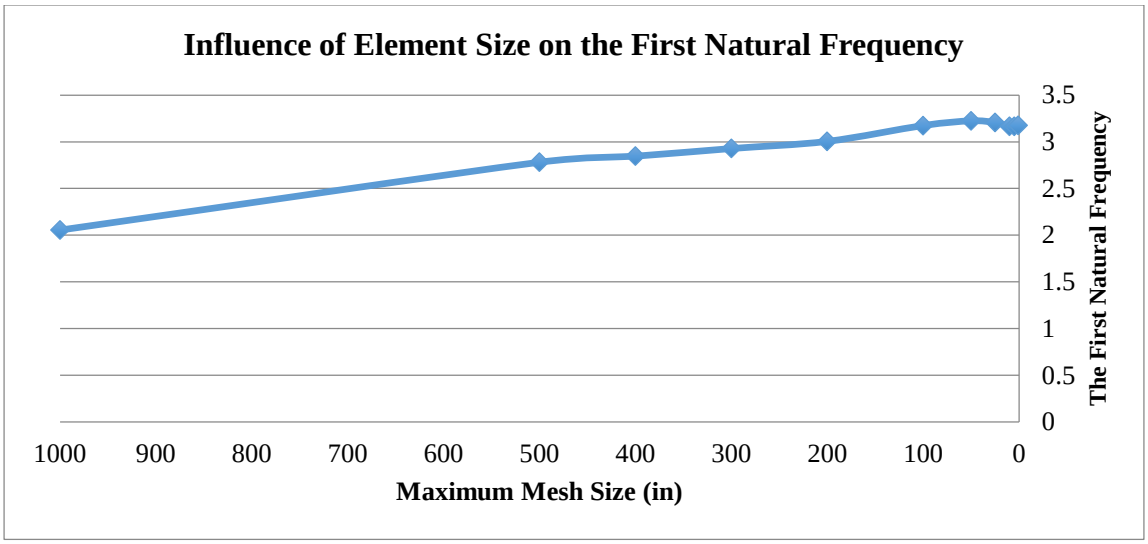

Figure 4.6 Influence of Element Size on the First Natural Frequency

The first natural frequency performed as the measurement during the convergence test. As displayed in Figure 4.6, as the maximum mesh size changed from 1000 in to 0.5 in, the results of the first natural frequency gradually approaching from 2 Hz to 3.20 Hz. The results of the first natural frequency were all below 3 Hz when the maximum mesh size of finite element models were smaller than 200 in, which means that the error rate of the first natural frequency was under 6.25%. When the maximum mesh size was equal to or less than 50 in, the results of the first natural frequency were accurate enough with an

error rate less than 2%. It can then be used as the basis for the selection of a new and accurate finite element mesh in ANSYS.

4.5 Model Validation

4.5.1 Modal Analysis

Modal analysis is used to determine the vibration modes of a structure. These modes are useful to understand the behavior of the structure. They can also be used as the basis for modal superposition in response-spectrum and modal time-history load cases.

Eigenvector analysis was used to determine the undamped free-vibration mode shapes and frequencies of the system. These natural modes can be provided by the generalized equation of motion:

$$(\mu^2[M] + \mu[C] + [K])\{\phi\} = 0 \qquad \text{Equation 4-1}$$

where, {M} is the mass matrix, [C] is the damping matrix, [K] is the stiffness matrix, μ is the eigenvalue and $\{\phi\}$ is the eigenvector. During eigenvalue extraction in CSiBridge and ANSYS, the damping was neglected.

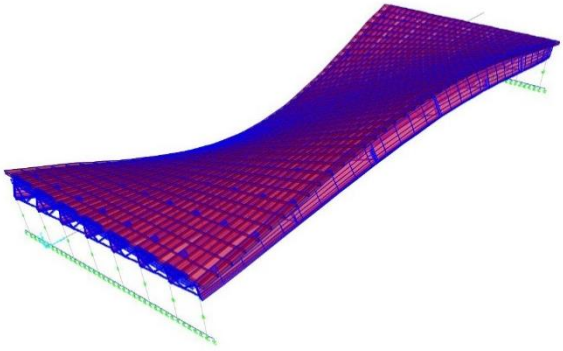

(a) Mode Shape 1 (First Torsion)

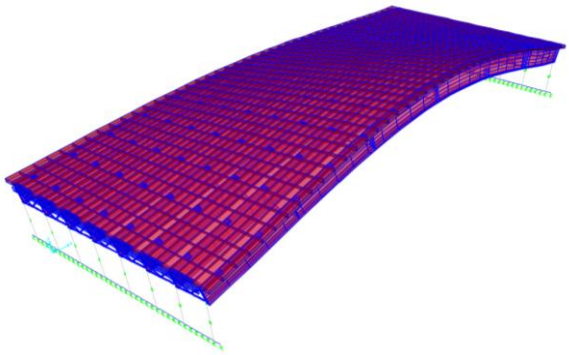

(b) Mode Shape 2 (First Vertical)

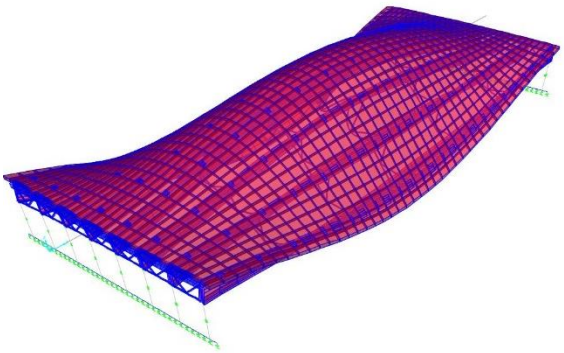

(c) Mode Shape 3 (Second Torsion)

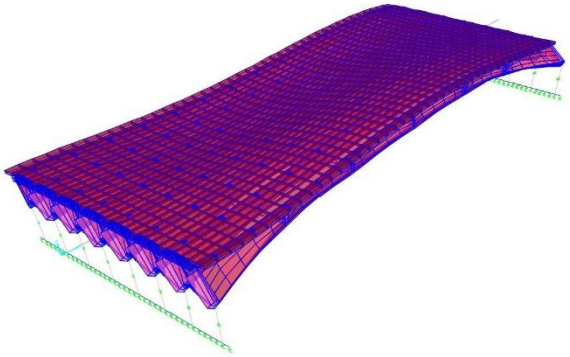

(d) Mode Shape 4 (First Lateral)

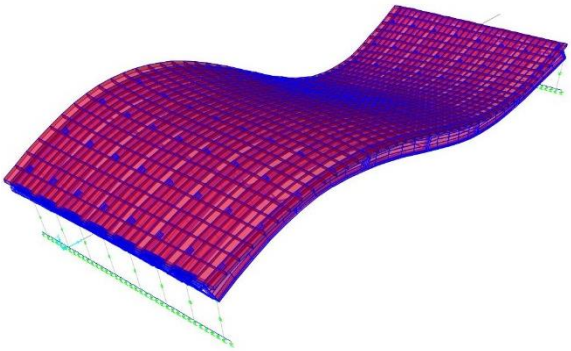

(e) Mode Shape 5 (Second Vertical)

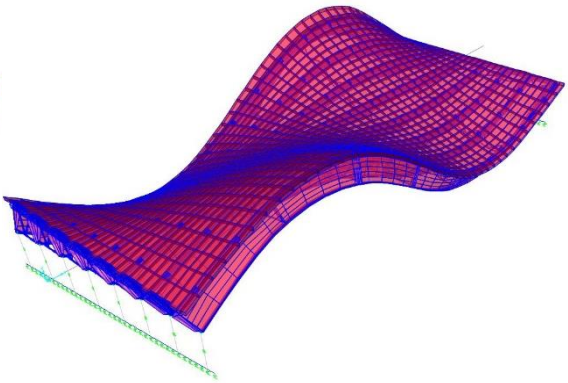

(f) Mode Shape 6 (Third Torsion)

Figure 4.7 Mode Shapes of I-270 Bridge over Middlebrook Road in CSiBridge

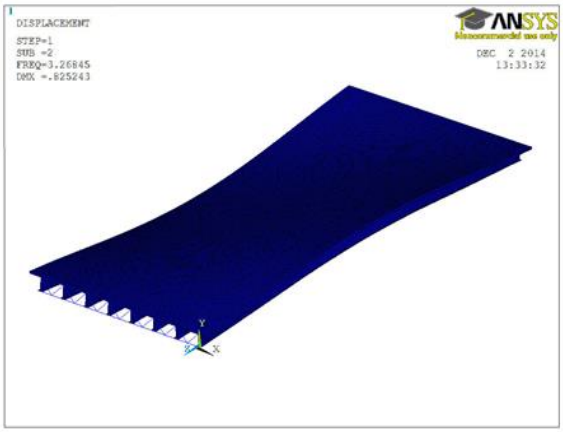

(a) Mode Shape 1 (First Torsion)

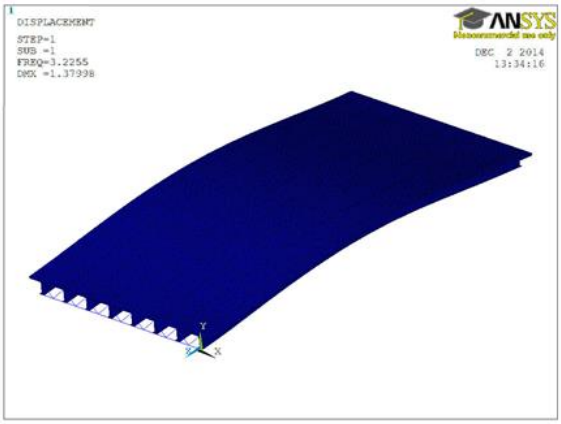

(b) Mode Shape 2 (First Vertical)

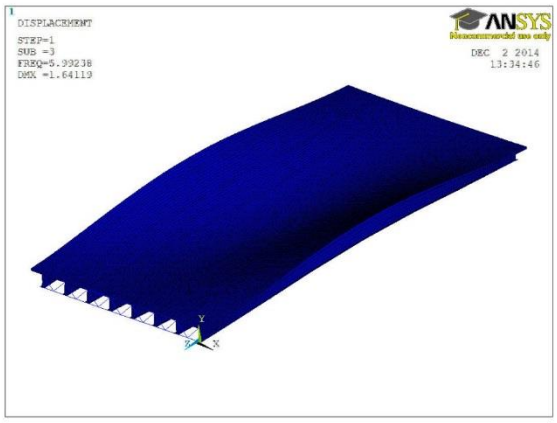

(c) Mode Shape 3 (Second Torsion)

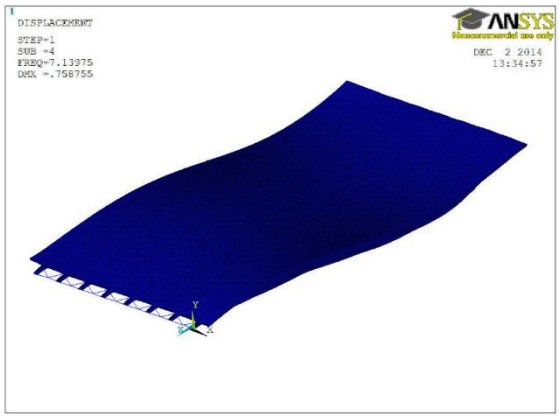

(d) Mode Shape 4 (First Lateral)

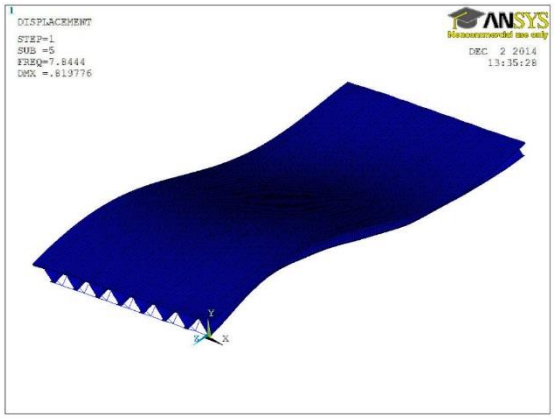

(e) Mode Shape 5 (Second Vertical)

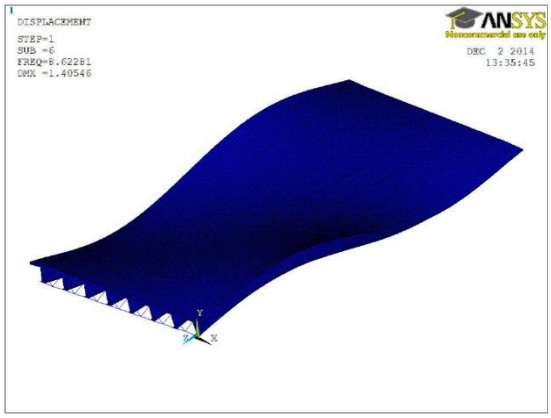

(f) Mode Shape 6 (Third Torsion)

Figure 4.8 Mode Shapes of I-270 Bridge over Middlebrook Road in ANSYS

As a matter of interest, the first six mode shapes of torsion, vertical and lateral modes were shown in Figure 4.7 and 4.8, respectively. To validate our finite element models, experimental data from the field test (will discussed in the next chapter) and numerical results from CSiBridge and ANSYS were studied. In both these numerical studies, the bridge was only subjected to dead load. Table 4-2 gave a comparison between the results obtained from our finite element models and field measurements, specifically for natural frequencies and mode shapes of the bridge. The differences of most of the compared frequencies varied between 0.05% and 6%, which was considered acceptable for the finite element analysis. All the mode shapes of these two models matched with

each other perfectly. Therefore, the CSiBridge model and ANSYS model would be considered as the same.

Table 4-2 Modal Analysis Comparison

Mode Number	Field Test	CSiBridge	ANSYS	Differences (%)	Mode Shape
1		3.2067	3.2255	0.59	First Torsion
2	3.22	3.2451	3.2685	0.72	First Vertical
3		5.6598	5.9924	5.88	Second Torsion
4		7.1363	7.1398	0.05	First Lateral
5		7.8050	7.8444	0.50	Second Vertical
6		8.4718	8.6228	1.78	Third Torsion

4.5.2 Live Load Analysis

Furthermore, both CSiBridge model and ANSYS model were subjected to the standard vehicular live load HS20 with a seed of 55 mph passing through right lane. Figure 4.9 and 4.10 showed the results of displacements and tension stresses of the bottom flange at mid-span of Girder 3. The results matched with each other with the maximum downward displacement of 0.22 in and the maximum tension stress of 1.2 ksi.

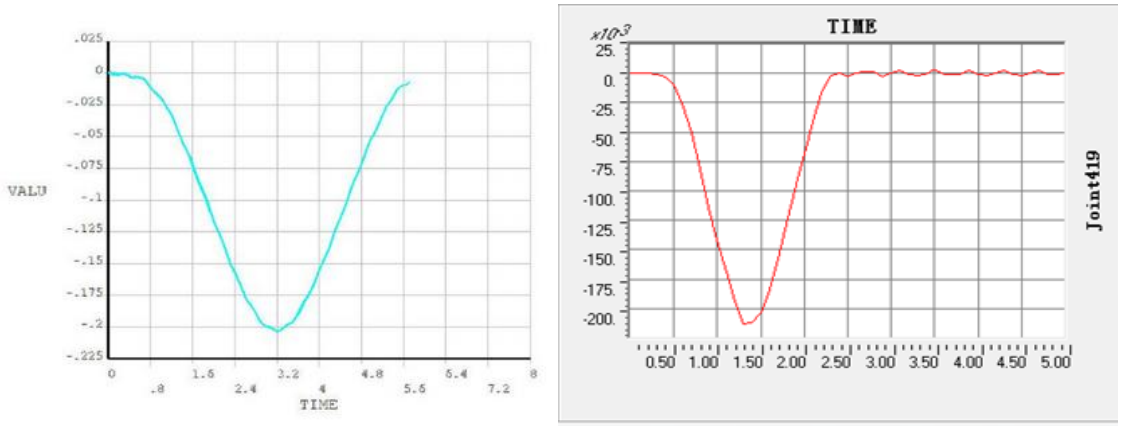

(a) ANSYS Model (b) CSiBridge Model

Figure 4.9 Mid-span Displacement of Girder 3 (a) ANSYS Model (b) CSiBridge Model

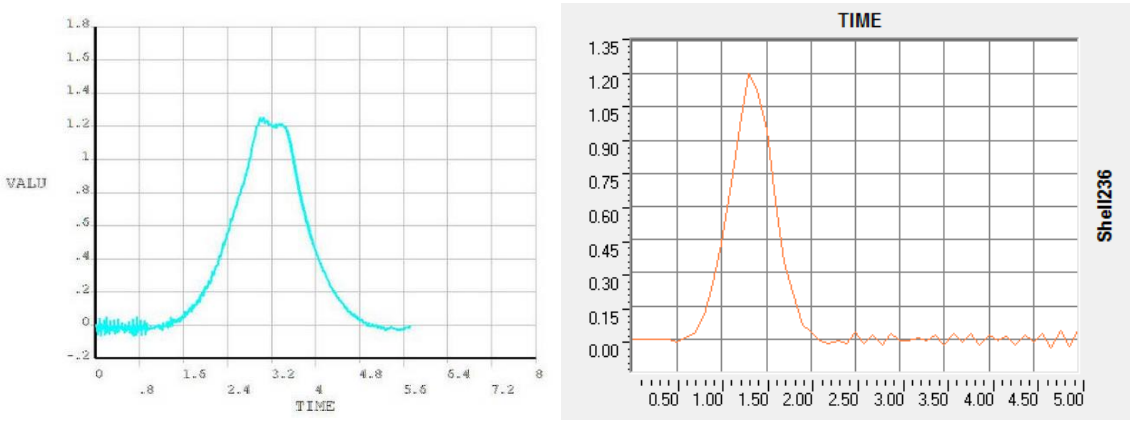

(a) ANSYS Model (b) CSiBridge Model

Figure 4.10 Bottom Flange Stress at Mid-span of Girder 3 (a) ANSYS Model (b) CSiBridge Model

4.6 Local Model: A Case Study

To investigate the stresses or strains of a certain area or a certain joint; and to determine the location of fatigue crack, crack path, and crack rate, there is a need for a series of small, refined sub-models, or local models, which are extracted from the global model, aiming at more effectively evaluate localized behavior for the design of certain components, connections, or systems. The global model of the whole bridge cannot be more refined with the computational time taken into account, and therefore the local model of this critical region can be facilitated for this purpose. When extracting local models, enough buffer zones surrounding the focus area should be included in the refined local models so that the effect of the notch stress concentration maybe negligible.

It is a common issue and also crucial in modeling a local refined model that the boundary conditions of a local model are set up correctly to truly reflect its mechanical connections to the global model. To set up the boundary conditions, the following guidelines should be followed: the boundary nodes should apply the same displacements

obtained from the global model, and the boundary nodes should apply the same external forces obtained from the global model as internal forces.

Since the global model is mesh with far coarser elements than the local model, not all the nodes at the local model correspond to a node on the global model. Therefore, nodes without a corresponding global model are given a displacement determined by bilinear interpolation. The bilinear interpolation is an extension of linear interpolation for interpolating functions of two variables (e.g., x and y) on a regular two-dimensional grid. The key idea is to perform linear interpolation first in one direction, and then again in the other direction. Although each step is linear in the sampled values and in the position, the interpolation as a whole is not linear but rather quadratic in the sample location.

Given the function F at the point P has the value of (Figure 4.11)

$$P = (x, y) \qquad \text{Equation 4-2}$$

Considering the value of F at the four points are:

$$Q_{11} = (x_1, y_1), Q_{12} = (x_1, y_2), Q_{21} = (x_2, y_1), Q_{22} = (x_2, y_2) \qquad \text{Equation 4-3}$$

Then, the value of the function at point P is interpolated having the values at four points at the corners of the grid using the following equations:

$$\begin{aligned} F(x,y)_P = {} & \frac{F(Q_{11})}{(x_2 - x_1)(y_2 - y_1)}(x_2 - x)(y_2 - y) \\ & + \frac{F(Q_{21})}{(x_2 - x_1)(y_2 - y_1)}(x - x_1)(y_2 - y) \\ & + \frac{F(Q_{12})}{(x_2 - x_1)(y_2 - y_1)}(x_2 - x)(y - y_1) \\ & + \frac{F(Q_{22})}{(x_2 - x_1)(y_2 - y_1)}(x - x_1)(y - y_1) \end{aligned} \qquad \text{Equation 4-4}$$

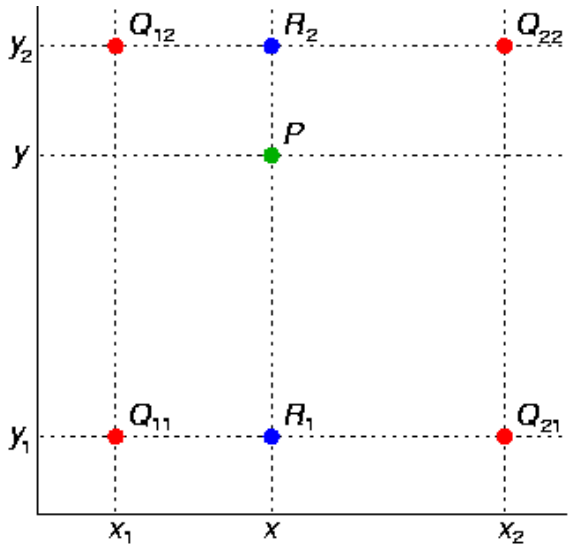

Figure 4.11 Bilinear Interpolation Illustration (Wikipedia, 2015)

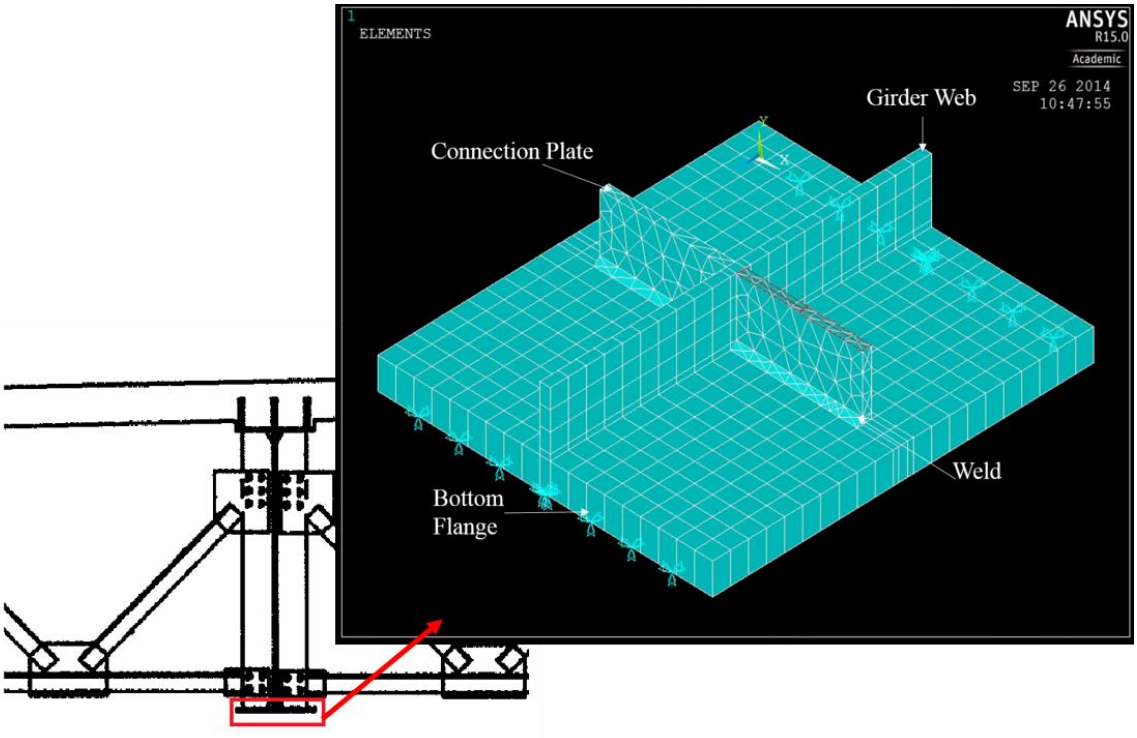

(a) Local Model

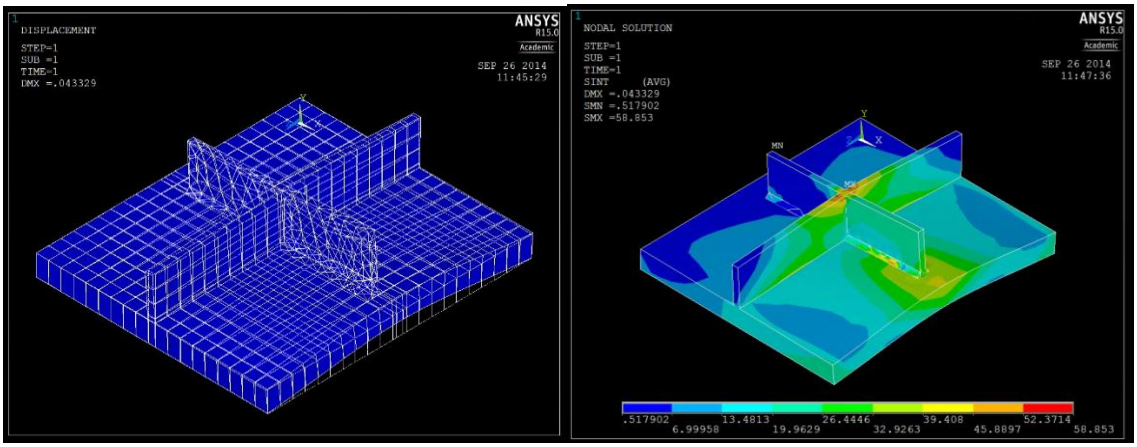

(b)Deformation Shape (c) Node Stress Intensity

Figure 4.12 Local Model

The local model of the welded connection between the lower end of the cross frame connection plate and the girder bottom flange of Girder 3 was generated by using SOLID185 in ANSYS. The local model was cut below the working point of cross frames. It consisted of 10.5-in-long girder web with 3.75-in height and 10.5-in-long bottom flange, two 7-in-wide connection plates with 3.75-in height, and four 7-in-long triangular prisms to simulate the welded connection, which were not taken into account in global models. The comparison between different meshing of the global and local model was displayed in Table 4-3. The more refined local model was subjected to the response determined from the global finite element analysis. The stress concentration is displayed in Figure 4.12.

Table 4-3 Comparison between Golbal and Local Model

Structural Components	Direction (Global Model)	Global Model		Local Model	
		Element Size	Element Divisions	Element Size	Element Divisions
Bottom Flange	Longitudinal	10”	2	1”	23
	Transverse	9”	2	1”	19
Girder Web	Longitudinal	10”	2	1”	23
	Transverse	-	-	9/16”	1
Connection Plate	Longitudinal	-	-	½”	1
	Transverse	7”	1	1”	7

4.7 Summary

This chapter aimed at developing global and local finite element models of highway bridges for fatigue analysis under traffic loading.

A brief review of martial properties and elements commonly used in finite element modeling was presented. As a case study, the three-dimensional global finite element model of the I-270 Bridge over Middlebrook Road was presented using two software: CSiBridge and ANSYS. The efficient mesh size of the elements was determined by the convergence test. The verification of the model was carried out with the help of the measured bridge model characteristics and standard vehicular live load analysis. After comparing the first six natural frequencies and the deflection and tension stress under standard vehicular live load, the two finite element models generated by CSiBridge and ANSYS could be consider as the same in the following study.

The local model of the welded connection between the lower end of the cross frame connection plate and the girder bottom flange of Girder 3 was employed to determine the stress intensification of the fatigue crack. The boundary condition of the local model were given by bilinear interpolation.

Chapter 5 Live Load Time-history Analysis and Results of Highway Bridges under Truck Loading

5.1 Introduction

This chapter focuses on conducting the time-history analysis of highway bridges under simulated truck loading. The single span composite steel I-girder bridge with inverted K-type bracing system is numerically studied with the proposed methodology in Section 5.2. The simulated responses such as displacement and stress of the bridge are examined. Later, preliminary field test and long term monitoring test of the studied bridge are also introduced in Section 5.3. Based on the information from field measurements, simulated numerical results are validated. Meanwhile, the vehicle bridge interaction and the cause of fatigue cracks are discussed in Section 5.4-5.5.Thus, the performance of highway bridges under truck load can be predicted in a more realistic way to estimate the fatigue performance of highway bridges.

5.2 Numerical Time-history Analysis: Case Study on I-270 Bridge over Middlebrook Road

The purpose of the finite elements analysis is to provide appropriate guidance for developing experimental designs and instrumentation plans, and performing experiments on structural elements. Also, it offers an alternative for accurate evaluation of the fatigue analysis for those highway bridges which has not been monitored. Meanwhile, the driving force for critical locations or fatigue cracks is also investigated.

In this case study of I-270 Bridge over Middlebrook Road, since all the fatigue cracks were developed along the horizontal fillet welds connecting the cross frame connection plates to the bottom flange of the girders, the finite element analysis focused on the vertical tensile and horizontal shear stresses along the connection welds due to vehicular loads. The simulated traffic loading obtained from probability based full velocity difference model was filtered before the numerical time-history analysis. Only the truck loading would be applied on the finite element model generated in Chapter 4. The influence of passage cars is negligible because that the total weight of a passage car is very light comparing with that of a truck, and a passage car passing through a bridge only induce a small stress range, usually below 1 ksi. The details of applied truck loading can be seen in Appendix B. Considering the computational efficiency, four 20-min truck flow loading cases would apply on the CSiBridge model of I-270 Bridge over Middlebrook Road.

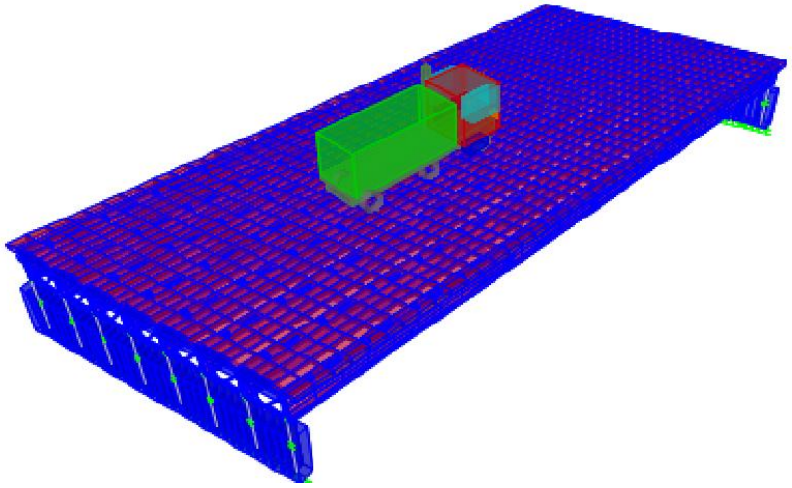

Figure 5.1 Truck Loading

5.2.1 Deflection

Table 5-1 Simulated Maximum Deflections (unit: in)

Girder Number	3	4	5
Midnight	0.1183	0.1363	0.1058
Early Morning and Night	0.1887	0.1952	0.1624
Morning Peak	0.2107	0.2648	0.1724
Noon to Evening	0.1791	0.1980	0.1633

Table 5-1 showed the maximum deflections at mid-span of Girdes 3, 4, and 5 during each 20-min simulation for the four different time periods of one weekday: midnight, early morning and night, morning peak, and noon to evening. The simulated maximum deflections were 0.2107 in at mid-span of Girder 3, 0.2648 in at mid-span of Girder 4, 0.1724 in at mid-span of Girder 5. All of them happened in the time period of morning peak hour, which was probably contributed to the high truck volume of this time period. For each time period, the deflection at mid-span of Girder 4 was always larger than that of Girder 3 and that of Girder 5; the deflection at mid-span of Girder 3 was always larger than that of Girder 5. This was because of the girder location. The right traffic lane is on the top of Girder 3, the middle traffic lane is on the top of Girder 4, and Girder 5 is located at the boundary between the middle and the left traffic lanes. From the traffic monitoring data, it has been shown that over 50% of trucks passing through the bridge by the right traffic lane, and over 98% of trucks passing through the bridge by the right and the middle traffic lanes. Therefore, Girder 4 located at the center left of the middle traffic lane, and Girder 3 located at the center right of the right traffic lane, became the most critical locations for bridge deflections.

5.2.2 Stress

Possible driving forces for the fatigue cracks as shown in Figure 4.2 would have to be vertical tensile stress, horizontal shear stress, or the principal tensile stress

due to their combined actions, along the connection welds. Live load induced stresses in the welded connections between the cross frame connection plates and the girder bottom flanges were extracted in the refined portion of finite element models. A total of four different cases were studied as describe d below and key results summarized in Table 5-2. For all the four cases analyzed, the longitudinal positions of trucks remained the same with previous deflection studies.

Table 5-2 Stresses in Cross Frame Connection Plate-to-Girder Bottom Flange Connections at G3 without Dynamic Impact (unit: ksi)

Time Period	Max Vertical Stress	Max Shear Stress	Max Principal Stress
Midnight	6.665	2.165	7.629
Early Morning and Night	7.586	2.563	8.70
Morning Peak	12.94	4.327	14.84
Noon to Evening	7.905	2.664	9.061

There were certainly many live load cases that can produce great tensile stresses in the connections of concern. The simulated truck loading contained most of the possible truck loading patterns. Magnitudes of tensile stresses in the connection plates depend on the magnitudes and positions of wheel loads of crossing vehicles. The stresses listed in Table 5-2 are for illustration and are taken from connection plates at Girder 3 for the four different time periods.

A comparison of live load cases for the four different time periods suggested that live loads during morning peak caused the highest tensile stress in the connection of concern with a value of 12.94 ksi. All the shear stresses in the connections welds were much lower than the vertical stresses at the same spot during each time period.

The detailed time-history results of the connection welds at Girder 3 corresponding to the four different time periods are shown in Figures 5.2-5.5. Each peak and valley corresponded to one truck loading pattern.

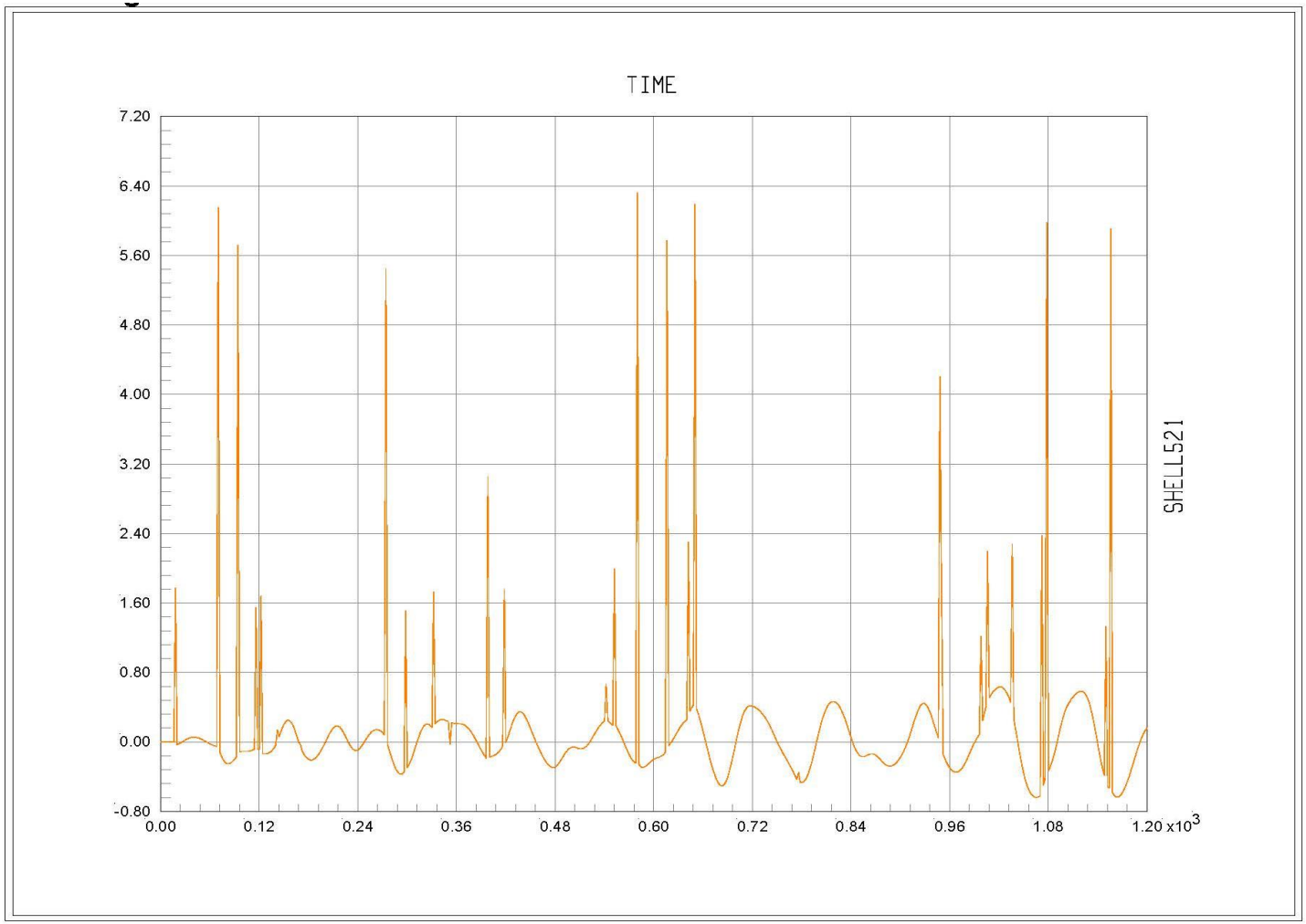

Figure 5.2 Time-History Results of Vertical Stress during Midnight

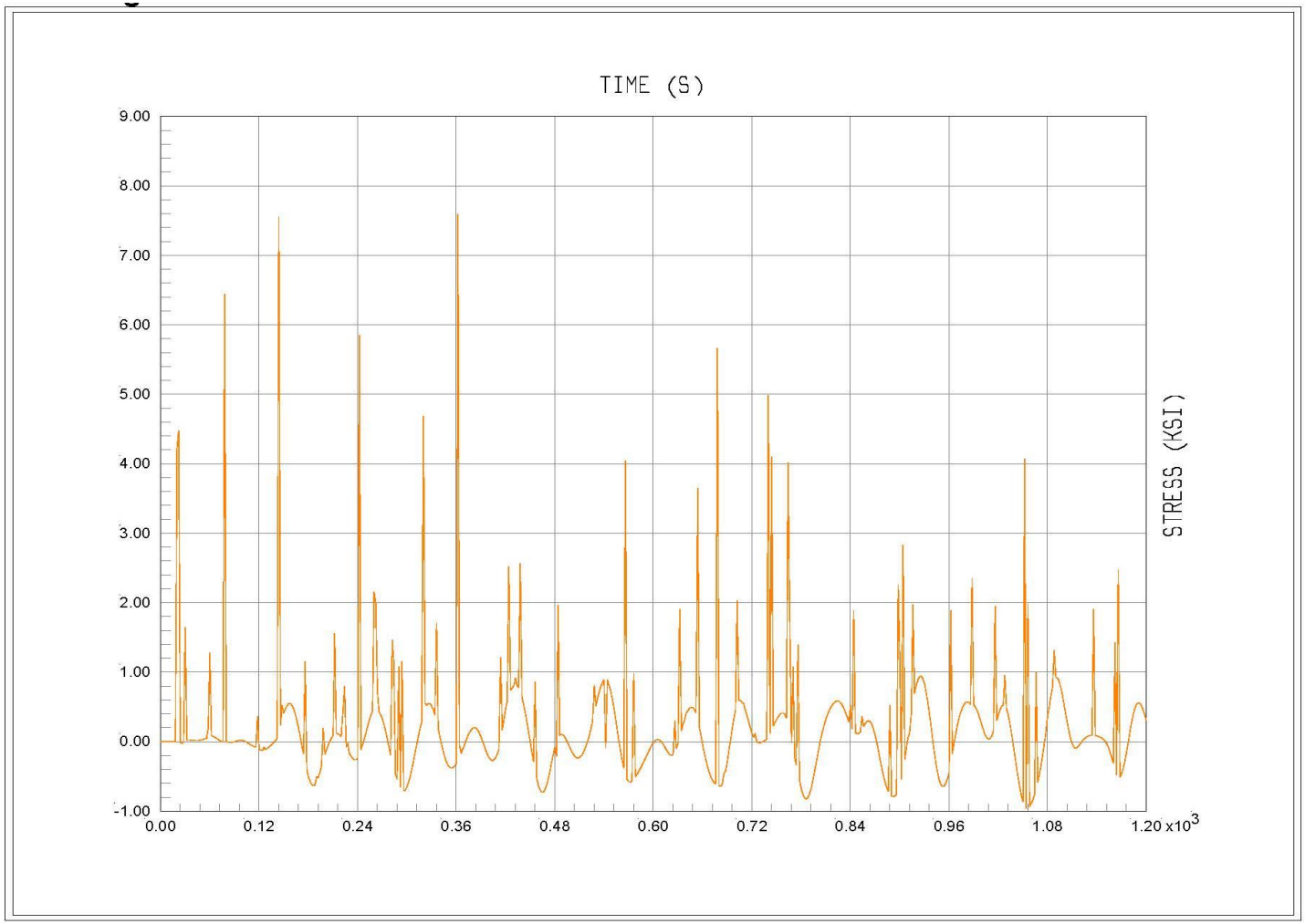

Figure 5.3 Time-History Results of Vertical Stress during Early Morning and Night

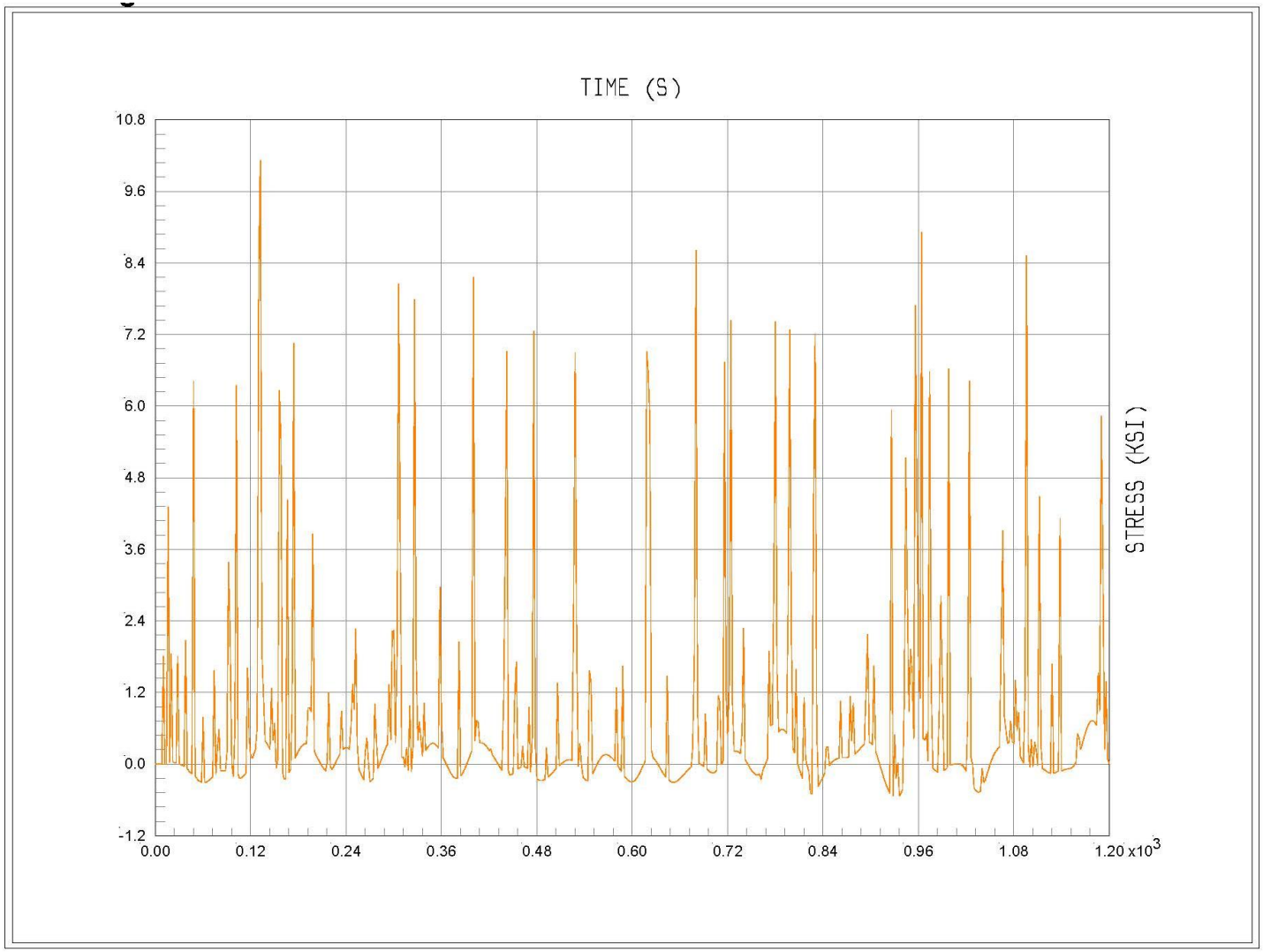

Figure 5.4 Time-History Results of Vertical Stress during Morning Peak

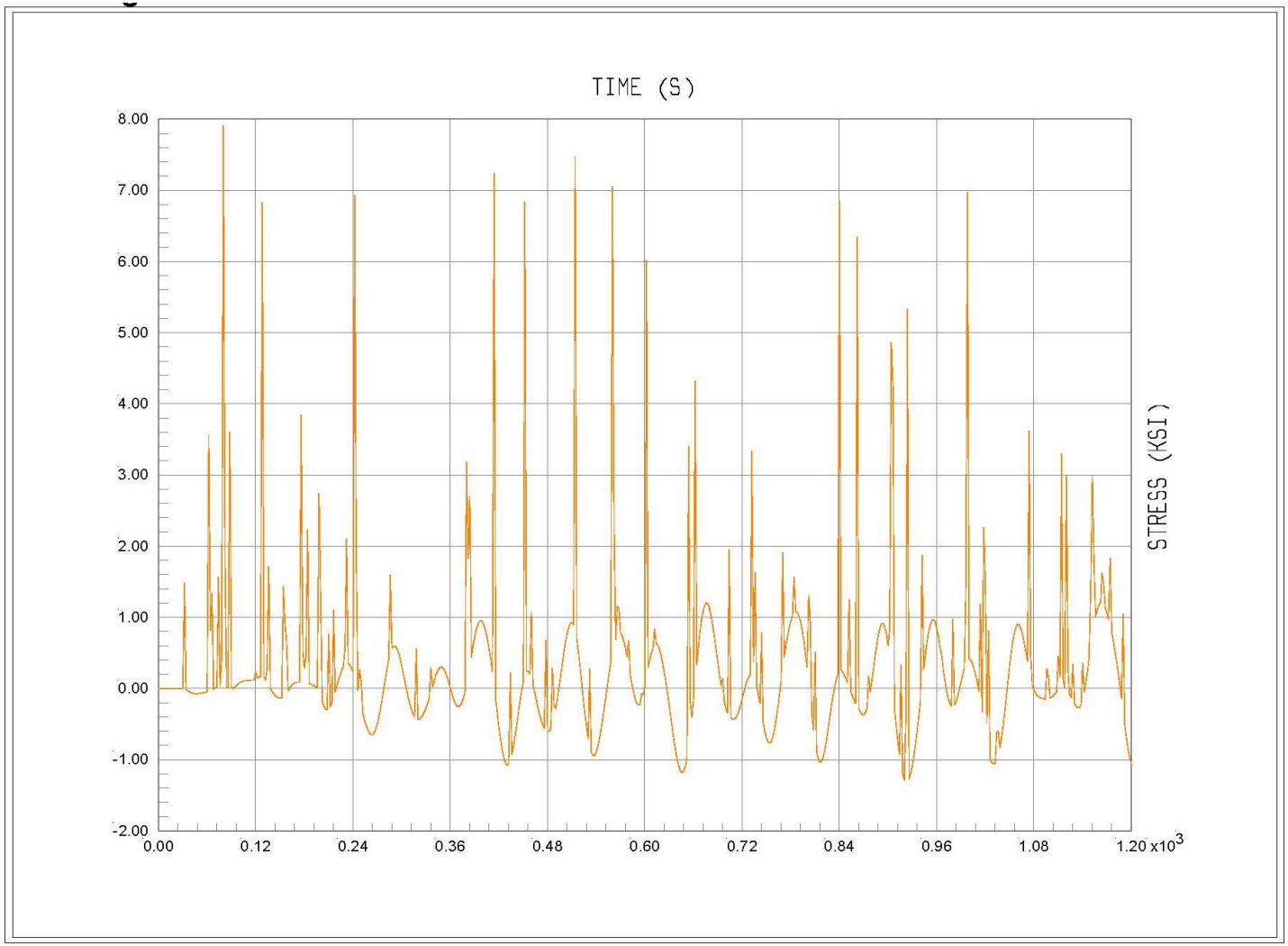

Figure 5.5 Time-History Results of Vertical Stress during Noon to Night

Compressive stress was observed at the symmetry position of the connection plate at the uncrack side on the north face. Figures 5.6 and 5.7 show the stress contour of the connection plates of Girders 3 and 4 at the most critical moments during morning peak hour. The blue area represents intensive tensile stress, the red area displays intensive compressive stress, and the yellow area reveals the balanced situation. The tensile stress concenters around the connection weld at the crack side, and the compressive stress concenters around the connection weld at the uncrack side. The stress also intensifies around the connection points of cross frames and connection plates. However, this is mainly because of the intersection area of cross frames and connection plates are modeled by a node. In fact, the stress would not be so high at the intersection area. The maximum tensile stress of connection plate at Girder 3 happened at the T=597 s; while the maximum tensile stress of connection plate at Girder 4 happened at the T=283 s due to the simulated truck loading. It should be noted that the live load induced stresses of connection plates were much localized around the weld connections. The stress would not spread from the bottom to the top of connection plates.

Time-history analysis of the crack side and uncrack side on the north face of Girder 3 and 4 has been carried out for further study. Figures 5.8 and 5.9 presents the time-history results during morning peak hour. The orange curve stand for the tensile stress, and the green curve is on behalf of the compressive. The same trend happened for the other three time periods. The crack side of the connection plates is always under tensile stress, while the uncrack side is always under compressive stress.

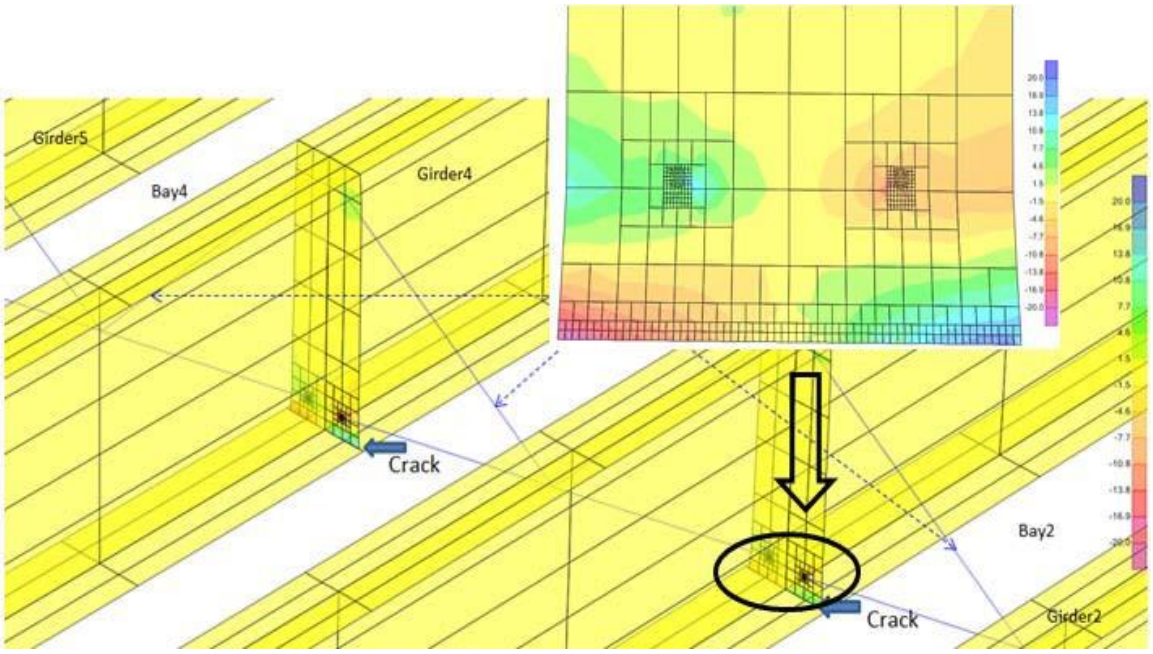

Figure 5.6 Zoom-in Stress Contour of Connection Plate (Girder 3 Diaphragm 3) at T=597second during Morning Peak

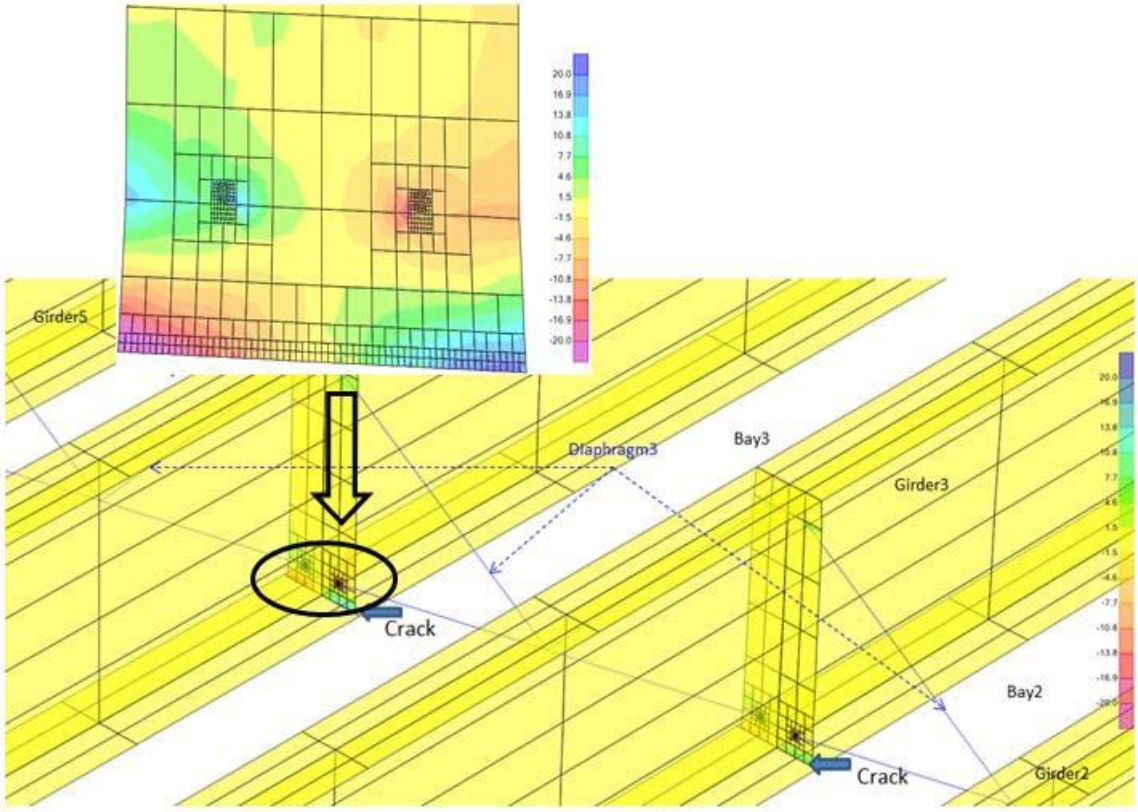

Figure 5.7 Zoom-in Stress Contour of Connection Plate (Girder 4 Diaphragm 3) at T=283second during Morning Peak

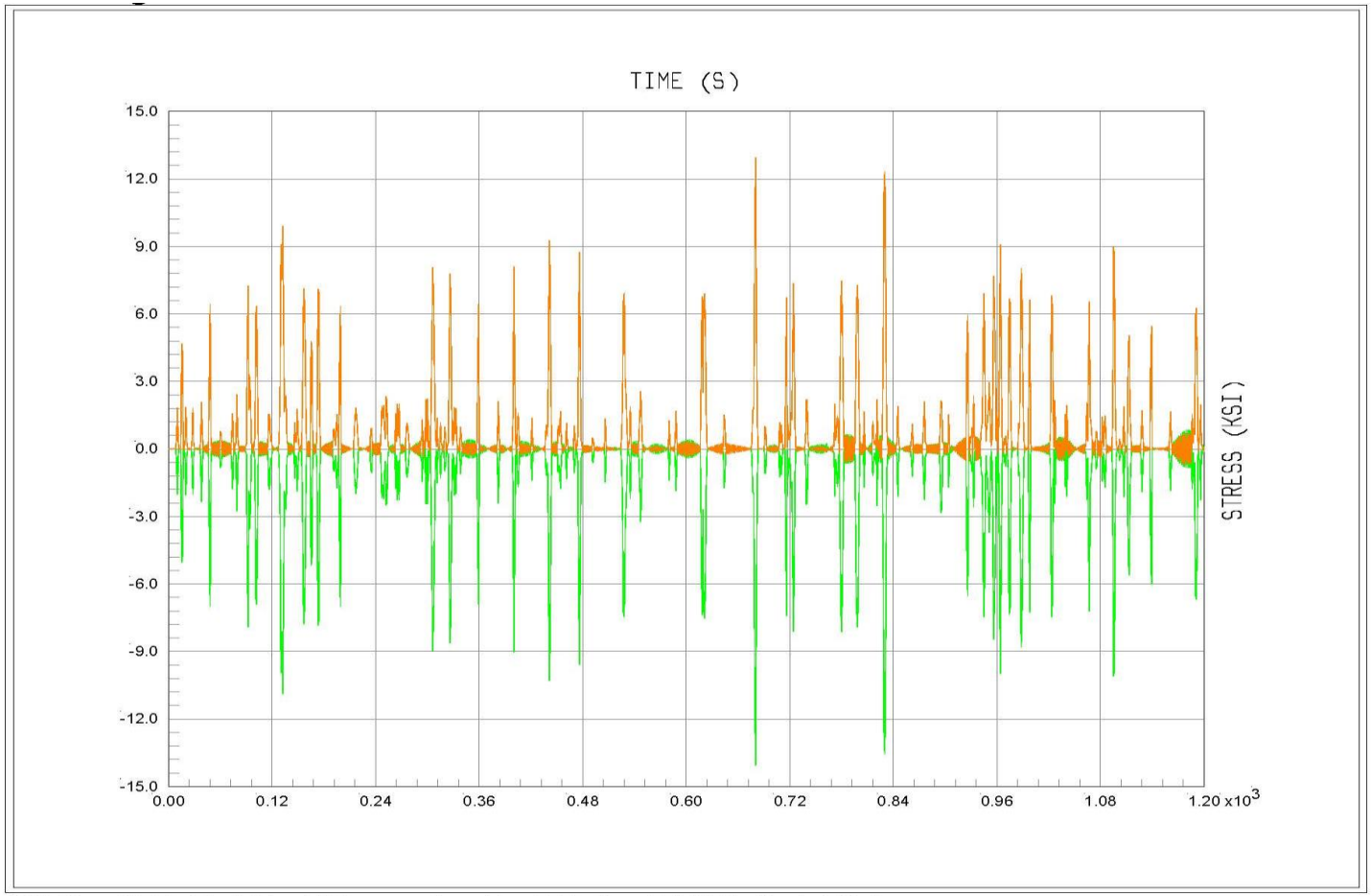

CSiBridge v15.2.0 - File:Bridge_I-270_connection plate - 5-10 - Case:TRUCKS - Kip, in, F Units
Shell655, Shell521 Vs TIME
Min is -1.407e+01 at 6.8000e+02 Max is 1.294e+01 at 6.8000e+02

Figure 5.8 Time-History Results of Vertical Stress on Crack side and Uncrack at Girder 3

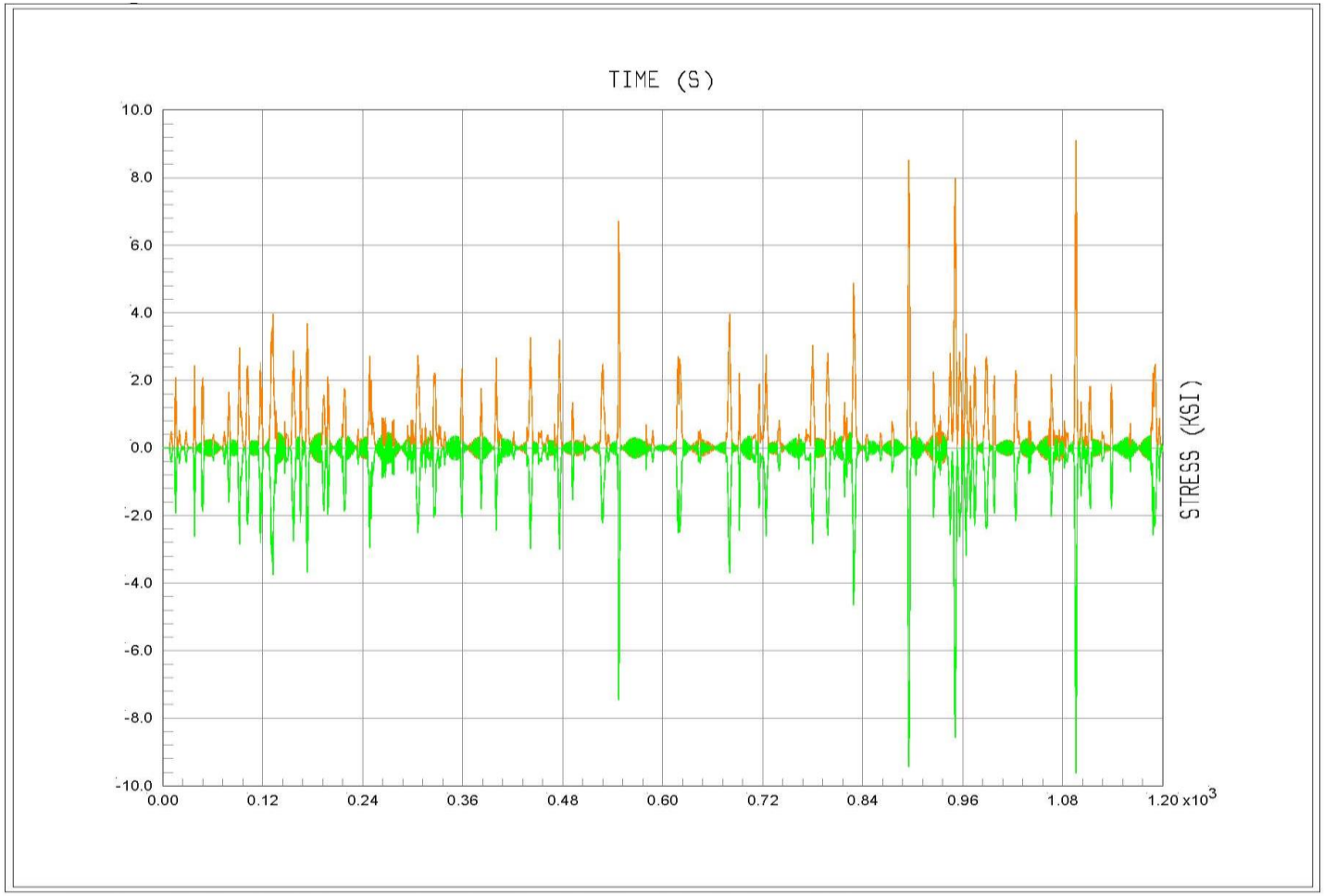

Figure 5.9 Time-History Results of Vertical Stress on Crack side and Uncrack at Girder 4

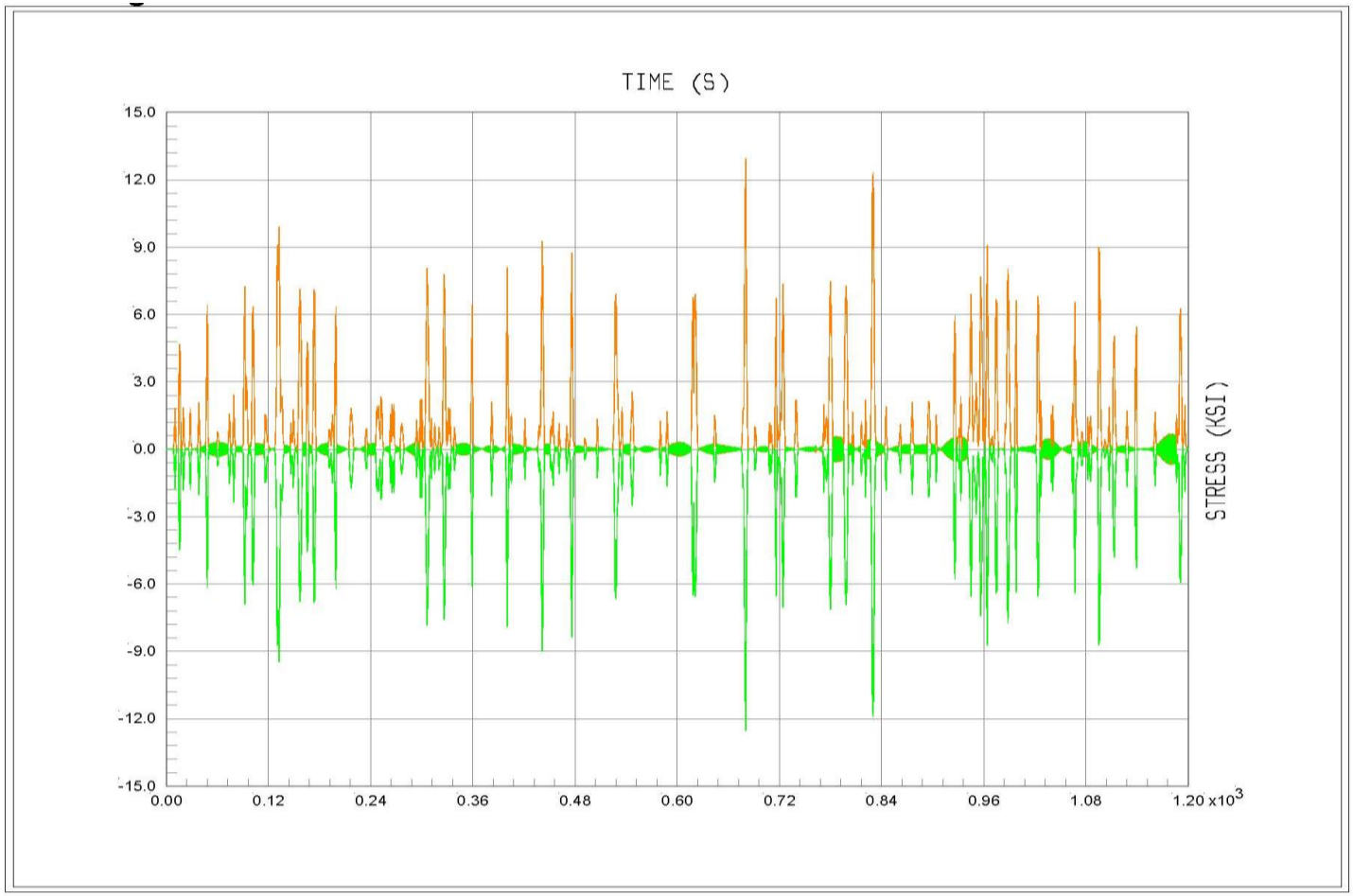

CSiBridge v15.2.0 - File:Bridge_I-270_connection plate - 5-10 - Case:TRUCKS - Kip, in, F Units
Shell521, Shell521-1 Vs TIME
Min is -1.253e+01 at 6.8000e+02 Max is 1.294e+01 at 6.8000e+02

Figure 5.10 Time-History Results of Vertical Stress on the north face and the south face of Girder 3

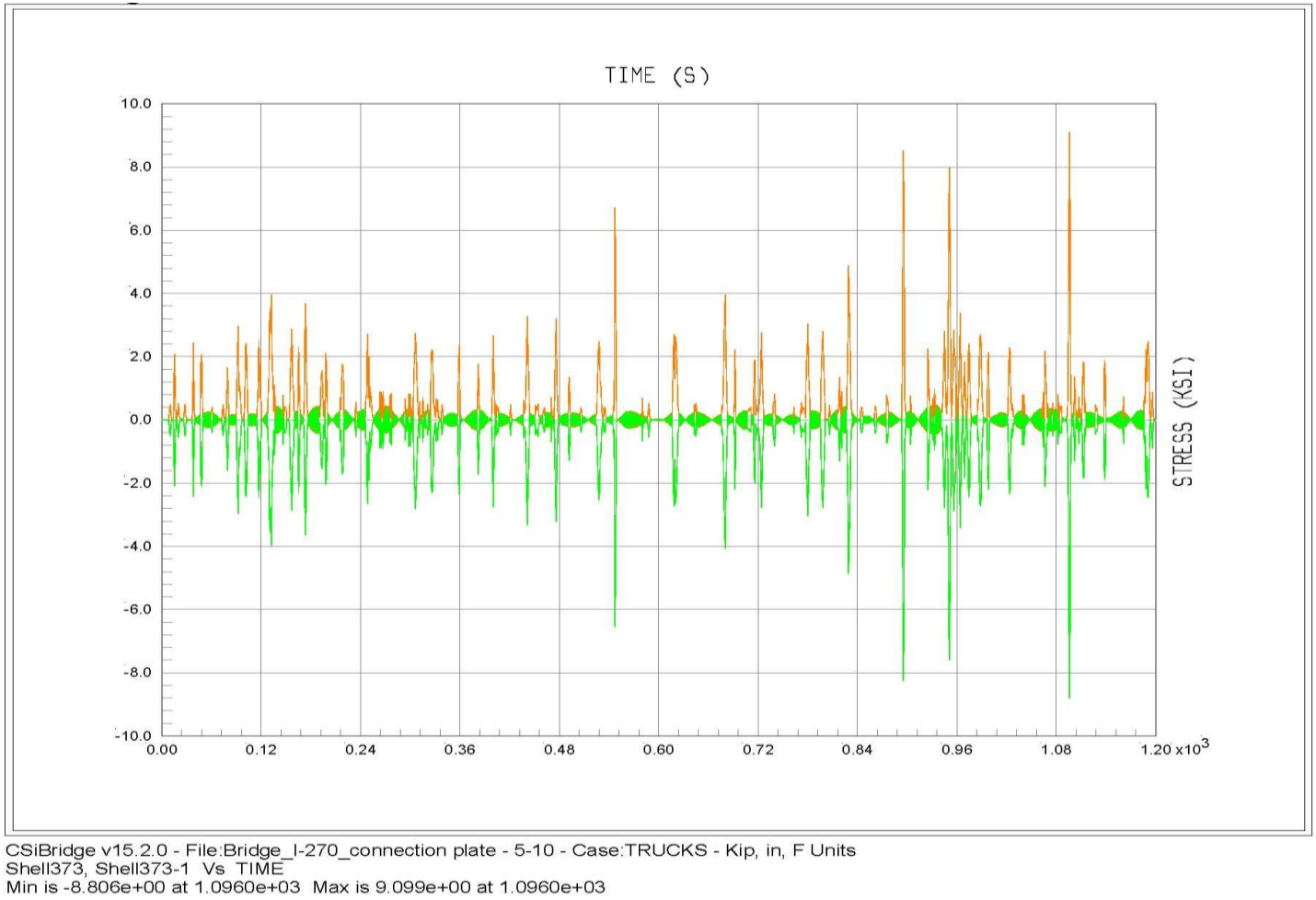

Figure 5.11 Time-History Results of Vertical Stress on the north face and the south face of Girder 4

Figures 5.10 and 5.11 are time-history results of the north face and the south face of the connection plate at the crack side of Girders 3 and 4. The orange curve stands for the tensile stress, and the green curve is on behalf of the compressive. The results reveal that at the same spot of the crack side, the north face and the south face bearing the same stress at the opposite direction.

The following observations can be made from the limited finite element analysis:

The passage of trucks on the bridge deck can cause vertical tensile stresses in the welded connections between cross frame connection plates and girder bottom flanges. These stresses are highest at the outer edge of the connection plate where all the existing fatigue cracks on the I-270 Bridge over Middlebrook Road have initiated from. Girder 4 located at the center left of the middle traffic lane, and Girder 3 located at the center right of the right traffic lane, are the most critical locations for bridge deflections.

The live load induced stresses of connection plates are much localized around the weld connections and would not spread from the bottom to the top of connection plates. For the same face of the connection plate, both tensile and compressive stresses are observed at the symmetry positions around the girder web. The crack side of the connection plates is always under tensile stress, while the uncrack side is always under compressive stress during each time period. At the same spot of the crack side, the north face and the south face bear the same stress at the opposite direction.

5.3 Field Test and Results of I-270 Bridge over Middlebrook Road

The field test of the I-270 Bridge over Middlebrook Road with active fatigue cracks was conducted through a Wireless Integrated Structural Health Monitoring (ISHM) System. This smart bridge condition monitoring system termed ISHM system, which features a number of technology innovations, including remote sensing capability, piezo paint acoustic emission sensors, wind and solar based energy harvesting devices to power sensor network, high-speed wireless sensing ability and advanced data analysis methods for remaining life estimation of aging bridges. Through successful advancement and commercialization in the state-of-the-art technology of remote infrastructure sensing, the ISHM system is promising to reduce life cycles costs while significantly maintaining the sustainability of the highway infrastructures in the US. Complete pilot testing was performed by using acoustic emission (AE), accelerometer, deflection, and strain sensors for bridge information collection.

5.3.1 Instrumentation Plan

The main data acquisition systems used in this test consisted of PXI-based data acquisition system by National Instruments, which was used for data collection by BDI strain transducers, string pots and AE sensors, and multi-channel data acquisition equipment CR5000 manufactured by Campbell Scientific, Inc. for extra BDI strain transducer. Types of sensors used in this project are: 1. piezoelectric paint AE sensors; 2. wireless accelerometers; 3.laser sensor; 4. ultrasonic distance sensors; 5. BDI strain transducers; and 6. String pots. Instrumentation plan is shown in Figure 5.12 Crack locations and sensor placement. Girder displacement and stress range records due to truck traffic were part of field measurements in this study.

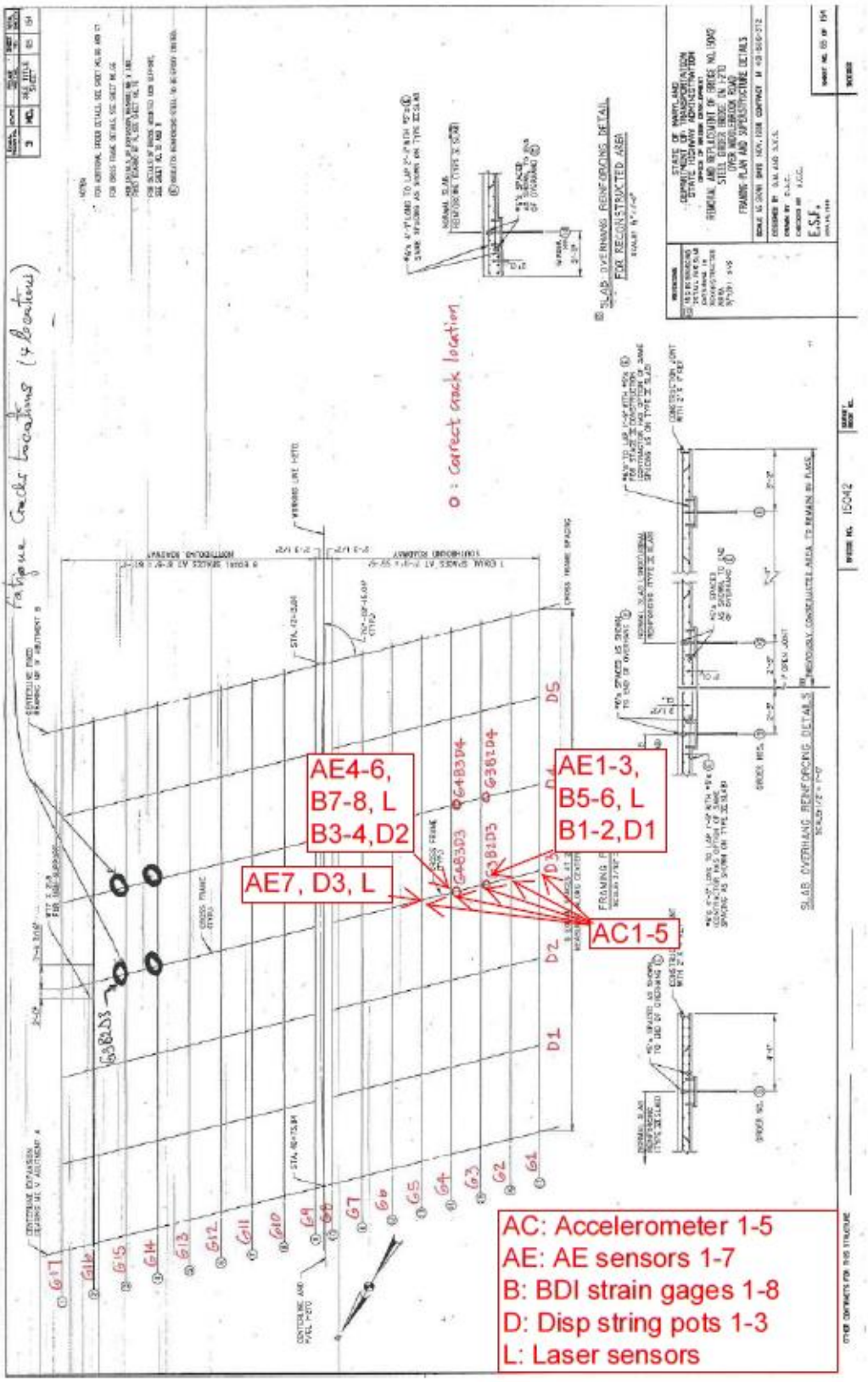

Figure 5.12 Crack Locations and Sensor Placements on the Framing Plan

5.3.2 Vibration Response

Figure 5.13 Wireless Sensor Imote2 (Measuring Acceleration and Temperature)

A total of four wireless accelerometers Imote2 were used to monitor the vibration responses of the bridge (Figure 5.13). One wireless sensor was installed on one of the girders (Girders 2 to 5) and acceleration data was acquired at 100 Hz sampling rate synchronically. The acceleration data was used to provide modal frequency information (Figure 5.14) that can be used to calibrate the finite element model of the bridge. The fundamental frequency thus measured is 3.22 Hz, which is very close to the value of the first vertical mode from finite element analysis (3.24 Hz) discussed in Chapter 4.

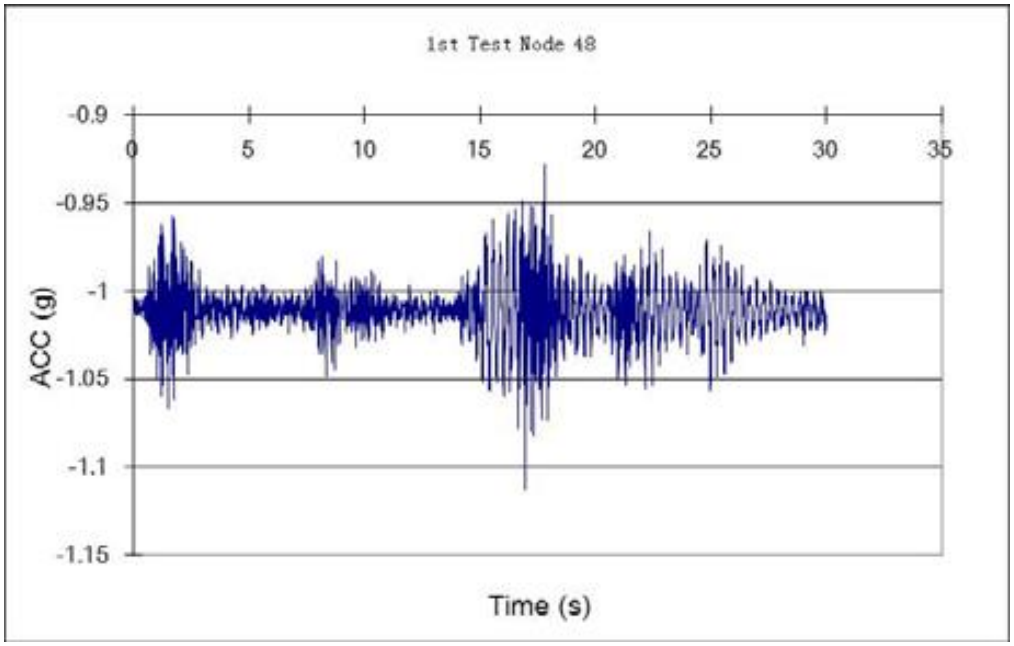

(a) Acceleration Time History

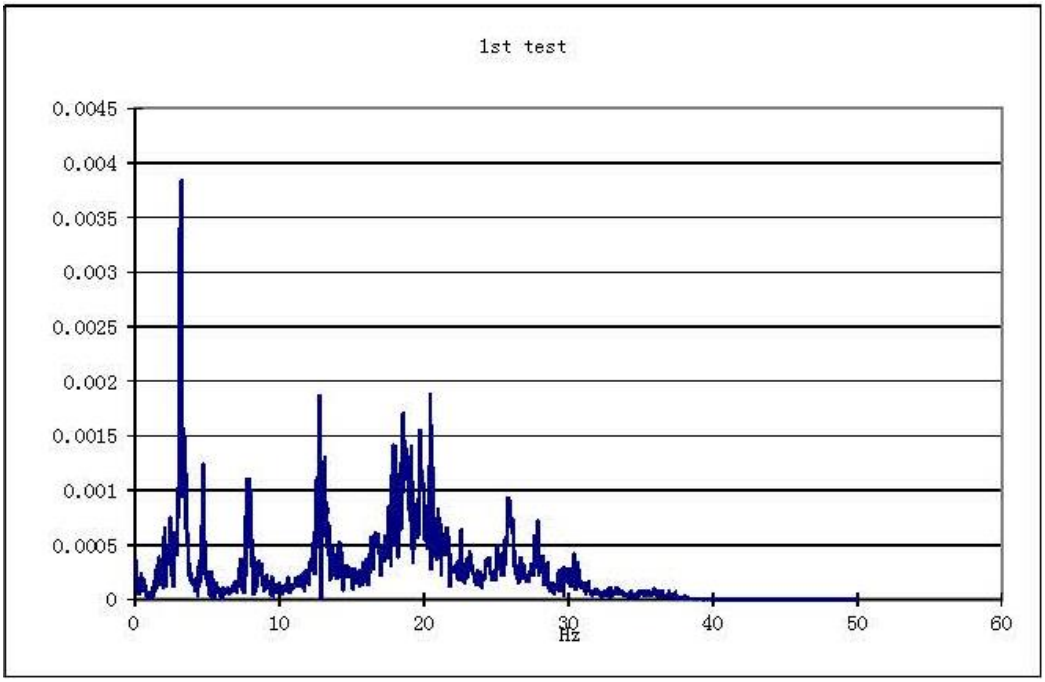

(b) FFT of Acceleration Data (Horizontal Axle: Frequency; Vertical Axle: FFT Amplitude)

Figure 5.14 Acceleration Data Measured by Wireless Sensor

Seven wireless piezoelectric sensors were also applied in the vibration test. The instrumentation plan and the first frequency results are displayed in Figure 5.15.

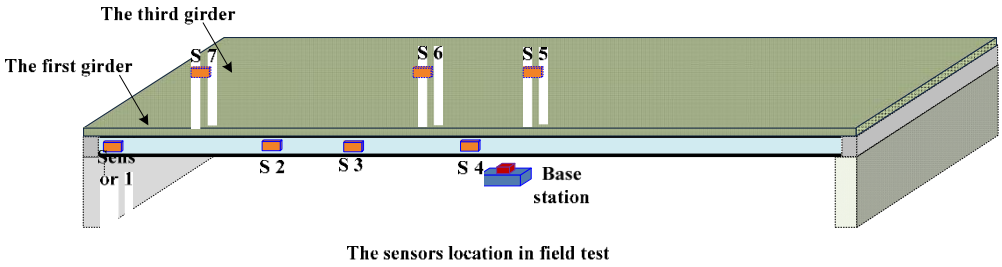

(a) instrumentation plan

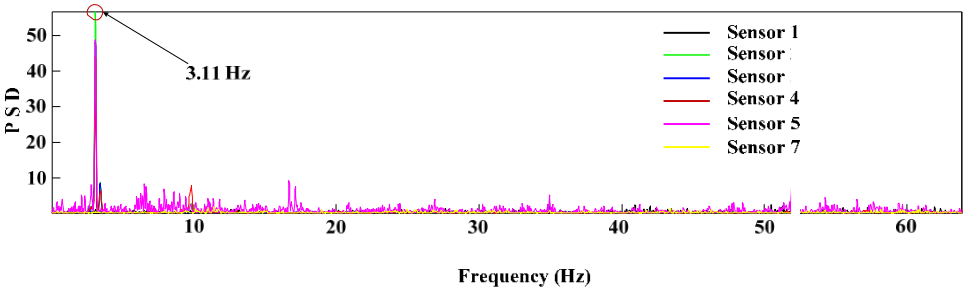

(b) Frequency

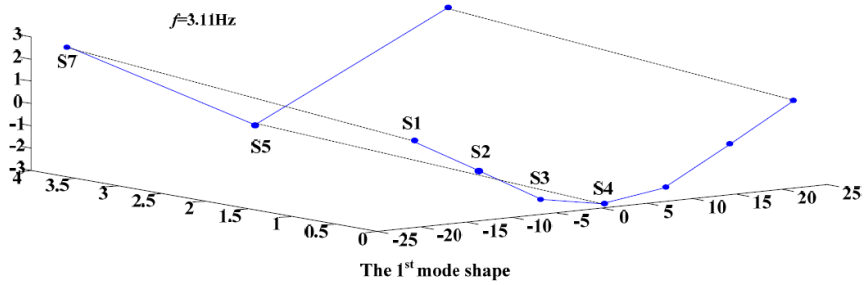

(c) The First Mode Shape

Figure 5.15 Frequency Results Measured by Wireless Piezoelectric Sensor

5.3.3 Bridge Deflection

Both laser sensor and ultrasonic distance sensors were used to measure the dynamic deflection of the bridge. Only one laser sensor and one ultrasonic distance sensor were used each time. The data from laser sensor is shown in Figure 5.15. The measured deflection value from the laser sensor agrees well with the string pot, and its

accuracy is also validated by the fundamental frequency indicated by FFT of the laser sensor measured deflection data (Figure 5.16).

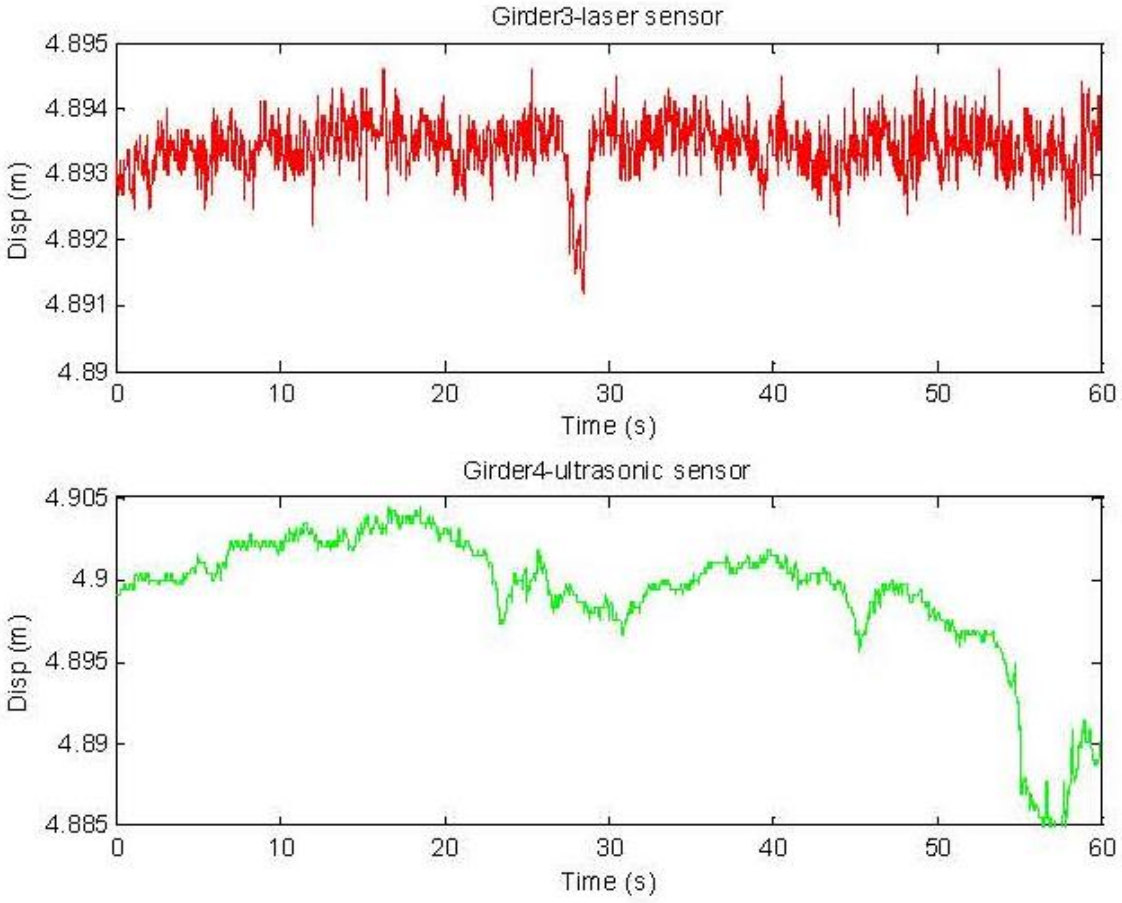

Figure 5.16 Bridge Deflection Data by Laser Sensor (Upper) and Ultrasonic Sensor (Lower) (The Measured Value is the Distance between the Sensor and Girder Bottom Surface)

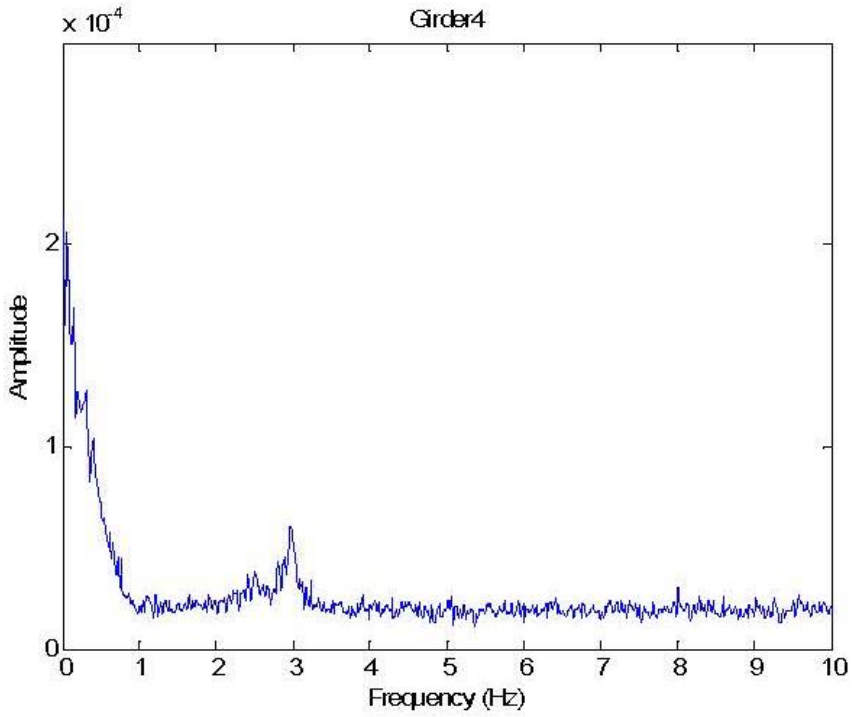

Figure 5.17 FFT of laser distance sensor (note the existence of fundamental frequency of the bridge near 3 Hz)

Table 5-3 Maximum Deflection Measured by Laser Sensor

Girder Number	3	4	5
MaxD (in)	0.2598	0.2717	0.2480

5.3.4 Stress

(b) Details at G3B2D3

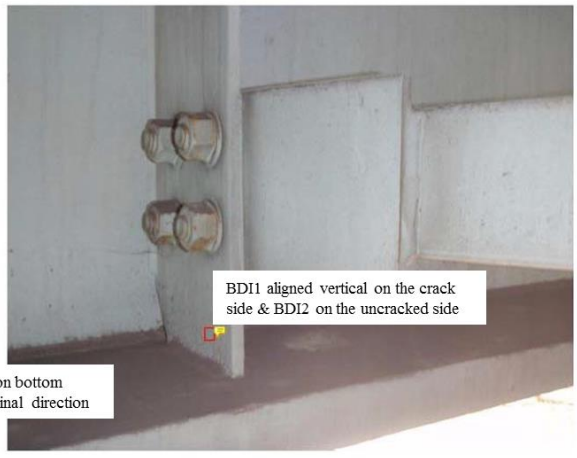

(c) Details at G3B3D3

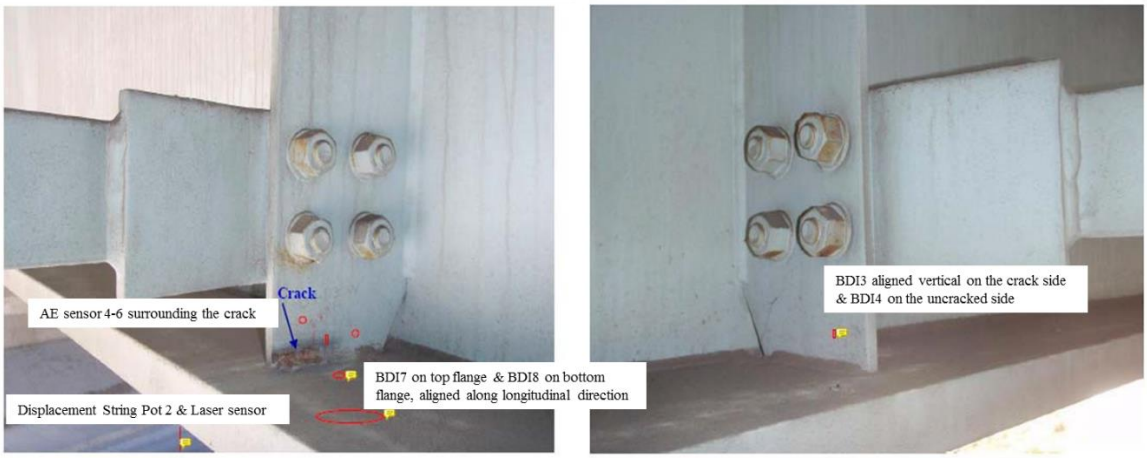

(d) Details at G4B3D3 (e) Details at G4B4D3

Figure 5.18 Crack Locations and Sensor Placements

Cracks always occur in the direction essentially perpendicular to the direction of principal tensile stress. In order to assess the driving force of the fatigue cracks in the connection welds, strain gages were placed vertically on the connection plate just beyond the tip of the existing crack. Strain gages were also placed longitudinally on the girder flanges to correlate with the occurrence of vehicular loads. Compared with analytical methods, field test is the most accurate method since no assumptions need to be made for uncertainties in load distribution such as unintended composite action between structural components, contribution of nonstructural members, stiffness of various connections, and behavior of concrete deck in tension. The actual strain histories experienced by bridge components are directly measured by strain gages at the areas of concern. The effects of varying vehicle weights and their random combinations in multiple lanes are also reflected in the measured strains.

BDI 1-4 strain transducers were placed on both sides of the connection plates while BDI 5- 8 were placed on the top and bottom flanges on Girders 3 and 4 (Figure 6.17). Since each transducer is unique and individually calibrated, their numbers are marked on Figure 6.18 for identification. Figures 6.19 and 6.20 were showing the stresses

on the flanges and connection plates, respectively. The maximum stress measured on the bottom flange was 1.604 ksi in tension for BDI 3215 on the bottom flange of Girder 3 due to regular traffic, which was low comparatively. As for the connection plates, the maximum stresses were 6.18 ksi in tension for BDI 1641 on Girder 3 and 16.1 ksi in tension for BDI 1644 on Girder 4.

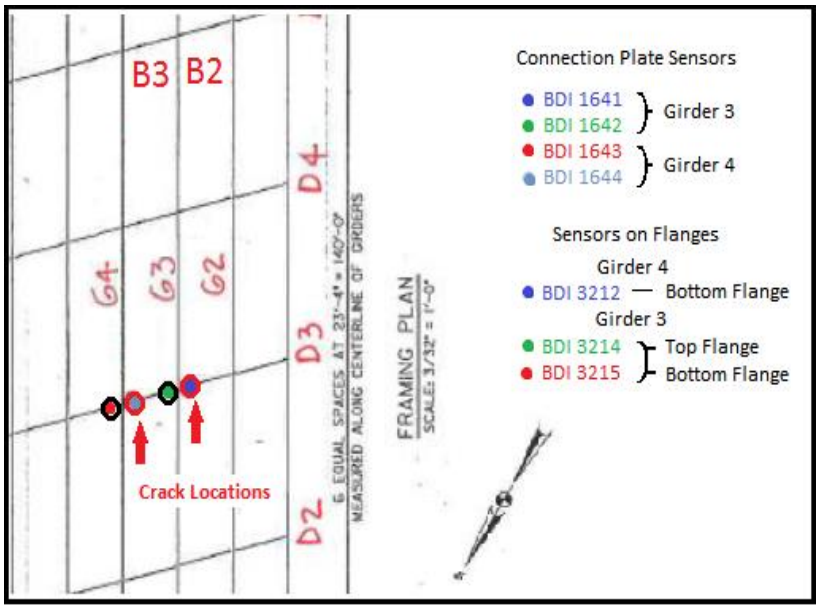

Figure 5.19 BDI Strain Transducer Locations and Marked Numbers

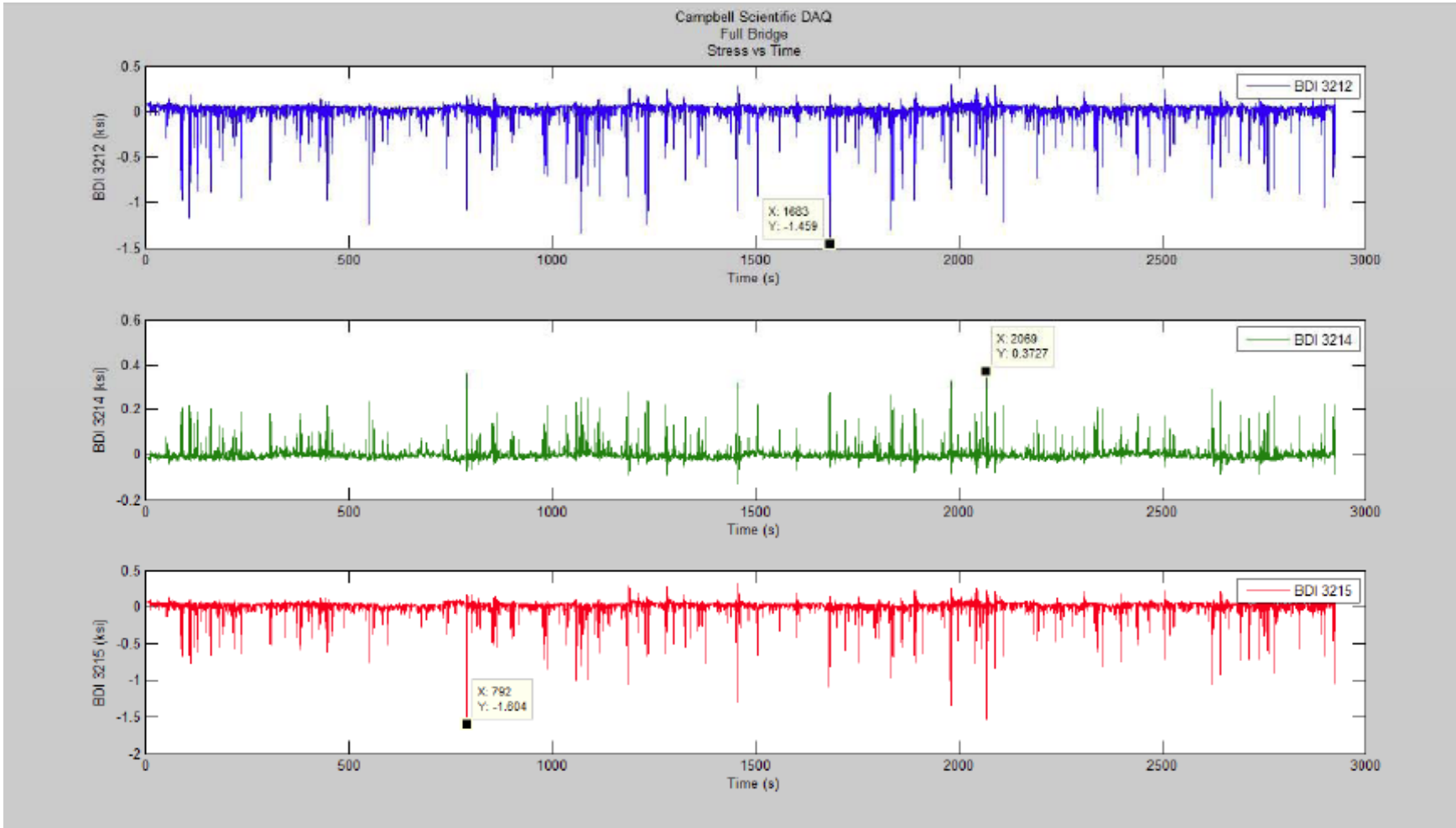

Figure 5.20 BDI Strain Transducer Flange Measurements on Girders 3 and 4 (Positive Indicates Compression; 3212 G4 Top Flange; 3214 G3 Top Flange and 3215 G3 Bottom Flange)

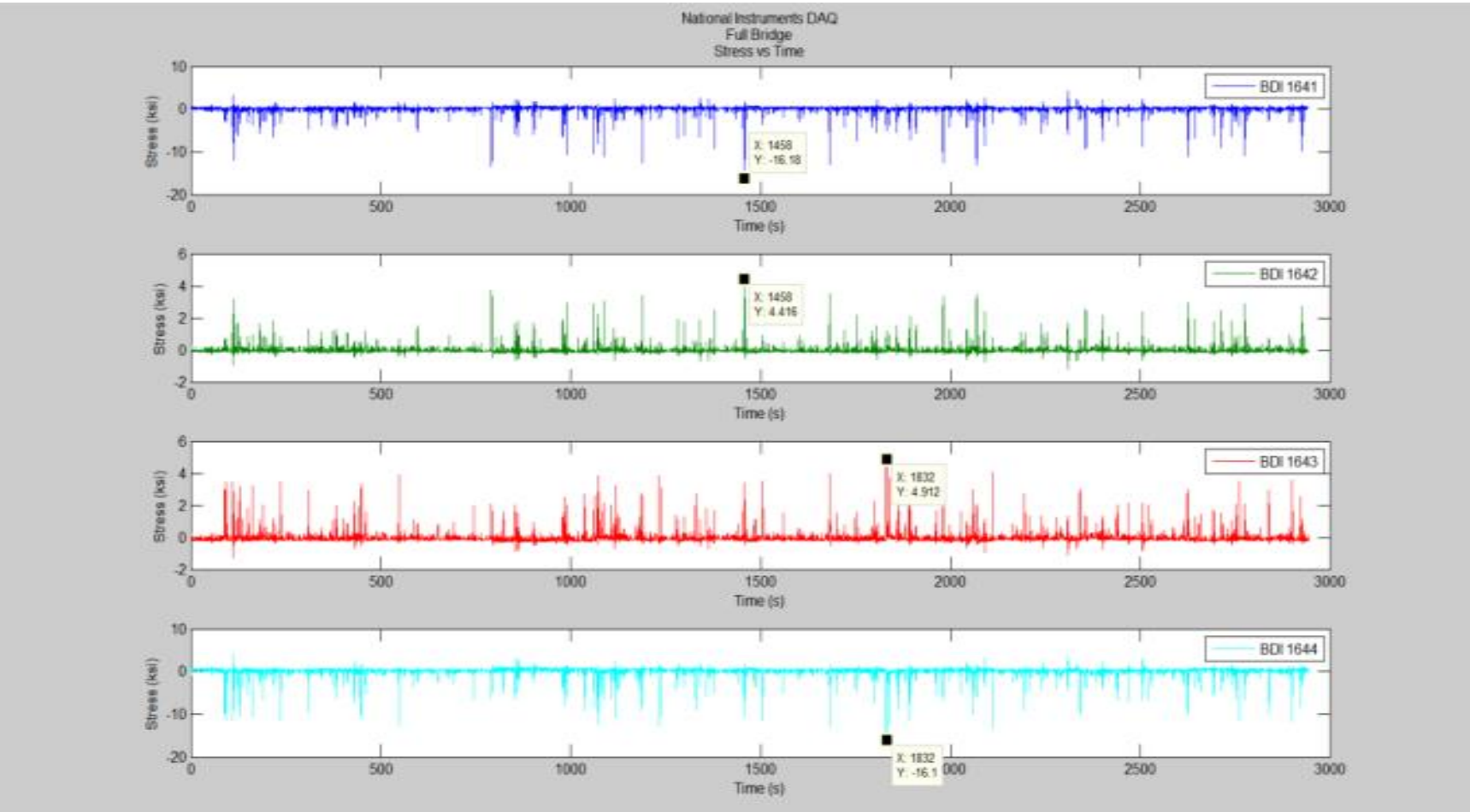

Figure 5.21 BDI Strain Transducer Connection Plate Measurements (Positive Indicates Compression; 1641 G3 Crack Side; 1642 G3 Uncrack Side, 1643 G4 Crack Side and 1644 G4 Uncrack Side)

5.4 Vehicle Bridge Interaction

Highway bridges are generally suffered from the dynamic effects due to moving vehicles. This dynamic effect could result in bridge deterioration decreasing of serviceability and increasing maintenance cost. Vehicle bridge dynamic interaction analysis has important economical and safety implications in making management decisions such as establishing permissible weight limits or issuing overload permits. All the measured data from the field test were dynamic responses under realistic traffic loading. However, due to the limitation of the software, the time-history analysis under simulated truck loading is only linear static analysis. Hence, the measured results are higher than the time-history results.

5.4.1 Dynamic Load Allowance

Usually, the moving vehicles are treated as vehicular live load of bridges in *AASHTO LRFD Bridge Design Specifications*. And, the dynamic effects are also been considered in the dynamic load allowance with increasing the static wheel load to simplify this problem. The factor to be applied to the static effect of the design truck shall be taken as:

$$1 + \frac{IM}{100}$$

Table 5-4 Dynamic Load Allowance, IM (*AASHTO LRFD Bridge Design Specifications*)

Component	IM
Deck Joints –All limit States	75
All Other Components: Fatigue and Fracture Limit Sate All other limit states	 15 33

Hongyi Li (2005) conducted a detailed research on dynamic response of highway bridges subjected to heavy vehicles. A typical multi-girder concrete bridge located in northern Florida was studied using static and dynamic field tests and finite element analysis with simple analytical models and detailed FE models in LS-DYNA. The parameters affecting vehicle bridge interaction were considered in this study, which included vehicle speed, vehicle weight, suspension parameters, truck position on bridge lanes, road surface condition and span length. The results claimed that the impact factor can far exceed the limit of 33% set by the AASHTO code, especially of the high speed and poor road conditions. The impact factors can be approximately taken to be linearly proportional to the vehicle speed. The effect of vehicle speed strongly depends on the road surface conditions. The rougher the surface is, the more rapidly the impact factor increases with the speed. For poor road surface and 70 mph, the impact factor can reach 2.

5.4.2 Vehicle-Bridge Interaction

However, the bridge and moving vehicles dynamic interaction effect should be consider as a coupled nonlinear dynamic problem. The idea of vehicle bridge interaction analysis is to model the bridge and moving vehicles as two elastic structures. These two subsystems interact with each other through the contact forces, such as the forces induced at the contact points between wheels and pavement surface. The main difficulty of this analysis is the nonlinearity and time dependent. Facts that contribute to this include the contact force may move from time to time and force magnitudes do not remain constant due to the relative movement of the two subsystems.

The dynamic effects in bridges can be modeled in three levels. The first analytical model is the pure motion of constant reaction forces exerted by a vehicle along a perfectly smooth bridge surface. However, idealized conditions result in unrealistically small dynamic bridge response. The second model includes characteristics of a vehicle suspension. This can be sufficient when the road surface is in good condition and the hammering load effect is negligible. The third vehicle-bridge interaction model is the most comprehensive since it includes impact forces induced by actual geometric surface imperfections which cause the most significant dynamic effects. High dynamic response was observed in the field test and obtained from FE analysis velocities which can cause extensive bridge vibrations.

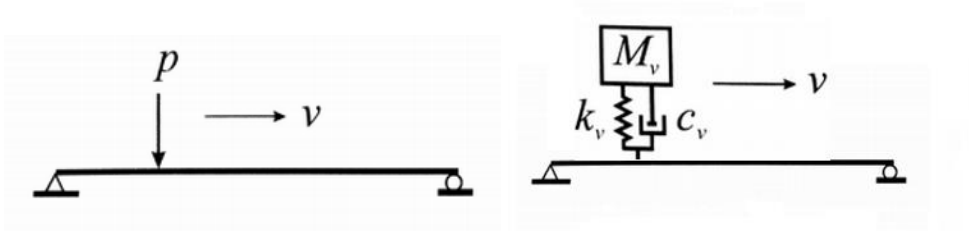

(a) First Analytical Model (b) Second and Third Analytical Model

Figure 5.22 Analytical Model of Vehicle-Bridge Interaction

The easiest model for vehicle and bridge interaction system may be given by a simply supported beam subjected to a single moving mass which represents the idealized vehicle. The governing formula is Bernoulli-Euler differential equation for a prismatic beam.

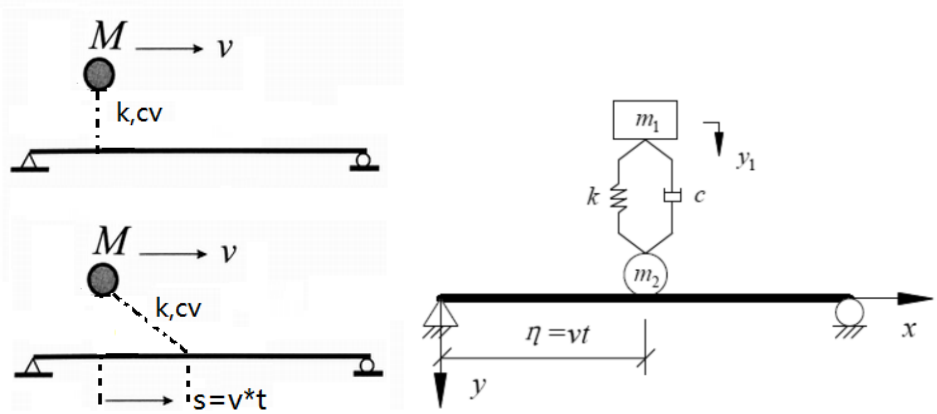

Figure 5.23 Simlified Analytical Model

$$EJ\frac{\partial^4 y(x,t)}{\partial x^4}+\mu\frac{\partial^2 y(x,t)}{\partial t^2}+2\mu\omega_d\frac{\partial y(x,t)}{\partial t} = \delta(x-vt)[P-m\frac{\partial^2 y(x,t)}{\partial t^2}] \quad \text{Equation 5-1}$$

Due to over simplicity of representation of moving vehicle, one moving mass is replaced by one-axle system with two degrees of freedom. The vehicle consists of sprung mass and unsprung mass, connected by a spring and a damper. The equation of motion for the bridge-vehicle system (Wang, et al, 2014)

$$m_1\frac{d^2 y_1(t)}{dt^2}+c\frac{d[y_1(t)-y(\eta,t)]}{dt}+k=m_1 g \quad \text{Equation 5-2}$$

$$EJ\frac{\partial^4 y(x,t)}{\partial x^4}+\mu\frac{\partial^2 y(x,t)}{\partial t^2}+2\mu\omega_d\frac{\partial y(x,t)}{\partial t} = \delta(x-\eta)\{m_2 g-m_2\frac{\partial^2 y(x,t)}{\partial t^2}\} \quad \text{Equation 5-3}$$
$$+k[y_1(t)-y(\eta,t)]+c\frac{d[y_1(t)-y(\eta,t)}{dt}$$

$$y(x,t)=\sum_{i=1}^{n} Y_i(x)T_i(t) \quad \text{Equation 5-4}$$

$$\begin{bmatrix} m_1 & 0 \\ 0 & H \end{bmatrix} \begin{Bmatrix} \ddot{y}_1 \\ \ddot{T} \end{Bmatrix} + \begin{bmatrix} c & B \\ E & C \end{bmatrix} \begin{Bmatrix} \dot{y}_1 \\ \dot{T} \end{Bmatrix} + \begin{bmatrix} k & D \\ F & K \end{bmatrix} \begin{Bmatrix} y_1 \\ T \end{Bmatrix} = \begin{Bmatrix} m_1 g \\ P \end{Bmatrix} \quad \text{Equation 5-5}$$

$$\{T\} = \{T_1, T_2, \dots, T_n\}^T \quad \text{Equation 5-6}$$

$$[H] = \begin{bmatrix} \mu + S_1 Y_1^2 & S_1 Y_1 Y_2 & \dots & S_1 Y_1 Y_n \\ S_2 Y_1 Y_2 & \mu + S_2 Y_2^2 & \dots & S_2 Y_2 Y_n \\ \vdots & \vdots & \ddots & \vdots \\ S_n Y_1 Y_n & S_n Y_2 Y_n & \dots & \mu + S_n Y_n^2 \end{bmatrix} \quad \text{Equation 5-7}$$

Consider two subsystems, i.e., the bridge and moving vehicles as two elastic structures. The two subsystems interact with each other through the contact forces.

5.4.3 Case study of I-270 Bridge over Middlebrook Road

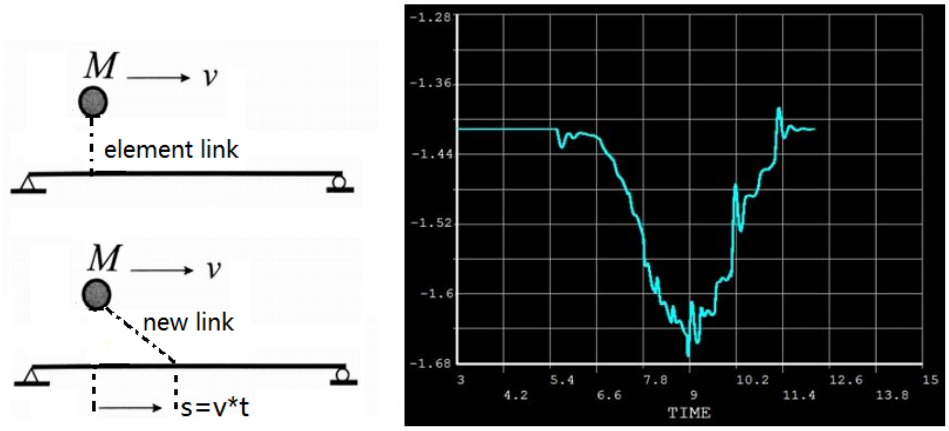

(a) Finite Element Model in ANSYS (b) Dynamic Deflection

Figure 5.24 Finite Element Model and Resluts

A simplified model with sprung and damping was developed to simulate the truck in order to minimize the calculation intensity. A three-dimensional finite element and an equivalent two-dimensional grid models were subjected to the standard vehicular live load HS20 with a seed of 55 mph passing through the right traffic lane. To simplify the dynamic problem, the three-dimensional finite element was only for static analysis, and the equivalent two-dimensional grid model was for dynamic analysis. Vehicle was modelled as a mass element and sprung-damping element, coupled with nodes from

bridge deck sharing the same degrees of freedom. While the mass was not moving itself, the effect of the mass element was spread alongside the bridge longitudinal direction. These two models were developed under the same loading and boundary condition. Figure 5.23 shows the displacement of Girder 3 at mid-span. The trend matches with the static case. Table 5-5 shows the static and dynamic deflections of Girder 3 at mid-span. The dynamic impact factor equals to 1.27 in this case study, between the fatigue limit state of 1.15 and other limit state of 1.3. Due to the simplification, the imperfection of pavement, a more detail truck model and traffic flow were not taken into consideration to fully analysis a vehicle bridge interaction. Thus, it is suggested to adopt the average value of 1.57 for average condition from the Hongyi Li's study.

Table 5-5 Static and Dynamic Deflections

		3D FEM (Static)	2D Grid (Dynamic)
First Natural Frequency (Vertical Mode)		3.26	3.05
Deflection at Mid-span of Girder 3	Dead Load	1.36	1.40
	Live Load	0.22	0.28

5.5 Parametric Study for the Cause of Fatigue Cracks

5.5.1 Connection Plates Configuration

The results of finite element analysis match with the filed test data; all the cracks located in western side of the connection plates. The vertical stress near the welded edges of connection plates follows the same pattern; the western sides of the connection plates are under tension, and the eastern sides of the connection plates are under compression. To further discuss the cause of this phenomenon, a series of controlled FEM tests were established for comparison study.

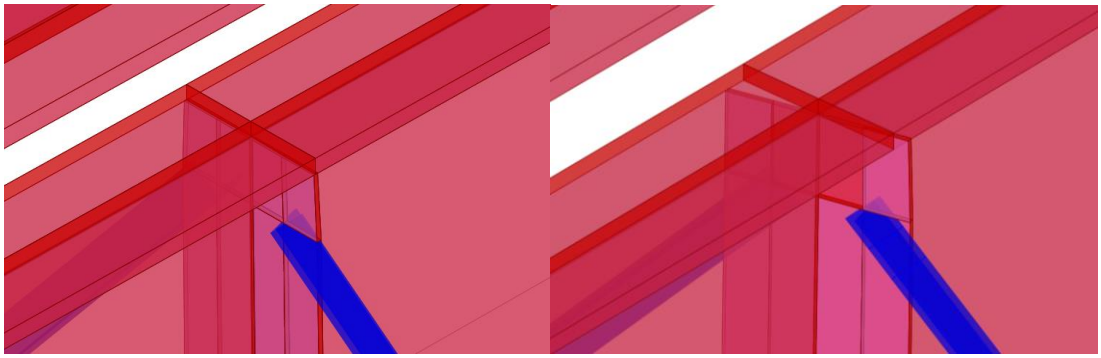

Figure 5.25 Skew (right) and non-skew (left) connection plates

According to the design drawing, cross frame connection plates and bearing stiffeners shall be normal to stringer and gusset plates shall be bent as required. Therefore, for the original FE model, all the connection plates are normal to the girders and the cross frames are parallel to two abutments with the angel of 76º. For the controlled model, all the connection plates were parallel to the cross frames with the same angel of 76º.

5.5.2 Bracing System Configuration

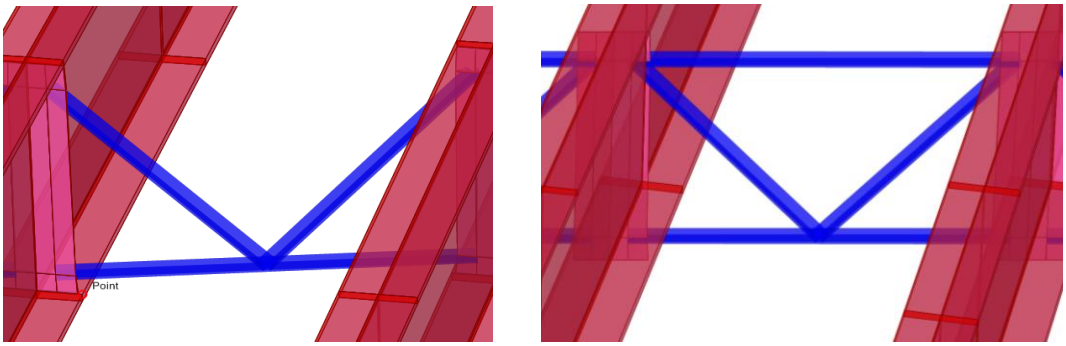

Figure 5.26 K-frame without top chord (left) and K-frame with top chord (right)

The K-type bracing system was modeled for studying the influence of bracing system configuration on the stress distribution of connection plates. The cross section of diagonal and bottom chords was employed for the added top chords. All the models were subjected to the same live load case. The live load case was defined as HS20 on right

traffic lane passing through the bridge from north to south at the limited speed of 55 mph. The vertical stress at the crack location (Girder 3 Diaphragm 3), and the axial forces of top chord located at Diaphragm 3 Bay 2, directly connecting with the crack side were analyzed and shown in Table 5-6. The maximum vertical stresses of non-skew models are much higher than those of skew models. The maximum axial forces of the models during the time history analysis were quiet small; the values were only 3.47 kip and 1.12 kip. The values of maximum vertical stresses do not change much due to the added top chord. It was represented that the connection plate configuration has a significant influence on the stress distribution of connection plates, while the top chord of K-type bracing plays a negligible role in this situation.

Table 5-6 Maximum vertical stress and axial force.

Connection plates configuration	Bracing system configuration	Max axial force (kip)	Max vertical stress of crack location (ksi)
Non-skew connection plats	K-frame without top chord	-	13.50
	K-frame with top chord	3.47	12.66
Skew connection plats	K-frame without top chord	-	0.33
	K-frame with top chord	1.12	0.30

The high vertical tensile stress around the connection welds was proven caused by the configuration of connection plates instead of the configuration of cross frames. The gusset plates, bent to be parallel to the skewed abutment, induced torsion to the connection welds. Differential displacements between girders cause one diagonal cross frame in tension and one in compression. Measured vertical tensile stresses up to 16.1 ksi in the connection plate explains why fatigue cracks have occurred at their connections to the girder bottom flange. Girders 3 and 4 are under the slow moving lane where most

heavy trucks are using while Girders 1 and 2 support a shoulder and thus large differential deflections occurred between Girders 2 and 3 (with up to 0.5” to 0.75” vertical deflections due to live load observed). The connection plate configuration is a key factor for the stress distribution of the connection plates.

5.6 Summary

This chapter consists of static and dynamic analytical work performed on the selected 3-lane highway bridge. The traffic loading obtained from Chapter 3 was converted to truck loading and applied on the finite element models form Chapter 4. The deflections and stresses has been examined.

The passage of trucks on the bridge deck can cause vertical tensile stresses in the welded connections between cross frame connection plates and girder bottom flanges. These stresses are highest at the outer edge of the connection plate where all the existing fatigue cracks on the I-270 Bridge over Middlebrook Road have initiated from. Girder 4 located at the center left of the middle traffic lane, and Girder 3 located at the center right of the right traffic lane, are the most critical locations for bridge deflections.

The live load induced stresses of connection plates are much localized around the weld connections and would not spread from the bottom to the top of connection plates. For the same face of the connection plate, both tensile and compressive stresses are observed at the symmetry positions around the girder web. The crack side of the connection plates is always under tensile stress, while the uncrack side is always under compressive stress during each time period. At the same spot of the crack side, the north face and the south face bear the same stress at the opposite direction.

The high vertical tensile stress around the connection welds was proven caused by the configuration of connection plates instead of the configuration of cross frames. The gusset plates, bent to be parallel to the skewed abutment, induced torsion to the connection welds. The connection plate configuration is a key factor for the stress distribution of the connection plates.

Meanwhile, the vehicle bridge interaction was investigated using finite element model with static and dynamic analysis. The bridge and moving vehicles were modeled as two elastic structures. A three-dimensional finite element and an equivalent two-dimensional grid models were subjected to the standard vehicular live load HS20 with a seed of 55 mph passing through the right traffic lane. To simplify the dynamic problem, the three-dimensional finite element was only for static analysis, and the equivalent two-dimensional grid model was for dynamic analysis. Vehicle was modelled as a mass element and sprung-damping element, coupled with nodes from bridge deck sharing the same degrees of freedom.

Chapter 6 Estimating Fatigue Life

6.1 Introduction

After obtaining the time-history result of stress at the connection welds from Chapter 5, the fatigue life and the remaining fatigue life for this detail can be calculated as a function of stress range and number of cycles. The widely used rainflow counting algorithm when determining the live load-induced stress range is introduced in Section 6.2. The Miner's rule is then applied for an equivalent stress range representing the actual variable-amplitude cyclic loading in Section 6.3. Case study is carried out in the last.

6.2 Rainflow Counting Algorithm

In bridge fatigue evaluation, one key component is to accurately determine the live load-induced stress range. The rainflow counting algorithm is widely used while fatigue life assessment of structural components under non-constant amplitude loading. Usually, the algorithm extract cycles from load, stress or strain history obtained from measurements or simulation results. As a result, the counted several cycles and half-cycles with different amplitude and mean value are obtained. With the advantage of fatigue damage accumulation hypothesis, the algorithm gives possibility to compute the expected fatigue life under random loading conditions.

The rainflow counting algorithm is used in the analysis of long term monitoring data in order to reduce a spectrum of varying stress into a set of simple stress reversals. Its importance is that it allows the application of Miner's rule in order to assess the

fatigue life of a structure subject to complex loading. The algorithm was developed by Tatsuo Endo and M. Matsuishi in 1968.

1. Reduce the time history to a sequence of (tensile) peaks and (compressive) valleys.

2. Imagine that the time history is a template for a rigid sheet (pagoda roof).

3. Turn the sheet clockwise 90° (earliest time to the top).

4. Each tensile peak is imagined as a source of water that "drips" down the pagoda.

5. Count the number of half-cycles by looking for terminations in the flow occurring when either: it reaches the end of the time history; it merges with a flow that started at an earlier tensile peak; or it flows when an opposite tensile peak has greater magnitude.

6. Repeat step 5 for compressive valleys.

7. Assign a magnitude to each half-cycle equal to the stress difference between its start and termination.

8. Pair up half-cycles of identical magnitude (but opposite sense) to count the number of complete cycles. Typically, there are some residual half-cycles.

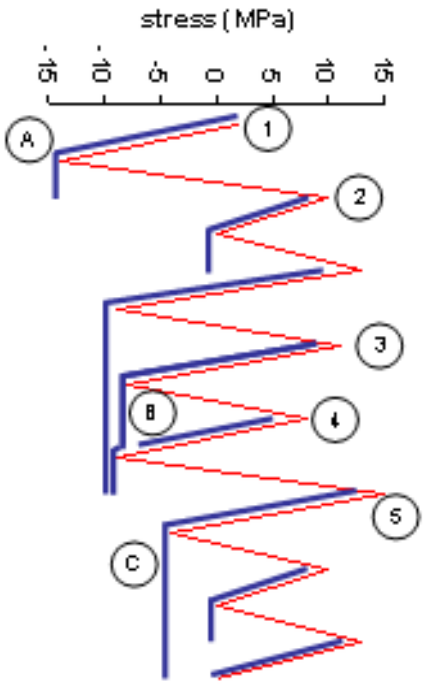

Figure 6.1 Rainflow Counting Algorithm

For example, Half-cycle (A) starts at tensile peak (1) and terminates opposite a greater tensile stress, peak (2); its magnitude is 16 MPa. Half-cycle (B) starts at tensile peak (4) and terminates where it is interrupted by a flow from an earlier peak, (3); its magnitude is 17 MPa. Half-cycle (C) starts at tensile peak (5) and terminates at the end of the time history.

6.3 Effective Stress Range

Since the fatigue strength S-N curves were developed primarily under constant-amplitude cyclic loading, an effective stress range needs to be determined to equivalently represent the actual variable-amplitude cyclic loading on bridge structures. For steel structures the root-mean cube stress range calculated from a variable amplitude stress range histogram has been found to produce the best results for this purpose, Miner's rule.

$$S_{re} = (\sum \gamma_i S_{ri}^3)^{1/3} \quad \text{Equation 6-1}$$

$$\gamma_i = \frac{n_i}{N} \quad \text{Equation 6-2}$$

Where, S_{re} is the effective stress range of a variable amplitude stress range histogram, S_{ri} is the i^{th} stress range in the stress range histogram, γ_i is the fraction of occurrence of stress range S_{ri}, n_i is the number of occurrences of tress range S_{ri}, and N is the total number of occurrence of all stress range in the histogram.

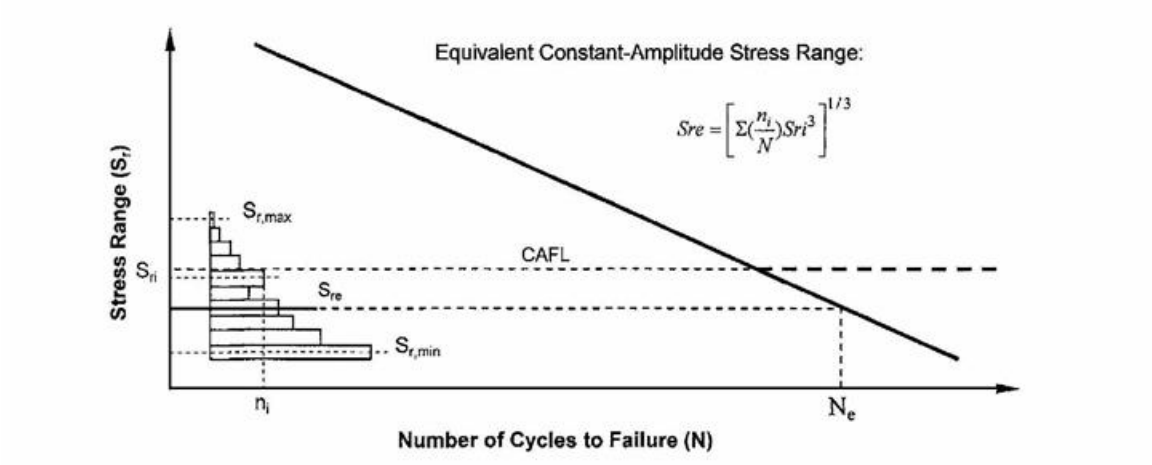

Figure 6.2 Fatigue Analysis using S-N Curve and Measured Stress Rang Histogram (Zhou, 2006)

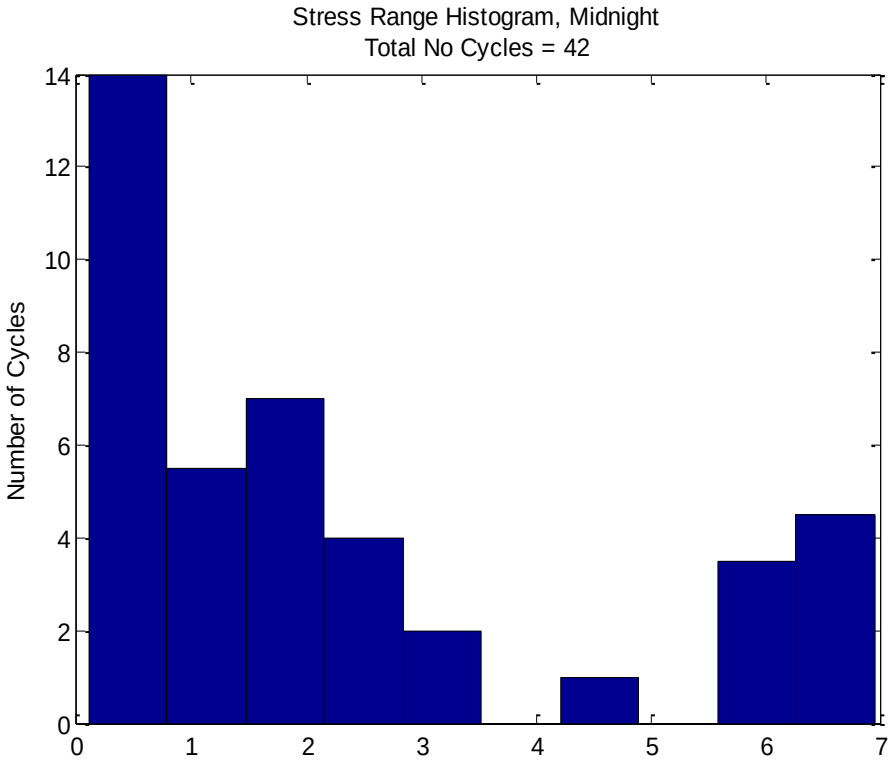

(a) Midnight

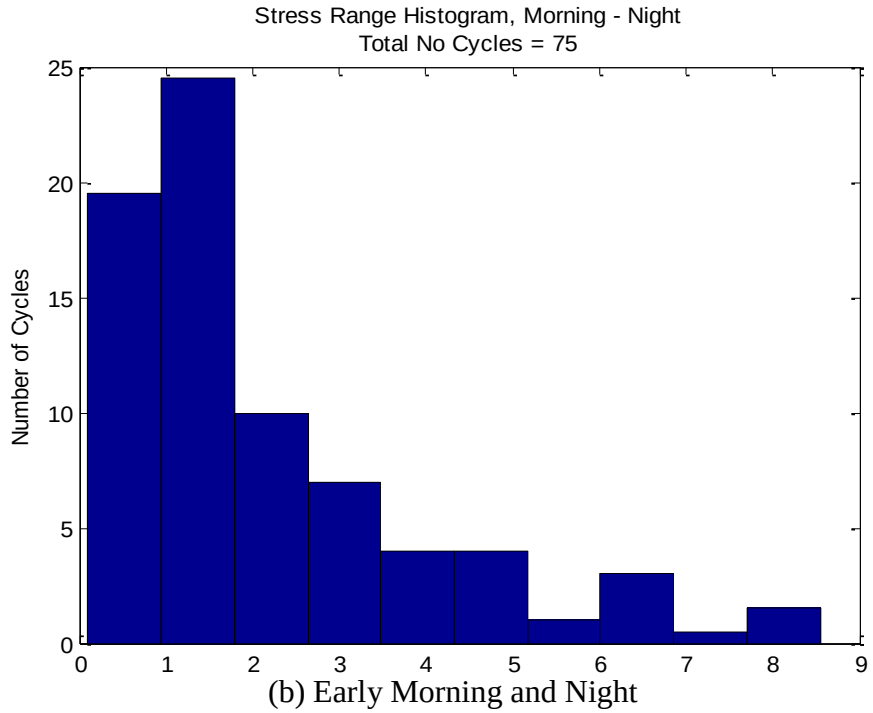

(b) Early Morning and Night

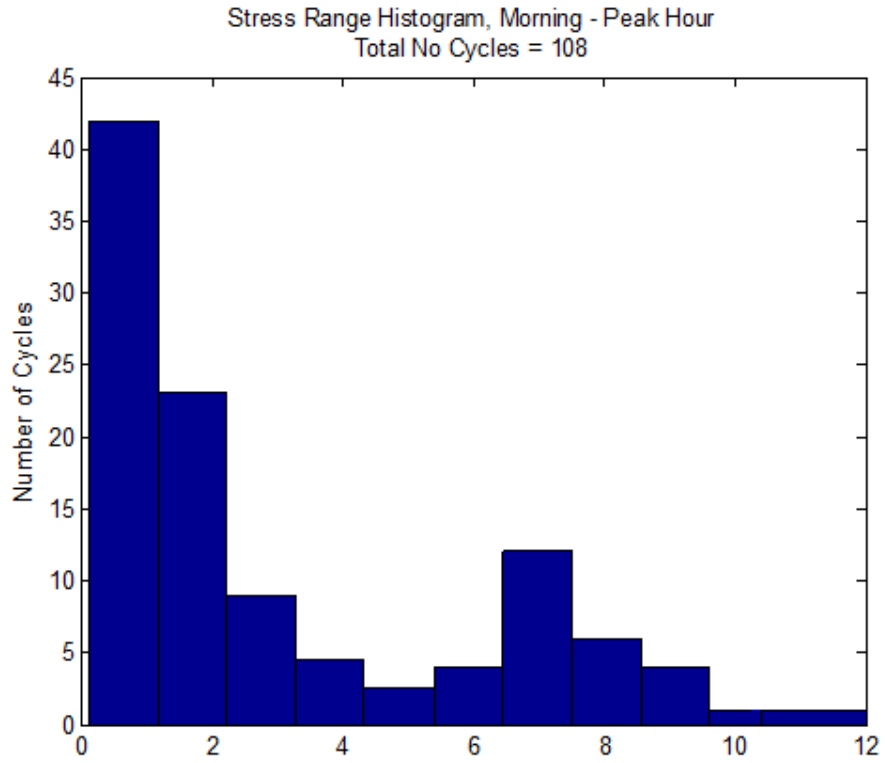

(c) Morning Peak

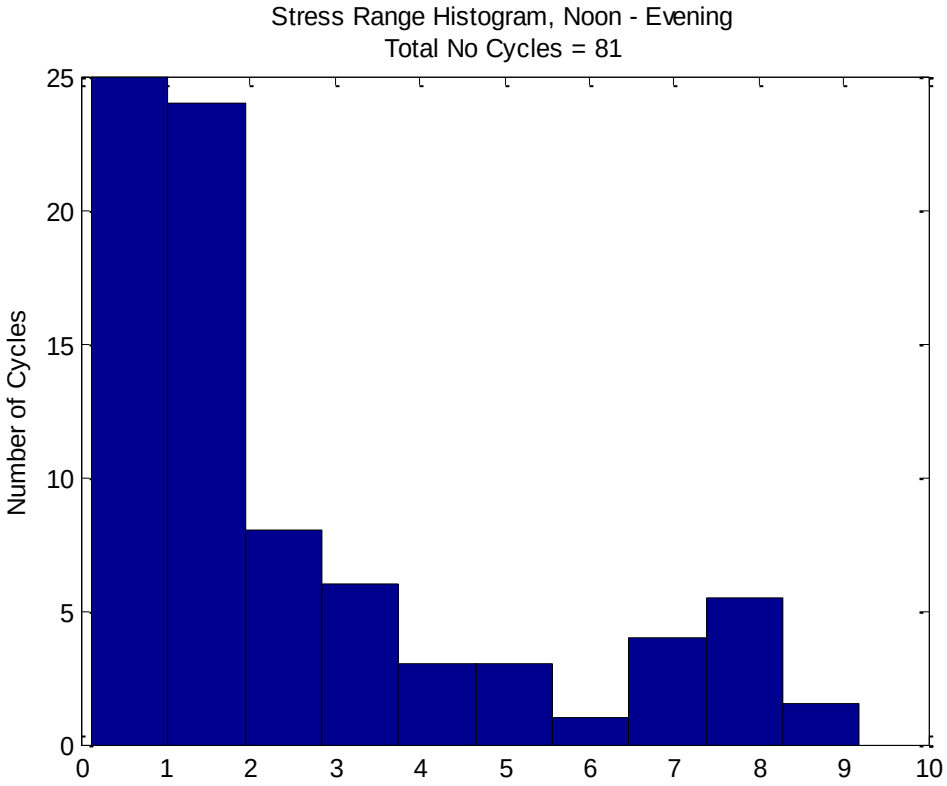

(d) Noon to Evening

Figure 6.2 Stress Range Histogram

The simulated results of the weld connection at Girder 3 during the different four time periods were analyzed by the rainflow counting algorithm and Miner's rule. The stress range histograms is shown in Figure 6.3, and the number of cycles and the effective static stress range during each time period are listed in Table 6-1. As can be seen, the highest tensile stress during morning peak caused the highest effective static stress range in the connection of concern with a value of 4.992 ksi. The number of cycles was related with the number of trucks passing through, but was not one-to-one correspondence.

Table 6-1 Number of Cycles and Effective Stress Range

Time Period	Number of Cycles (20-min)	Number of Cycles (1hr)	Static Effective Stress Range (ksi)
1. Midnight	42	126	3.815
2. Early Morning & Night	75	225	3.424
3.Moring Peak	108	324	4.992
4. Noon to Evening	81	243	4.251

The effective stress range considering the dynamic effects during one typical day can be computed as

$$S_{re} = (\sum \frac{n_i t_i}{N} S_{di}^3)^{1/3} \quad \text{Equation 6-3}$$

$$N = 365 \sum_{1}^{4} n_i t_i \quad \text{Equation 6-4}$$

$$S_{di} = (1 + IM) S_{si} \quad \text{Equation 6-5}$$

n_i is the number of cycles during one hour simulation for each time period, t_i is the total hours of the time period. For example, t_i is 5 for time period of midnight, early morning and night, and morning peak, and is 9 for the time period of noon to evening. N is the total number of cycles the fatigue-prone experienced during one typical day. S_{re} is

the effective stress range considering the dynamic effects, S_{si} is the static effective stress range of the i^{th} time period, S_{di} is the dynamic effective stress range of the i^{th} time period The dynamic impact has been considered in the dynamic load allowance with the value of 57%, as discussed in Section 5.4.3.

The total fatigue life of the fatigue-prone detail will be computed by the following equation:

$$Y = \frac{R_R A}{365n(ADTT)_{SL}((\Delta f)_{eff})^3} = \frac{R_R A}{N(R_s 0.75 S_{re})^3} \quad \text{Equation 6-6}$$

$$R_s = R_{sa} R_{st} \quad \text{Equation 6-7}$$

The resistant factor for evaluation and the detail category constant are given in the Table 6-2 and 6-3, as describe in *AASHTO LRFD Design Specifications* and *Manual for Bridge Evaluation.* 75 percent of the calculated stress range due to the passage of the fatigue track determined by weigh-in-motion study. R_s is the stress-range estimate partial load factor, contributed by the uncertainty associated with analysis R_{sa} and assumed effective truck weight R_{st}. The value of the partial load factor can be taken as 0.95 for the determination of evaluation or minimum fatigue life, and 1.0 for the mean fatigue life.

Table 6-2 Resistance Factor for Evaluation R_R

Detail Category	Evaluation Life	Minimum Life	Mean Life
A	1.7	1.0	2.8
B	1.4	1.0	2.0
B’	1.5	1.0	2.4
C	1.2	1.0	1.3
C’	1.2	1.0	1.3
D	1.3	1.0	1.6
E	1.3	1.0	1.6
E’	1.6	1.0	2.5

Table 6-3 Detail Category Constant A

Detail Category	Constant A (ksi^3)	CAFL (ksi)
A	250×10^8	24.0
B	120×10^8	16.0
B’	61×10^8	12.0
C	44×10^8	10.0
C’	44×10^8	12.0
D	22×10^8	7.0
E	11×10^8	4.5
E’	3.9×10^8	2.6

The calculated evaluation fatigue life is 19.704 years based on the current traffic volume, the minimum fatigue life is 16.42 years and the mean fatigue life is 21.346 years. Designed in 1988, these bridge was open to public after two-year construction. And the actually fatigue life is 20 years from the beginning to the time when the first crack has been observed.

Chapter 7 Conclusions

7.1 Fatigue Assessments Framework of Highway Bridges under Traffic Loading

Figure 7.1 illustrates the framework of the proposed fatigue assessments methodology. The above chapters decomposes the system into three primary stage and specifies the corresponding numerical model at each stage.

This system includes three continued procedures. The first step is fatigue loading simulation based on the probability-based full velocity difference model. Combined the historical truck information with historical traffic flow information, the simulated vehicles are inputted to the simulated network representing the studies bridge. Each simulated vehicle would follow the full velocity difference model of car-following behavior. The results would provide the vehicle type, vehicle position and speed at each time step.

In the following step, the three-dimensional global and local bridge models have studied using finite element method. The finite element model would be verified by the comparison with measurements from field tests. Then, the truck loading from step 1 would be applied on the bridge model. The modal analysis, time-history analysis of bridge deflection, stress at hot spot would be studies as well.

In the last step, Miner's rule and the rainflow counting algorithm are used in the analysis of simulated data from the finite element modeling, in order to reduce a spectrum of varying stress into a set of simple stress reversals. The stress cycles would be calculated as the results to prediction the remaining fatigue life.

For long-term monitoring, the update data of truck information and traffic information would be taken as input of this system to replace the historical data. The analytical procedures could be performed step by step, and the results would provide the updated remaining fatigue life according to the update information. The proposed methodology could be used as a tool accompanying a monitoring program to obtain the fatigue reliability levels associated with the fatigue sensitive bridge details that were not monitored.

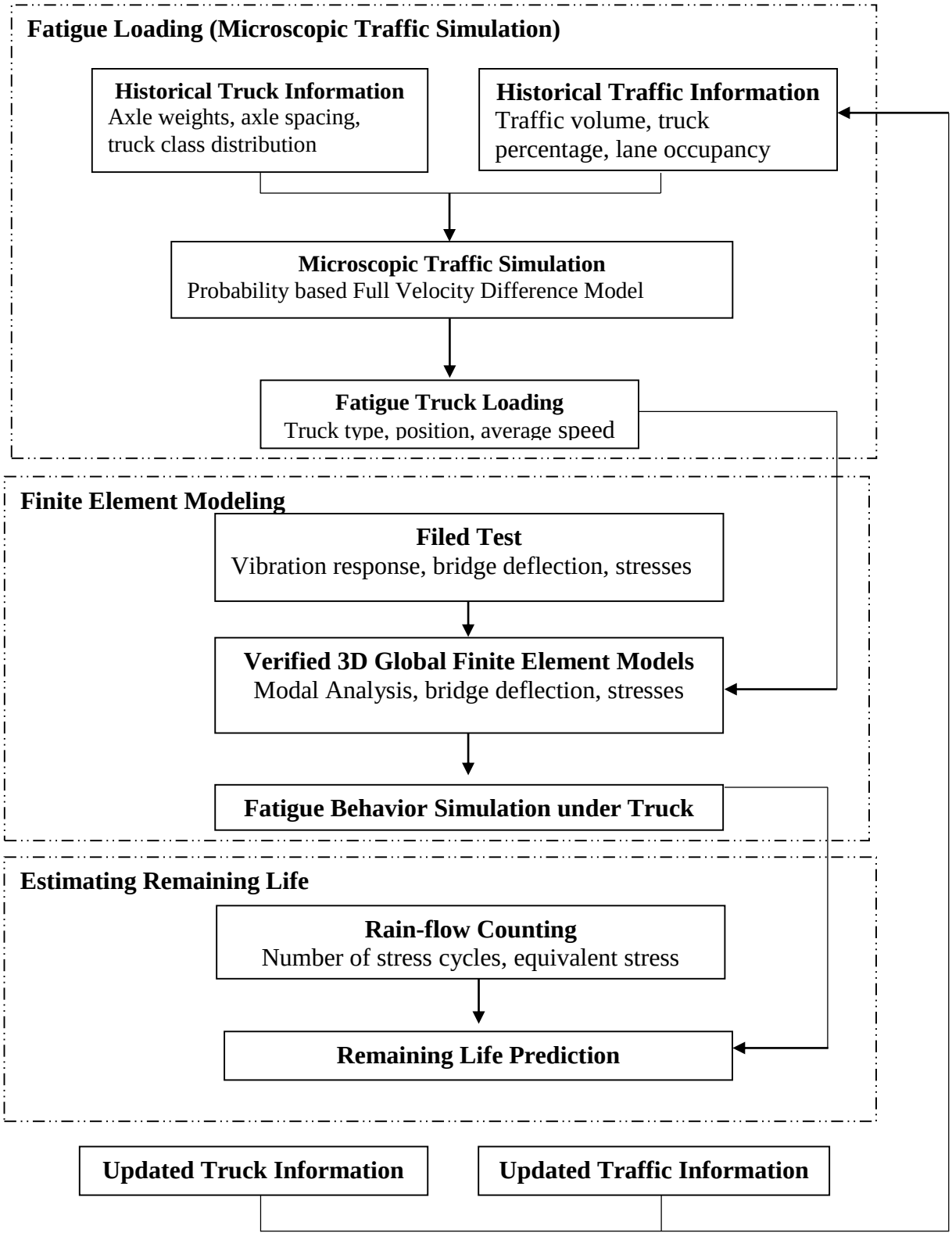

Figure 7.1 Framework of the Fatigue Assessment

7.2 Results and Findings

1. For fatigue analyses based on a traffic load model and a structural model, the effectiveness of the analyses is determined by the accuracy of the traffic load model and the structure model.

2. Different from the explicit equation-based method, the proposed approach combines a comprehensive traffic loading model, including information on vehicle types, axle weights, axle spacing, and the lane occupation, and a detailed 3D FE model, which enables fatigue analyses on unreachable or complicated details where complex stress conditions may exist.

3. It is worth mentioning that axle weight, axle spacing, vehicle position and speed at each time step can be obtained from the probability-base full velocity difference model, combining the historical traffic monitoring data (traffic volume, truck percentage, lane distribution) with weigh station measurements (vehicle type, axle weight, axle spacing). The more detailed information obtains, the better results achieves.

4. The passage of trucks on the bridge deck can cause vertical tensile stresses in the welded connections between cross frame connection plates and girder bottom flanges. The live load induced stresses of connection plates are much localized around the weld connections and would not spread from the bottom to the top of connection plates. The high vertical tensile stress around the connection welds is proven caused by the configuration of connection plates instead of the configuration of cross frames. The gusset plates, bent to be parallel to the skewed abutment, induced torsion to the connection welds. The connection plate configuration is a key factor for the stress distribution of the connection plates.

5. The impact factor can far exceed the limit of 15% for fatigue limit state set by the AASHTO code, or even 33% for other limit state, especially of the high speed and poor road conditions. The dynamic impact factor equals to 1.27 in this case study, between the fatigue limit state of 1.15 and other limit state of 1.3. Due to the simplification, the imperfection of pavement, a more detail truck model and traffic flow were not taken into consideration to fully analysis a vehicle bridge interaction. This results matches with Dr. Hongyi Li's study that the impact factors for simplified sprung-mass model are usually below the AASHTO value, even at the high speed of 70 mph. Thus, it is suggested to adopt the average value of 1.57 for average condition from the Hongyi Li's study.

6. The proposed approach may be used as a tool accompanying a monitoring program to find the stresses in un-monitored details or to reduce the frequency of SHM, resulting in lower costs in fatigue assessment. In such case, the proposed approach provides a tool to predict the fatigue reliabilities of these hard-to-reach details. When combined with the fracture damage mechanics, the proposed approach can provide a better understanding of the accumulation of fatigue damage and crack propagation.

7.3 Future Study

In the current study, the time-history stresses responses of the welded connection are obtained from the global finite element model. The local finite element model was only used for stress concentration analysis. The refined local model with the active crack will be analyzed under time-history loading from the global model for a more accurate analysis.

Much detailed vehicle model is need for vehicle bridge interaction analysis. More scenarios of vehicle-bridge interaction need to be investigated, including different configurations of vehicles, surface imperfections and discontinuities, and traffic flow pattern should take into consideration to a fully analysis.

The uncertainty associated with the analysis is considered in the stress-range estimate partial load factor. Much work is need for the fatigue reliability analysis for future study.

Appendices

A. WIM Data and Traffic Data Accessibility

For the method required high quality of WIM data, it is difficult to apply for many states. The National Cooperative Highway Research Program's report *Protocols for Collecting and Using Traffic Data in Bridge Design (2011)* claimed that approximate 500 permanent WIM sites in operation in 47 states for several years, but they all concentrated in California, New Jersey, New York, Oklahoma, Washington, etc. For national-wide use, it may be sufficient enough to represent the current truck information in US. However, many states only have one or two WIM sites covering one or two lanes, like Maryland. For studies in these states, the WIM sites cannot cover most of the area and could not be reliable source to generate truck loading.

Table A-1 WIM Data Distribution

State	WIM Program Installed	WIM Data Available For A Whole Year	WIM System Coverage	
			WIM Sites More Than 5	Covering Lanes More Than One Per Site
Alabama	Yes	No	Yes	Yes
Alaska	Yes	Yes	Yes	Yes
Arizona	Yes	No	Yes	No
Arkansas	No	Yes	No	No
California	Yes	Yes	Yes	Yes
Colorado	Yes	No	No	No
Connecticut	Yes	Yes	No	Yes
DC (Washington)	Yes	No	No	Yes
Delaware	Yes	No	No	No
Florida	Yes	Yes	Yes	No
Georgia	No	No	No	No
Hawaii	Yes	Yes	Yes	Yes

Idaho	Yes	Yes	No	Yes
Illinois	Yes	No	No	No
Indiana	Yes	Yes	Yes	Yes
Iowa	Yes	Yes	No	No
Kansas	Yes	Yes	No	No
Kentucky	Yes	No	No	Yes
Louisiana	Yes	No	No	No
Maine	Yes	No	No	No
Maryland	Yes	No	No	No
Massachusetts	Yes	No	No	Yes
Michigan	Yes	Yes	Yes	Yes
Minnesota	Yes	Yes	Yes	Yes
Mississippi	Yes	Yes	No	Yes
Missouri	Yes	Yes	Yes	Yes
Montana	No	No	No	No
Nebraska	No	No	No	No
Nevada	Yes	Yes	No	Yes
New Hampshire	Yes	No	No	Yes
New Jersey	Yes	Yes	Yes	Yes
New Mexico	Yes	Yes	No	Yes
New York	Yes	Yes	Yes	Yes
North Carolina	No	No	No	No
North Dakota	Yes	Yes	No	No
Ohio	Yes	Yes	No	No
Oklahoma	Yes	No	Yes	Yes
Oregon	Yes	Yes	Yes	Yes
Pennsylvania	Yes	No	Yes	No
Rhode Island	Yes	No	No	Yes
South Carolina	No	No	No	No
South Dakota	Yes	Yes	Yes	Yes
Tennessee	No	No	No	No
Texas	Yes	No	No	Yes
Utah	Yes	No	No	Yes
Vermont	Yes	No	Yes	Yes
Virginia	Yes	Yes	No	No
Washington	Yes	Yes	Yes	Yes
West Virginia	No	No	No	No
Wisconsin	No	No	No	No
Wyoming	Yes	Yes	No	Yes

The table above is the summary of state department of transportation survey from National Cooperative Highway Research Program's report *Protocols for Collecting and*

Using Traffic Data in Bridge Design (2011). Three major WIM program details were compared between 50 states, including the WIM system installation, duration of available WIM data, and WIM system coverage. The four charts below represented the results. Although 41 out of 50 states have installed WIM system, there is still over half of 50 states cannot provide WIM data for a whole year. The WIM system coverage is another issue. About two-thirds of the states only have few WIM sites, and almost half of them cannot covering more than one traffic lane. Like Delaware, Illinois, Louisiana, Maryland, there is only one WIM site covering only one traffic lane.

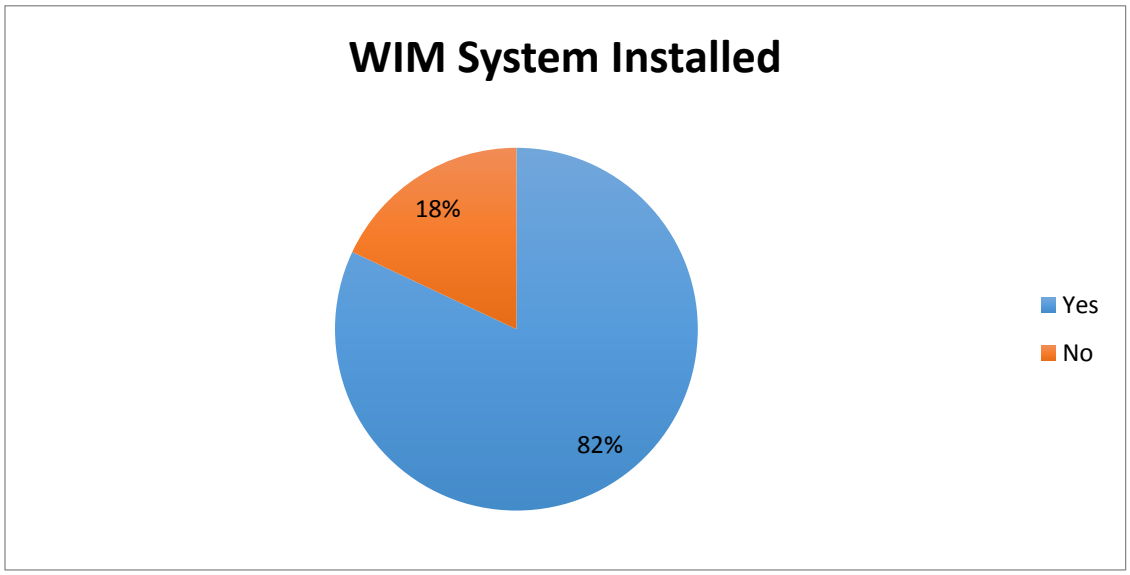

(a)The percentage of WIM system installed in the US

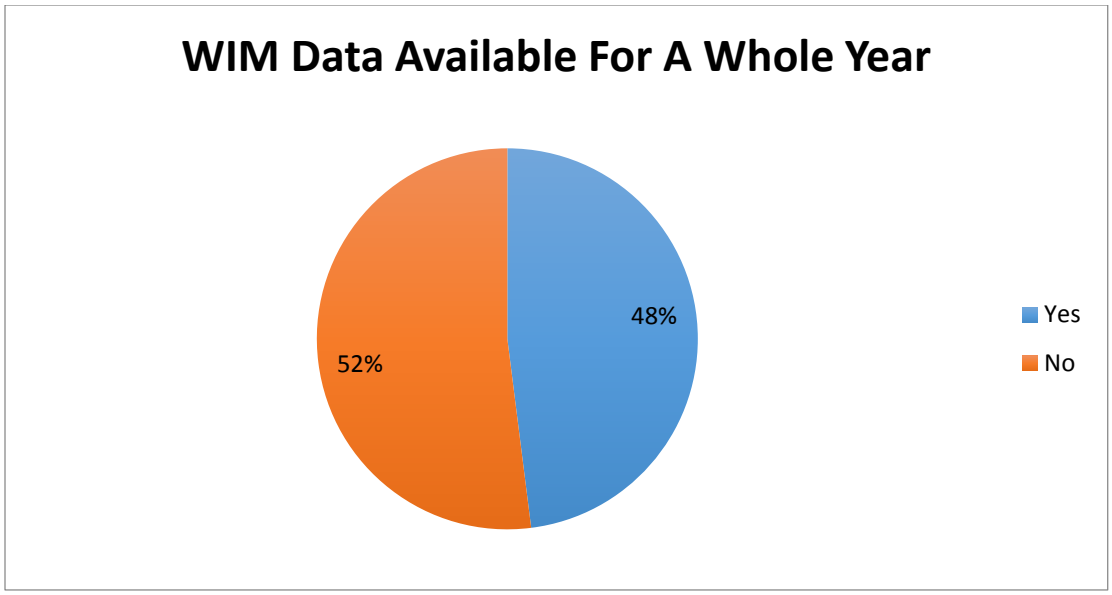

(b) WIM Data Available For a Whole Year

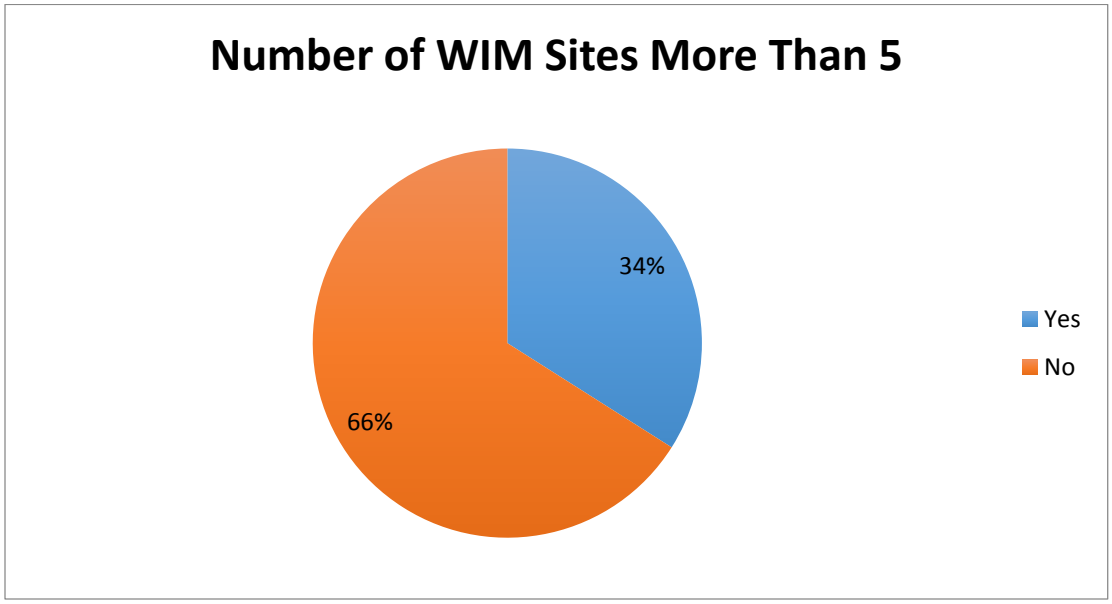

(c) Number of WIM sites more than 5

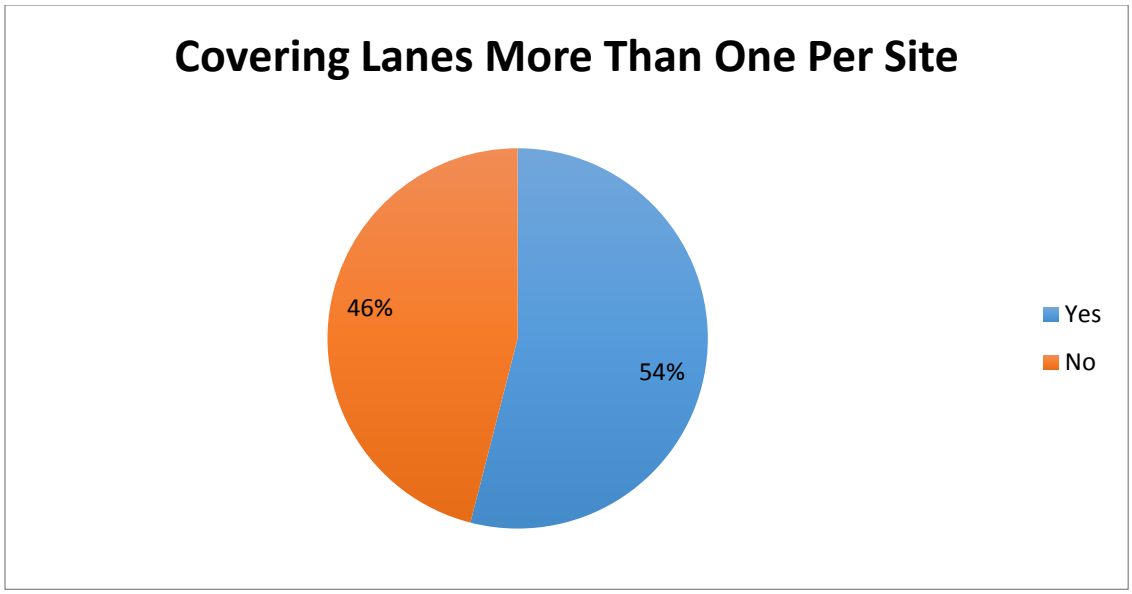

(d) Covering Lanes per site
Figure A.1 WIM Data Accessibility

B. MATLAB Code for Probability-based Full Velocity Difference Model

```
clc;
clear;

%**************************************************************************
***%
% Define settings and parameters necessary for the simulation

% read the truck data
DATA2=readCsv2('axle2.csv');
DATA3=readCsv3('axle3.csv');
DATA4=readCsv4('axle4.csv');
DATA5=readCsv5('axle5.csv');
DATA6=readCsv6('axle6.csv');

% number of cars
% 100 for Midnight
% 250 for Early Morning
% 500 for Morning Peak
% 400 for Noon
Ncars_Lane1 = 400;
Ncars_Lane2 = 400;
Ncars_Lane3 = 400;

% segment length
ROAD_LENGTH = 100; %m, part of which is the bridge 140ft (43m from 20m
to 63m)

% stept is the time of every step (in seconds)
stept = 0.2;
```

```
% n is the steps of simulation, equal to 20 mins simulation
n = 6000;

% vehicle characteristics
MIN_SPEED = 14.31; % m/s, 45mph
MAX_SPEED = 23.24; % m/s, 65mph
MAX_ACCELERATION = 5; %?
MIN_ACCELERATION = -5; %?
MEAN_SPEED=( MIN_SPEED + MAX_SPEED ) / 2;
VAR_SPEED=sqrt( (MAX_SPEED - MIN_SPEED ) / 2 );

% Truck Distribution
Truck_Prob=0.1039*3; % 0.201/0.114/0.1082/0.1039
Lane_Prob=[0.0145,0.4484,0.5371];
Type=[526,34,63,1438,54]; % number of different types of trucks
Type_Prob=Type./sum(Type);
TIMEGAP_EXPECT = 3600/(3021/3); % headway, divided by per lane volume,
revise 505/1934/4215/3021

LAMBDA=0.5;
%*****************************************************************
***%
% Simulation input generation

cars_Lane1 = cell(Ncars_Lane1,1);
cars_Lane2 = cell(Ncars_Lane2,1);
cars_Lane3 = cell(Ncars_Lane3,1);
% cars: .xtrace, along the lane
%       .xv, along the lane, velocity
%       .xa, along the lane, accelerate rate
%       .type, vehicle type, 1: passenger car, 2: truck
%       .axleno
%       .weight
%       .length
%       .appeartime, the appear time of the car
%       .appeared, true or false.

for k=7:7
    % initialization for lane 1 (most left)
    for i = 1:Ncars_Lane1
        intervaltime = poissrnd(TIMEGAP_EXPECT);
        if i==1
            cars_Lane1{i}.appeartime = 0;
            cars_Lane1{i}.appeared = true;
        else
            cars_Lane1{i}.appeartime = cars_Lane1{i-1}.appeartime +
intervaltime;
            cars_Lane1{i}.appeared = false;
        end
        cars_Lane1{i}.xtrace = zeros(n,1);
        cars_Lane1{i}.xa = zeros(n,1);
        cars_Lane1{i}.xv = ones(n,1) * randn() * VAR_SPEED+MEAN_SPEED;

[ cars_Lane1{i}.type,cars_Lane1{i}.axleno,cars_Lane1{i}.weight,cars_Lan
e1{i}.length ] = RandomNumberGenerator(1-
Truck_Prob*Lane_Prob(1,1),Type_Prob,DATA2,DATA3,DATA4,DATA5,DATA6);
```

```
    end
    % initialization for lane 2 (middle)
    for i = 1:Ncars_Lane2
        intervaltime = poissrnd(TIMEGAP_EXPECT);
        if i==1
            cars_Lane2{i}.appeartime = 0;
            cars_Lane2{i}.appeared = true;
        else
            cars_Lane2{i}.appeartime = cars_Lane2{i-1}.appeartime +
intervaltime;
            cars_Lane2{i}.appeared = false;
        end
        cars_Lane2{i}.xtrace = zeros(n,1);
        cars_Lane2{i}.xa = zeros(n,1);
        cars_Lane2{i}.xv = ones(n,1) * randn() * VAR_SPEED+MEAN_SPEED;

[ cars_Lane2{i}.type,cars_Lane2{i}.axleno,cars_Lane2{i}.weight,cars_Lan
e2{i}.length ] = RandomNumberGenerator(1-
Truck_Prob*Lane_Prob(1,2),Type_Prob,DATA2,DATA3,DATA4,DATA5,DATA6);
    end
    % initialization for lane 3 (most right)
    for i = 1:Ncars_Lane3
        intervaltime = poissrnd(TIMEGAP_EXPECT);
        if i==1
            cars_Lane3{i}.appeartime = 0;
            cars_Lane3{i}.appeared = true;
        else
            cars_Lane3{i}.appeartime = cars_Lane3{i-1}.appeartime +
intervaltime;
            cars_Lane3{i}.appeared = false;
        end
        cars_Lane3{i}.xtrace = zeros(n,1);
        cars_Lane3{i}.xa = zeros(n,1);
        cars_Lane3{i}.xv = ones(n,1) * randn() * VAR_SPEED+MEAN_SPEED;

[ cars_Lane3{i}.type,cars_Lane3{i}.axleno,cars_Lane3{i}.weight,cars_Lan
e3{i}.length ] = RandomNumberGenerator(1-
Truck_Prob*Lane_Prob(1,3),Type_Prob,DATA2,DATA3,DATA4,DATA5,DATA6);
    end

%*********************************************************************
***%


%*********************************************************************
***%
    % Start the simulation for lane 1, 2, & 3
    % simulate the speed of the first leading vehicle
    cars_Lane1{1}.xv(1:n) = 18.77; % 55 mph
    cars_Lane2{1}.xv(1:n) = 18.77; % 55 mph
    cars_Lane3{1}.xv(1:n) = 18.77; % 55 mph
    %cars_Lane1{1}.xv(n/2:n) =0 ;
    for i = 1:n % every step
        i
        for j = 1:Ncars_Lane1 % the behavior of every car
            if  (cars_Lane1{j}.appeared == true)
                if ( j == 1) % the first car cares nothing
```

```
                    cars_Lane1{j}.xtrace(i+1) =
cars_Lane1{j}.xtrace(i) + cars_Lane1{j}.xv(i)*stept;
                    cars_Lane1{j}.xv(i+1) = cars_Lane1{j}.xv(i);
                else % other cars_Lane1, take care:)
                    delta_x = cars_Lane1{j-1}.xtrace(i) -
cars_Lane1{j}.xtrace(i);
                    delta_v = cars_Lane1{j-1}.xv(i) -
cars_Lane1{j}.xv(i);
                    cars_Lane1{j}.xa(i) =
get_acceleration(cars_Lane1{j}.xv(i), ...
                                                    delta_x,
delta_v, ...
                                                    LAMBDA,
sum(cars_Lane1{j-1}.length)*0.3048);
                    if( cars_Lane1{j}.xa(i) >= 0 )
                        cars_Lane1{j}.xa(i) = min(MAX_ACCELERATION, ...
                                                  cars_Lane1{j}.xa(i));
                    else
                        cars_Lane1{j}.xa(i) =
max(MIN_ACCELERATION,cars_Lane1{j}.xa(i));
                    end

                    % calculate speed and position
                    % normal condition
                    if cars_Lane1{j}.xv(i)+cars_Lane1{j}.xa(i)*stept >
0
                        cars_Lane1{j}.xv(i+1) =
cars_Lane1{j}.xv(i)+cars_Lane1{j}.xa(i)*stept;
                        cars_Lane1{j}.xtrace(i+1) =
cars_Lane1{j}.xtrace(i) +
(cars_Lane1{j}.xv(i)+cars_Lane1{j}.xa(i)*stept/2)*stept;
                    elseif cars_Lane1{j}.xa(i)==0 % this means that
velocity has already been 0
                        cars_Lane1{j}.xv(i+1) = 0;
                        cars_Lane1{j}.xtrace(i+1) =
cars_Lane1{j}.xtrace(i);
                    else
                        cars_Lane1{j}.xtrace(i+1) =
cars_Lane1{j}.xtrace(i) - cars_Lane1{j}.xv(i)^2/( 2 *
cars_Lane1{j}.xa(i) );
                        cars_Lane1{j}.xv(i+1) = 0;
                    end
                    if (cars_Lane1{j}.xtrace(i + 1)<0)
                        disp('What?');
                    end
                end
            elseif (i*stept >= cars_Lane1{j}.appeartime)  % if j has
not appeared...
                cars_Lane1{j}.appeared = 1;
            else
                break;
            end
        end
        for j = 1:Ncars_Lane2 % the behavior of every car
            if  (cars_Lane2{j}.appeared == true)
                if ( j == 1) % the first car cares nothing
```

```
                    cars_Lane2{j}.xtrace(i+1) =
cars_Lane2{j}.xtrace(i) + cars_Lane2{j}.xv(i)*stept;
                    cars_Lane2{j}.xv(i+1) = cars_Lane2{j}.xv(i);
                else % other cars_Lane2, take care:)
                    delta_x = cars_Lane2{j-1}.xtrace(i) -
cars_Lane2{j}.xtrace(i);
                    delta_v = cars_Lane2{j-1}.xv(i) -
cars_Lane2{j}.xv(i);
                    cars_Lane2{j}.xa(i) =
get_acceleration(cars_Lane2{j}.xv(i), ...
                                                    delta_x,
delta_v, ...

LAMBDA,sum(cars_Lane2{j-1}.length)*0.3048);
                    if( cars_Lane2{j}.xa(i) > 0 )
                        cars_Lane2{j}.xa(i) = min(MAX_ACCELERATION, ...
                                                  cars_Lane2{j}.xa(i));
                    else
                        cars_Lane2{j}.xa(i) =
max(MIN_ACCELERATION,cars_Lane2{j}.xa(i));
                    end

                    % calculate speed and position
                    if cars_Lane2{j}.xv(i)+cars_Lane2{j}.xa(i)*stept >
0
                        cars_Lane2{j}.xv(i+1) =
cars_Lane2{j}.xv(i)+cars_Lane2{j}.xa(i)*stept;
                        cars_Lane2{j}.xtrace(i+1) =
cars_Lane2{j}.xtrace(i) +
(cars_Lane2{j}.xv(i)+cars_Lane2{j}.xa(i)*stept/2)*stept;
                    elseif cars_Lane2{j}.xa(i)==0 % this means that
velocity has already been 0
                        cars_Lane2{j}.xv(i+1) = 0;
                        cars_Lane2{j}.xtrace(i+1) =
cars_Lane2{j}.xtrace(i);
                    else
                        cars_Lane2{j}.xtrace(i+1) =
cars_Lane2{j}.xtrace(i) - cars_Lane2{j}.xv(i)^2/( 2 *
cars_Lane2{j}.xa(i) );
                        cars_Lane2{j}.xv(i+1) = 0;
                    end
                    if (cars_Lane2{j}.xtrace(i + 1)<0)
                        disp('What?');
                    end
                end
            elseif (i*stept >= cars_Lane2{j}.appeartime)  % if j has
not appeared...
                cars_Lane2{j}.appeared = 1;
            else
                break;
            end
        end
        for j = 1:Ncars_Lane3 % the behavior of every car
            if  (cars_Lane3{j}.appeared == true)
                if ( j == 1) % the first car cares nothing
                    cars_Lane3{j}.xtrace(i+1) =
cars_Lane3{j}.xtrace(i) + cars_Lane3{j}.xv(i)*stept;
```

```
                    cars_Lane3{j}.xv(i+1) = cars_Lane3{j}.xv(i);
                else % other cars_Lane3, take care:)
                    delta_x = cars_Lane3{j-1}.xtrace(i) -
cars_Lane3{j}.xtrace(i);
                    delta_v = cars_Lane3{j-1}.xv(i) -
cars_Lane3{j}.xv(i);
                    cars_Lane3{j}.xa(i) =
get_acceleration(cars_Lane3{j}.xv(i), ...
                                                    delta_x,
delta_v, ...

LAMBDA,sum(cars_Lane3{j-1}.length)*0.3048);
                    if( cars_Lane3{j}.xa(i) > 0 )
                        cars_Lane3{j}.xa(i) = min(MAX_ACCELERATION, ...
                                                  cars_Lane3{j}.xa(i));
                    else
                        cars_Lane3{j}.xa(i) =
max(MIN_ACCELERATION,cars_Lane3{j}.xa(i));
                    end

                    % calculate speed and position
                    if cars_Lane3{j}.xv(i)+cars_Lane3{j}.xa(i)*stept >
0
                        cars_Lane3{j}.xv(i+1) =
cars_Lane3{j}.xv(i)+cars_Lane3{j}.xa(i)*stept;
                        cars_Lane3{j}.xtrace(i+1) =
cars_Lane3{j}.xtrace(i) +
(cars_Lane3{j}.xv(i)+cars_Lane3{j}.xa(i)*stept/2)*stept;
                    elseif cars_Lane3{j}.xa(i)==0 % this means that
velocity has already been 0
                        cars_Lane3{j}.xv(i+1) = 0;
                        cars_Lane3{j}.xtrace(i+1) =
cars_Lane3{j}.xtrace(i);
                    else
                        cars_Lane3{j}.xtrace(i+1) =
cars_Lane3{j}.xtrace(i) - cars_Lane3{j}.xv(i)^2/( 2 *
cars_Lane3{j}.xa(i) );
                        cars_Lane3{j}.xv(i+1) = 0;
                    end
                    if (cars_Lane3{j}.xtrace(i + 1)<0)
                        disp('What?');
                    end
                end
            elseif (i*stept >= cars_Lane3{j}.appeartime)  % if j has
not appeared...
                cars_Lane3{j}.appeared = 1;
            else
                break;
            end
        end
    end
end
```

C. Truck Loading during Different Time Periods

Table C-1 Midnight Loading

Lane 1(Left)	Lane 2 (Middle)	Lane 3 (Right)	Time (s)	Speed (mph)
		m	68	57.95455
	m	m	91	49.09091
		s	114	53.18182
	s	s	167	52.5
		m	272	54.54545
	s		296	56.59091
		l	329	60.68182
	m		395	53.86364
	m		577	42.95455
		s	585	54.54545
		m	613	49.09091
	m		639	57.27273
		m	648	55.90909
	s		773	49.77273
	m		946	49.77273
		s	948	62.04545
		m	995	61.36364
		s	1004	54.54545
		s	1027	56.59091
		m	1069	54.54545
		m	1076	58.63636
		s	1105	54.54545
		m	1154	59.31818
	m		16	49.09091
		m	120	49.09091
	s		139	49.09091
	m		416	49.09091
	s		540	57.95455
		s	549	49.09091
		s	1034	51.81818
	m		1148	49.09091
m			350	54.54545

Table C-2 Early Morning and Night Loading

Lane 1 (Left)	Lane 2 (Middle)	Lane 3 (Right)	Time (s)	Speed (mph)
		m	18	49.77273
		m	20	51.13636
		s	21	51.81818
	s		28	53.18182
		s	55	49.09091
	s		57	39.54545
	m		75	47.72727
		s	123	51.81818
		m	141	47.04545
		s	145	47.72727
	s		174	50.45455
	s		187	50.45455
	s		210	50.45455
		s	221	39.54545
		s	225	49.77273
		m	239	51.81818
	s		240	54.54545
		s	258	53.86364
	s		280	55.22727
		s	288	53.86364
	s		292	57.27273
		s	293	54.54545
	s		295	57.95455
	m		317	51.81818
		s	319	50.45455
		s	334	49.77273
		m	359	34.09091
	m		411	60.68182
		s	422	57.95455
	s		425	57.95455
	s		436	57.95455
	s		454	47.72727
		s	525	58.63636
		m	564	51.13636
		s	574	51.81818
	s		58	56.59091
		s	116	49.77273
	m		141	60.68182
		s	196	51.13636

		s	220	57.27273
	L		260	45
		m	281	53.86364
	s		429	49.77273
		m	482	51.13636
	s		526	61.36364
	s		541	53.18182
s			480	49.09091
m			540	60
		s	623	57.95455
	s		624	51.13636
		s	627	55.90909
		s	630	56.59091
		s	637	52.5
	m		652	55.22727
		s	652	49.09091
		l	676	60
		s	683	50.45455
		s	700	51.13636
		s	707	52.5
		s	721	49.77273
		l	737	52.5
		m	741	52.5
		m	762	47.72727
		s	764	54.54545
		m	767	60.68182
		s	774	57.95455
	s		837	45
	s		842	54.54545
		s	851	47.72727
		s	886	47.72727
		m	895	54.54545
	m		898	51.81818
		m	901	53.86364
m			909	58.63636
		s	914	49.77273
		m	959	56.59091
		m	985	57.95455
		s	1014	54.54545
	s		1026	52.5
		m	1049	50.45455

		m	1053	54.54545
		s	1064	53.86364
		s	1077	51.81818
		s	1085	58.63636
	s		1086	51.81818
		s	1111	60
		s	1134	60.68182
		s	1147	54.54545
		s	1160	59.31818
		m	1163	53.86364
s			1164	53.86364
	s		1165	55.22727
		m	1199	54.54545

Table C-3 Morning Peak Loading

Lane 1 (Left)	Lane 2 (Middle)	Lane 3(Right)	Time	Speed (mph)
		s	7	30
		m	13	51.81818
		s	17	30
		s	25	30.68182
		s	35	27.27273
	s		36	53.86364
		m	45	44.31818
		s	58	45
		s	71	32.04545
		s	76	30
	s		77	42.95455
		s	88	27.27273
		m	89	42.95455
		s	90	19.77273
		s	91	25.90909
		m	98	27.95455
		s	113	25.22727
	s		114	27.95455
	s		117	49.77273
		m	126	21.81818
		s	128	49.77273
		m	129	30.68182
	s		132	30
		s	133	27.95455
		s	144	45

		s	146	27.27273
		m	152	19.77273
		m	163	51.13636
		m	170	30
	s		171	42.95455
		s	189	45.68182
	s		190	30
		s	192	27.95455
		m	196	47.04545
		s	213	36.13636
s			214	25.90909
	s		215	25.22727
		s	232	36.81818
		s	244	30
	s		245	30
		s	246	30
	s		248	47.72727
		s	249	30
		s	261	49.77273
		s	262	30
		s	264	30
		s	273	36.13636
		s	275	42.27273
		s	291	38.18182
		s	295	30
		s	297	29.31818
		m	301	17.72727
		s	309	49.77273
		s	313	45
		s	318	45
		m	322	23.18182
		s	328	30.68182
		s	330	30
		s	336	40.22727
		m	356	42.95455
		s	379	30
		s	380	47.72727
		m	397	34.77273
		s	402	30
		s	419	51.13636
		s	435	36.13636

		m	437	23.18182
		s	438	23.18182
		s	449	36.13636
		s	451	30
		s	459	45
		s	468	44.31818
		m	472	25.90909
		s	473	30
	s		489	34.77273
		s	504	49.77273
		s	523	34.77273
		m	524	30
		s	526	25.90909
		s	527	25.90909
		s	532	32.04545
		s	543	29.31818
	m		545	53.18182
		s	578	47.72727
		s	585	30.68182
		m	615	44.31818
		m	616	19.77273
		s	641	27.27273
		s	674	27.27273
		m	676	32.04545
		m	677	30
		s	689	42.95455
	s		690	54.54545
		s	706	47.04545
		s	708	45
		m	713	45.68182
		s	716	42.95455
		s	718	27.27273
		m	720	25.22727
		s	736	30
		s	737	30
s			760	36.13636
		s	769	27.27273
		s	772	30
		m	775	21.13636
		s	778	30
		m	793	19.77273

		s	797	45.68182
		s	804	51.13636
		s	814	49.77273
	s		816	49.77273
		s	818	30
		m	825	25.22727
		m	826	23.86364
		s	842	30
		s	859	38.18182
		s	872	25.90909
		s	874	43.63636
	m		892	32.04545
		s	902	49.09091
		m	923	47.72727
		s	928	44.31818
		s	930	27.95455
		s	940	49.09091
		m	941	27.27273
		s	946	42.95455
	m		947	27.27273
		m	952	21.81818
		s	956	47.72727
		s	958	49.09091
		m	960	29.31818
		s	961	30
		s	962	30.68182
	s		966	27.95455
		m	971	30
		s	983	45
		s	984	27.95455
		m	984	21.81818
		m	995	45
		m	1020	30
		s	1024	30
		s	1037	45
		s	1039	51.81818
		s	1061	27.95455
		m	1064	47.04545
		s	1065	23.18182
		s	1073	45
		s	1080	45

		s	1082	27.27273
		m	1092	32.72727
	m		1093	42.95455
		s	1095	45
	s		1100	47.72727
		s	1104	30
s			1106	30
		m	1110	51.13636
		s	1111	27.95455
		s	1125	29.31818
		m	1136	49.77273
		s	1158	30.68182
		s	1184	42.27273
	s		1185	27.27273
		m	1187	27.27273
		s	1193	40.90909
		s	1194	45

Table C-4 Noon to Evening Loading

Lane 1	Lane 2	Lane 3	Time	Speed (mph)
		s	30	51.13636
		m	60	47.04545
		s	62	40.22727
		s	63	34.77273
		s	72	51.81818
		m	76	23.18182
		m	86	47.04545
		s	117	49.77273
		m	125	45
		s	131	47.72727
		s	133	32.72727
	m		152	44.31818
		s	153	40.22727
		s	155	40.22727
		m	174	47.72727
	s		175	23.18182
		s	180	30
		s	181	30
		s	195	44.31818
	m		196	64.09091
		s	197	34.09091

		s	208	44.31818
		s	214	47.04545
		s	228	23.86364
	s		229	34.77273
		m	239	40.22727
		s	241	30
		s	246	30
		s	284	45
		s	316	42.95455
		s	333	45
		s	339	53.18182
		m	378	45
	m		380	42.27273
		s	381	30
		m	411	38.18182
		s	432	47.04545
		m	449	45.68182
		s	458	42.27273
		s	476	47.72727
		s	483	45.68182
		s	484	32.04545
		m	511	45
		s	530	45
		m	557	30
		s	559	45
		s	564	30
		s	577	45
		s	593	49.77273
		m	599	49.09091
		s	609	47.04545
		s	621	55.22727
		m	652	49.77273
	s		653	40.22727
		m	660	49.77273
		s	693	47.04545
	m		701	45
		m	730	45
		s	734	51.81818
		s	742	45.68182
	s		768	53.18182
	s		781	42.95455

		s	800	47.04545
		s	802	45
		s	808	47.72727
	m		837	44.31818
		s	850	47.04545
		m	859	44.31818
	s		873	45
	s		899	44.31818
	m		901	25.90909
		s	914	49.77273
	m		920	30
	s		939	30
		s	963	51.13636
	s		978	47.04545
		s	994	44.31818
		m	995	47.04545
		s	1012	49.09091
		m	1016	42.95455
	m		1018	44.31818
	m		1022	47.72727
		s	1032	30
		s	1071	30.68182
	m		1072	44.31818
		s	1094	30.68182
		s	1108	32.04545
		m	1112	45.68182
		m	1118	44.31818
		s	1125	42.95455
		s	1137	42.95455
		s	1148	40.22727
	m		1149	30
		s	1162	30.68182
		s	1171	38.18182
		s	1188	49.09091

s: small trucks, including 2-alxe and 3-axle;
m: medium trucks, including 4-axle and 5-axle;
l: large trucks, 6-axle and above.

Bibliography

AASHTO. (1989). *Guide Specifications for Fatigue Design of Steel Bridges.* Washington D.C.: American Assocation of State Highway and Transporation Officals.

AASHTO. (1990). *Guide Specifications for Fatigue Evaluation of Existing Steel Bridges.* Washington, D.C.: American Association of State Highway and Transportation Officials.

AASHTO. (2010). *The Manual for Bridge Evaluation.* Washington, D.C.: American Association of State Highway and Transportation Officials.

AASHTO. (2013). *LRFD Bridge Design Specifications.* Washington, D.C.: American Association of State Highway and Transportation Officials.

Andrzej S. Nowak, Hani Nassif, and Leo DeFrain. (1993). Effect of Truck Loads on Bridges. *Journal of Transportation Engieering*, 119:853-867.

Averill M. Law and W. David Kelton. (2000). *Simualtion Modeling and Analysis.* McGraw-Hill.

Boulent M. Lmam, Timothy D. Righiniotis, and Marios K. Chryssanthopoulos. (2008). Probabilistic Fatigue Evaluation of Riveted Railway Bridges. *Journal of Bridge Engineering* , 13: 237-244.

Colin MacDougall, Mark F. Green, Scott Shillinglaw. (2006). Fatigue Damage of Steel Bridges Dut to Dynamic Vehicle Loads. *Jounal of Bridge Engineering*, 11:320-328.

Dan M. Frangopol, Alfred Strauss and Sunyong Kim. (2008). Bridge Reliability Assessment Based on Monitroing . *Journal of Bridge Engineering*, 13: 258-270.

Guo Tong, Li Aiqun and Li Jianhui. (2008). Fatigue Life Prediction of Welded Joints in Orthotropic Steel Decks considering Temperature Effect and Increasing Traffic FLow. *Structural Health Monitoring*, 7: 189-202.

Jeffrey A. Laman and Andrzej S. Nowak. (1996). Fatigue-Load Models for Girder Bridges. *Jouranl of Structural Engineering*, 122:726-733.

Nawal Kishor Banjara and Saptarshi Sasma. (2013). Evaluation of Fatigue Remaining Life of Typical Steel Plate Girder Bridge under Railway Loading. *Structural Longevity*, 10: 151-166.

NCHRP. (2011). *Protocols for collecting and using traffic data in bridge design.* Washington, D.C.: Transportation Research Board.

NCHRP. (2012). *Fatigue Evaluation of Steel Bridges.* Washington, D.C.: Transportation Research Board.

Nur Yazdani and Pedro Albrecht. (1987). Risk Analysis of Fatigue Failure of Highway Steel Bridges. *Journal of Structural Engineering*, 113: 483-500.

Piya Chotickai and Mark D. Bowman. (2006). Truck Models for Improved Fatigue Life Predictions of Steel Bridges. *Journal of Bridge Engineering*, 11: 71-80.

Rui Jiang, Qingsong Wu, Zuojin Zhu. (2001). Full Velocity Difference Model for a Car-following Theory. *Physical Review E*, 64:017101,1-4.

Suren Chen and Jun Wu. (2010). Dynamic Performance Simulation of Long-Span Bridge under Combined Loads of Stochastic Traffic and Wind. *Journal of Bridge Engineering*, 15: 219-230.

Suren Chen and Jun Wu. (2011). Modeling Stochastic Live Load for Long-span Bridge based on Microscopic Traffic Flow Simulation. *Computers and Structures*, 89:813-824.

Suren Chen, and C.S. Cai. (2007). Equivalent Wheel Load Approach for Slender Cable-Stayed Bridge Fatigue Assessment under Traffic and Wind: Feasibility Study. *Journal of Bridge Engineering*, 12: 755-764.

T. F. Fwa and S. Li. (1995). Estimation of Lane Distriction of Truck Traffic for Pavement Design. *Journal of Transportaion Engineering* , 121:241-248.

T. F. Fwa, B. W.Ang, H. S. Toh, and T. N. Goh. (1993). Estimation of Axle Loads of Heavy Vehicles for Pavement Studies. *Transportation Reserach Record, No. 1388, Rigid and Flexible Pavement Design and Rehabilitation.*, 70-79.

T. J. Miao and T.H.T. Chan. (2002). Bridge Live Load Models from WIM Data. *Engineering Structures*, 24: 1071-1084.

Tommoy H.T. Chan, T. Q. Zhou, Z. X. Li and L. Guo. (2005). Hot Spot Stress Approach for Tsing Ma Bridge Fatigue Evaluation under Traffic using Finite Element Method. *Structural Engineering and Mechanics*, 19: 261-279.

Tommy H.T. Chan, L. Guo, and Z. X. Li. (2003). Finite ELement Modelling for Fatigue Stress Analysis of Large Suspension Bridges. *Jouranl of Sound and Vibration*, 261:443-464.

Tong Guo, Dan M. Frangopol, Yuwen Chen. (2012). Fatigue Reliability Assessment of Steel Bridge Details Integrating Weigh-in-motion Data and Probabilistic Finite Element Analysis. *Computers and Structures*, 112-113:245-257.

Ton-Lo Wang, Chunhua Liu, Dongzhou Huang, and Mohsen Shahawy. (2005). Truck Loading and Fatigue Damage Analysis for Girder Bridges Based on Weigh-in-Motion Data. *Journal of Bridge Engineering*, 10:12-20.

W. Zhang, C. S. Cai and F. Pan. (2013). Fatigue Reliability Assessment for Long-Span Bridges under Combinaed Dynamic Loads from Winds and Vehicles. *Journal of Bridge Engineering*, 18: 735-747.

W. Zhang, C.S.Cai, and F. Pan. (2013). Fatigue Reliability Assessment for Long-Span Bridge under Combined Dynamic Loads from Winds and Vehicles. *Journal of Bridge Engineering*, 18: 735-747.

Wikipedia. (2015). *Bilinear Interpolation*. Retrieved from Wikipedia.

Xiaomin Shi, C. S. Cai, and Suren Chen. (2008). Vehicle Induced Dynamic Behavior of Short-Span Slab Bridges Considering Effect of Approach Slab Condition. *Journal of Bridge Engineering*, 13: 83-92.

Z. W. Chen, Y. L. Xu, and X. M. Wang. (2012). SHMS-Based Fatigue Reliability Analysis of Multiloading Suspension Bridges. *Journal of Structural Engineering*, 138: 299-307.

Zhou, Y. E. (2006). Assessment of Bridge Remaining Fatigue Life through Field Stran Measurement. *Journal of Bridge Engieering*, 11:737-744.

Cai, C. S. , Shi, X. M. , Araujo, M. , and Chen, S. R. (2007). “Effect of approach span condition on vehicle-induced dynamic response of slab-on-girder road bridges.” Eng. Structures , 29 (12), 3210–3226.

Cao, Y. H. , Xiang, H. F. , and Zhou, Y. (2000). “Simulation of stochastic wind velocity field on long-span bridges.” J. Eng. Mech. , 126 (1), 1–6.

Chan, T. H. T. , Li, Z. X. , and Ko, J. M. (2001). “Fatigue analysis and life prediction of bridges with structural health monitoring data—Part II: Application.” Int. J. Fatigue , 23 (1), 55–64.

Chan, T. H. T. , Yu, Y. , Wong, K. Y. , and Li, Z. X. (2008). “Condition-assessment-based finite element modeling of long-span bridge by mixed dimensional coupling method.” 3rd World Congress on Engineering Asset Management and Intelligent
Maintenance Systems Conference: Engineering Asset Management-A Foundation for Sustainable Development, J. Gao, J. Lee, J. Ni, L. Ma, and J. Mathew, eds., WCEAM World Congress on Engineering Asset Management, Daejeon, Korea.

Chen, S. R. , and Wu, J. (2010). “Dynamic performance simulation of long-span bridge under combined loads of stochastic traffic and wind.” J. Bridge Eng. , 15 (3), 219–230.

Chen, Z. W. (2010). “Fatigue and reliability analysis of multiload suspension bridges with WASHMS.” Ph.D. thesis, Hong Kong Polytechnic Univ., Hong Kong.

Chen, Z. W. , Xu, Y. L. , Li, Q. , and Wu, D. J. (2011a). “Dynamic stress analysis of long suspension bridges under wind, railway, and highway loadings.” J. Bridge Eng. , 16 (3), 383–391.

Chen, Z. W. , Xu, Y. L. , Xia, Y. , Li, Q. , and Wong, K. Y. (2011b). “Fatigue analysis of long-span suspension bridges under multiple loading: Case study.” Eng. Structures , 33 (12), 3246–3256.

Chung, H. (2004). “Fatigue reliability and optimal inspection strategies for steel bridges.” Ph.D. thesis, Univ. of Texas, Austin, TX.

Deng, L. , and Cai, C. S. (2010). “Development of dynamic impact factor for performance evaluation of existing multi-girder concrete bridges.” Eng. Structures , 32 (1), 21–31.

Dodds, C. J. , and Robson, J. D. (1973). “The description of road surface roughness.” J. Sound Vibrat. , 31 (2), 175–183.

Donnell, E. T. , Hines, S. C. , Mahoney, K. M. , Porter, R. J. , and McGee, H. (2009). “Speed concepts: Informational guide.” Publication No. FHWA-SA-10-001, U.S. Department of Transportation and Federal Highway Administration, Washington, DC.

Ge, Y. , Yang, Y. , and Zhang, Z. (2003). “Report on the wind tunnel experiments of Donghai cable-stayed bridge.” Dept. of Bridge Engineering, Tongji Univ., Shanghai, China.

Gu, M. , Xu, Y. L. , Chen, L. Z. , and Xiang, H. F. (1999). “Fatigue life estimation of steel girder of Yangpu cable-stayed bridge due to buffeting.” J. Wind Eng. Ind. Aerodyn. , 80 (3), 383–400.

Guo, W. H. , and Xu, Y. L. (2001). “Fully computerized approach to study cable-stayed bridge-vehicle interaction.” J. Sound Vibrat. , 248 (4), 745–761.

Honda, H. , Kajikawa, Y. , and Kobori, T. (1982). “Spectra of road surface roughness on bridges.” J. Struct. Div. , 108 (9), 1956–1966.

ISO. (1995). “Mechanical vibration; Road surface profiles; Reporting of measured data.” ISO 8608:1995, Geneva.

Keating, P. B. , and Fisher, J. W. (1986). “Evaluation of fatigue tests and design criteria on welded details.” NCHRP Report 286, Transportation Research Board, Washington, DC.

Kwon, K. , and Frangopol, D. M. (2010). “Bridge fatigue reliability assessment using probability density functions of equivalent stress range based on field monitoring data.” Int. J. Fatigue , 32 (8), 1221–1232.

Laman, J. A. , and Nowak, A. S. (1996). “Fatigue-load models for girder bridges.” J. Struct. Eng. , 122 (7), 726–733.

Li, Z. X. , Chan, T. H. T. , and Ko, J. M. (2002). “Evaluation of typhoon induced fatigue damage for Tsing Ma bridge.” Eng. Structures , 24 (8), 1035–1047.

Miner, M. A. (1945). “Cumulative damage in fatigue.” J. Appl. Mech. , 12 (3), A159–A164.

Nyman, W. E. , and Moses, F. (1985). “Calibration of bridge fatigue design model.” J. Struct. Eng. , 111 (6), 1251–1266.

Oh, B. H. , Lew, Y. , and Choi, Y. C. (2007). “Realistic assessment for safety and service life of reinforced concrete decks in girder bridges.” J. Bridge Eng. , 12 (4), 410–418.

Shi, X. , Cai, C. S. , and Chen, S. (2008). “Vehicle induced dynamic behavior of short-span slab bridges considering effect of approach slab condition.” J. Bridge Eng. , 13 (1), 83–92.

Texas Department of Transportation (TxDOT). (2006). Procedures for establishing speed zones, Texas Department of Transportation, Austin, TX.

Transportation Research Board (TRB). (2000). Highway capacity manual. Washington, DC.

Troitsky, M. S. (1987). Orthotropic bridges; Theory and design, 2nd Ed. The James F. Lincoln Arc Welding Foundation, Cleveland.

Virlogeux, M. (1992). “Wind design and analysis for the Normandy Bridge.” Aerodynamics of large bridges, A. Larsen, ed., Balkema, Rotterdam, Netherlands, 183–216.

Wang, T.-L. , and Huang, D. (1992). Computer modeling analysis in bridge evaluation, Florida Dept. of Transportation, Tallahassee, FL.

Wolchuk, R. (1963). Design manual for orthotropic steel plate deck bridges, American Institute of Steel Construction, Chicago.

Wu, C. , Zeng, M. G. , and Dong, B. (2003). Report on the performance of steel-concrete composite beam of Donghai cable-stayed bridge, Dept. of Bridge Engineering, Tongji Univ., Shanghai, China.

Wu, J. (2010). “Reliability-based lifetime performance analysis of long-span bridges.” Ph.D. thesis, Colorado State Univ., Fort Collins, CO.

Xu, Y. L. , and Guo, W. H. (2003). “Dynamic analysis of coupled road vehicle and cable-stayed bridge systems under turbulent wind.” Eng. Structures , 25 (4), 473–486.

Xu, Y. L. , Liu, T. T. , and Zhang, W. S. (2009). “Buffeting-induced fatigue damage assessment of a long suspension bridge.” Int. J. Fatigue , 31 (3), 575–586.

Zhang, W. (2012). “Fatigue performance of existing bridges under dynamic loads from winds and vehicles.” Ph.D. thesis, Louisiana State Univ., Baton Rouge, LA.

Zhang, W. , and Cai, C. S. (2012). “Fatigue reliability assessment for existing bridges considering vehicle and road surface conditions.” J. Bridge Eng. , 17 (3), 443–453.

Zhang, Z. T. , and Ge, Y. J. (2003). “Static and dynamic analysis of suspension bridges based on orthotropic shell finite element method.” Struct. Engineers , 2003 (4), 21–25, 6.